THE ANISOTROPY OF THE SECOND-ORDER NONLINEAR SUSCEPTIBILITY OF RI$_3$*3S$_8$ CRYSTALS
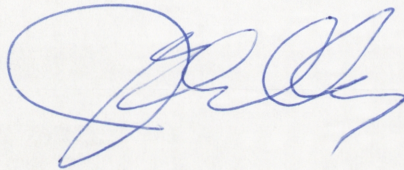
Julian F. Kelly

November 1997

A thesis submitted for the degree of Doctor of Philosophy of the Australian National University

DECLARATION

The work presented in this thesis is my own, except where due reference has been given in the text. To the best of my knowledge, no part of the research described in the thesis has been submitted or accepted for the award of any other Degree at any other University.

Julian Kelly

ABSTRACT

Numerous molecules with large hyperpolarisabilities are now known. Yet prediction of the bulk, non-linear susceptibilities ($\chi^{(2)}$) for their molecular crystals is not straightforward. This is because of the need to accurately know:
- the *in-crystal* molecular polarisability (and hyperpolarisability) and
- the local-field factors applicable to the particular crystal lattice.

Both of these quantities affect the other and special methods must be used in their determination.

This thesis reports on such $\chi^{(2)}$ 'construction' in the interesting series of charge-transfer addition compounds, RI_3*3S_8, where R = CH, As, Sb. An unresolved question concerning the erratic anisotropy of the $\chi^{(2)}$ tensor coefficient across this series appears to have been at least partly solved through comparison of these predicted $\chi^{(2)}$ with the experimentally determined coefficients.

In the course of this work, hyperpolarisabilities of the free triiodide molecules have been calculated -including β tensors for AsI_3 and SbI_3 which have been predicted for the first time. The ab initio computations incorporated consideration of electron correlation via the MP2 perturbation-theory approach which represents an improvement over earlier β calculations for CHI_3.

Second-order NLO susceptibility measurements were performed for CHI_3*3S_8 and AsI_3*3S_8 crystals using the second-harmonic Maker-Fringe Technique. An electro-optic coefficient was also determined for the AsI_3*3S_8 crystal.

Estimation of local electric fields involved calculation of Lorentz-factor tensors and local-field factor tensors for the adduct crystals. This approach gives a more realistic description of the local-field at a molecular site than the anisotropic Lorentz approximation. A complete specification of the *hetero*-molecular lattice is important for obtaining representative local-field-factor tensors.

By doing this, one may incorporate hyperpolarisabilities from both molecule types into the NLO-susceptibility calculation. This requires assumptions about each polarisability of the different molecules as they exist in the adduct crystal. This procedure for calculating $\chi^{(2)}$ for a hetero-molecular crystal had not previously been performed.

Contributions to $\chi^{(2)}$ from the octa-sulfur molecule are important in some of these complexes and this seems to be correlated with the extent of S_8 ring distortion in the complex. Electronic absorption also influences the size of $\chi^{(2)}$ and can confuse the $\chi^{(2)}$ anisotropy in these rather birefringent crystals. These two factors are primarily responsible for the $\chi^{(2)}$ anisotropy differences in the $RI_3{*}3S_8$ series. However, this could not have been deduced without using the extended local-field description.

PUBLICATIONS

J.F. Kelly, R.W. Munn and M.J. Samoc, The local electric field and dipole moment of CHI_3 in the $CHI_3{*}3S_8$ complex.
    submitted to *Chemical Physics Letters.*

R.W. Munn, J.F. Kelly and F.M. Aicken, Nature or Nurture: Environmental effects on molecular response in crystals of CHI_3, S_8 and their 1:3 complex.
    Engineering Foundation Conference "Molecular Electronics - Science and Technology", Puerto Rico, 14-18 Dec 1997.

J.F. Kelly, E.R. Krausz, A.C. Willis, A. Samoc and M.J. Samoc, The second-order nonlinear susceptibility of the addition complex, $AsI_3{*}3S_8$. submitted to *Aust.J.Chem.*

CONTENTS

ACKNOWLEDGMENTS

CHAPTER ONE

Physical characteristics of condensed molecular media originate ultimately from properties of the molecules themselves. Thus, it is the response of the molecule to incident light fields which determines the bulk optical properties, for example, one notes that more polarisable compounds have greater refractive indices in condensed phases. Yet it is also the manner in which molecules aggregate which helps define a macroscopic optical property. This is, in turn, determined by the physico-chemical properties of the molecule.

In the domain of Nonlinear Optical (NLO) response of molecular materials, it is also true that bulk NLO properties are determined by the properties and behaviour of the molecules from which they are composed. The relationship between microscopic and macroscopic NLO response is of fundamental interest and is not necessarily straightforward [1,30-36,39]. A major theme in this thesis is the macroscopic$\leftrightarrow$microscopic relationship between second-order nonlinear optical response of a certain group of crystals and that of their constituent molecules.

Introduction

1. NONLINEAR OPTICS IN GENERAL

Electronic charge distributions in molecules are distorted by applied electric fields. In the low field limit, the resulting polarisation scales linearly with the applied field strength. Thus, linear optical properties arise from irradiation with ambient electromagnetic radiation of optical frequency. Larger applied field strengths may be beyond this range of linear response. The domain of Nonlinear Optics refers to the situation in which incident light intensity provides a strong electric field such that the polarisation of the molecule is beyond the linear response regime.

When a molecule is polarised, its dipole moment, μ_i, can be described by an expansion in powers of the electric field, F, acting on it[1]:

$$\mu_i = \mu_i^{(0)} + \alpha_{ij}F_j + \beta_{ijk}F_jF_k + \gamma_{ijkl}F_jF_kF_l + ...$$

(1)

where $\mu_i^{(0)}$ is the permanent dipole moment in the absence of any polarising field and α_{ij} is the polarisability tensor accounting for the linear response. The tensors, β_{ijk} and γ_{ijkl} are, respectively, the second-order and third-order *hyperpolarisabilities*. The indices refer to cartesian coordinates of the molecule and the convention of summation over repeated indices is assumed.

The analogous expression describing macroscopic polarisation in any medium (whether molecular or ionic) including linear and nonlinear response is:

$$P_I = \chi_{IJ}^{(1)}F_J + \chi_{IJK}^{(2)}F_JF_K + \chi_{IJKL}^{(3)}F_JF_KF_L + ...$$

(2)

where P_I is the polarisation vector and a term for a permanent macroscopic polarisation is omitted. The $\chi^{(n)}$ coefficients are the nth-order *susceptibility tensors*. The indices in this case correspond to the chosen axis system for the macroscopic sample (crystal axes, for example).

When the electric fields are time-varying, the polarisation also becomes a function of time. A nonlinearly oscillating polarisation can be included in a wave equation derived from the Maxwell Equations to describe the propagation of an electromagnetic wave arising from this nonlinear polarisation. This is illustrated in the next Chapter. Bulk nonlinear polarisation can manifest as numerous

---

[1] See, for example, Ref [1] or any one of: G.D. Stucky *et al*, D.J. Williams, P.N. Prasad or J.W. Perry in [3b].

interesting and useful phenomena; Harmonic Generation, Frequency Mixing and Intensity Dependent Refractive Index are just a few examples.

A symmetry requirement exists: for a medium possessing a centre of inversion, the second-order susceptibility (quadratic in F) must be zero (*i.e.* $\chi^{(2)} \neq 0$). This is not the case for third order NLO response and all materials have a non-zero $\chi^{(3)}$.

The molecules of interest in this study are iodoform and the triiodides of arsenic and antimony. These three compounds form crystalline complexes with molecules of sulfur, S_8. The composition of these complexes is RI_3*3S_8. The three complexes are the materials of interest to this study.

This investigation falls into two topical areas within the domain of NLO properties of molecular materials. These are:
- the study of NLO phenomena in "addition-complex" type crystalline materials and in particular, in those formed between non-π-electron molecules
- the investigation of second-order molecular NLO response in structures with 'nontraditional' architectures. In most cases, the required molecular noncentrosymmetry is present in 'dipolar' asymmetry[2] and it is along the dipole moment axis that the strongest second-order NLO polarisation occurs. Symmetry groups also exist which are noncentrosymmetric yet based on elements of three-fold symmetry. These are called octupolar classes. 'Quadratic' NLO response has been shown [6] from molecules possessing such structural elements but this domain is still relatively little-studied.

Both areas are of interest since the existence of new classes of NLO-active materials offers greater scope in the development of compounds with specific (large) NLO responses. This chapter provides a background to these two fields.

Differences in the second-order NLO susceptibility, $\chi^{(2)}$, between two of the isomorphous RI_3*3S_8 complexes were noted in earlier studies (as described later). Possible explanations for this are proposed in this chapter and are of central concern in the thesis.

---

[2] Such structures are typified by the organic Donor-Acceptor molecule:
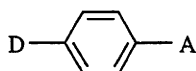
Examples of NLO studies on such molecules may be found in Refs [1-3].

2. *SECOND-ORDER NONLINEAR OPTICS IN MULTIPOLAR MEDIA*

Dipolar and Octupolar Molecules

The elements of the third-rank β or $\chi^{(2)}$ tensor quantify the quadratically dependent electronic polarisation induced by an applied electric field. The associated electron density changes are related to the spatial electronic structure of the molecule or crystal respectively.

These tensors may be rather complicated -especially for low symmetry systems. A procedure exists, however, whereby a tensor is *decomposed* into a number of simpler parts. The formalism is outlined here. Further detailed description with respect to NLO in molecular media is found in Refs [10].

A general tensor of rank n can be decomposed into a number of irreducible 'sub-tensors' of the same rank which by definition are invariant upon rotation in any dimension. Irreducible tensors[1] are linear combinations of parent-tensor elements and are described by a quantity called the 'weight', j, defining the number of independent components; $2j+1$. They may appear as lower rank tensors and be considered as such (with rank, j) [10a] or they may be expressed in the higher rank tensor space of the parent tensor [10c]. The sum of independent components from all invariants equals the number of independent components of the parent tensor.

The method by which the irreducible tensors are obtained is described by Coope *et al* [11a] and by Juretschke [11b]. Briefly, (following Juretschke), consider a diagonal $3^{\ell} \times 3^{\ell}$ transformation matrix for the rotation operation on a rank ℓ parent tensor. This matrix contains certain 'blocks' of dimension $(2j+1) \times (2j+1)$ and each corresponds to an irreducible tensor of weight j. This gives the *types* of irreducible parts in the decomposition. For the *number* of each type, one takes the expression for the trace of the individual irreducible tensor blocks, $\chi_{(2j+1)}$. This is a function

only of rotation angle, ϕ, and is given by:

$$\chi_{(2j+1)}(\phi) = \frac{\sin(j + \frac{1}{2})\phi}{\sin \frac{1}{2}\phi} \qquad (3)$$

The transformation matrix of the parent tensor has a trace determined by the ℓ-fold product of the transformation of the vectors and equals:

$$\chi_{3^{\ell}}(\phi) = (1 + 2\cos\phi)^{\ell} \qquad (4)$$

---

[1]   Juretschke refers to irreducible tensors as 'invariants'. In accordance with Jerphagnon, however, this term is reserved for describing 'scalar invariants' in this work.

Since the sum of the traces of each of the blocks must equal the trace of the 'parent' transformation matrix, one can easily work out integer combinations of each j term of Eq (3) to match the appropriate Eq (4) (expanded to order ℓ).

Following this, any rank-two tensor, T_{ij}, is decomposed into: a scalar part (j =0) which is the trace, a vector part (j =1) and an irreducible tensor of weight j =2 (often called a deviator). The sum of components of these irreducible tensors (1+3+5) equals the nine components of the original rank-two tensor. A general third-rank tensor, T_{ijk}, is decomposed into: a scalar part, three vectors, two deviators and a 'septor' (j=3) part giving 1+(3×3)+(2×5)+7= the 27 components for a third-rank tensor.

The number and type of irreducible tensors arising from the parent tensor may be simplified depending on the intrinsic symmetry of the physical process being described; a symmetric second rank tensor (such as the strain or polarisability tensor) decomposes to just a scalar and a deviatric (j=2) part. This treatment has been performed for the specific case of a fully symmetric[2] third-rank tensor as for β or $\chi^{(2)}$ [10a]. This analysis shows that the only non-zero irreducible parts for these tensors are a vector and a septor part[3].

Because the irreducible sub-tensors are rotationally invariant, they cannot mix when the coordinate system is changed. This means that for a macroscopic response made up entirely of molecules with a non-zero β, an irreducible part of the decomposed $\chi^{(2)}$ has its origins *entirely* in the same irreducible part of β, even if the symmetries on which the two tensors apply are different.

---

[2]   for SHG, $\omega_1 = \omega_2$, allowing free permutation of j and k elements in the β_{ijk} tensor. The Kleinman symmetry condition allows full index permutation in the non-resonant case.

[3]   The combination of parent-tensor elements in the irreducible parts can be worked out:

The vector parts, $t^{(1)}_{ijk}$, are the traces of the parent third-rank tensor. In the fully symmetric case they are all equal and thus:

$$t^{(1)}_{ijk} = \frac{1}{5}\left(\sum_{m=1}^{3} \left(t_{imm}\delta_{jk} + t_{jmm}\delta_{jk} + t_{kmm}\delta_{jk} \right) \right) \qquad \text{where} \quad \begin{array}{l} \delta_{jk} = 1 \text{ if } j = k \\ \delta_{jk} = 0 \text{ if } j \neq k \end{array} \text{ etc and}$$

m is a dummy variable.

The septor-part describes the "octupolar deviation" from isotropy. Each component is given by:

$$t^{(3)}_{ijk} = t_{ijk} - t^{(1)}_{ijk}$$

As an example, the 311 component of the septor derived from the β-tensor for SHG in 3m symmetry is: $\beta^{(3)}_{311} = \frac{1}{5}\left(3\beta_{311} - \beta_{333}\right)$. And the total septor part is the sum of all $t^{(3)}_{ijk}$ (many of which will be zero).

5

The definition has been established by Zyss whereby a material with a structure having a symmetry group such that its β tensor decomposes into a vector (j=1) part *only* is deemed to be a purely **dipolar** material. A material with a structure of symmetry for which the decomposed β tensor has *no* vector part and *only* the septor (j=3) part is a purely **octupolar** material.

These names reflect the fact that the irreducible parts of $\chi^{(2)}$ or β describe the NLO interaction of the dipolar/octupolar parts of the charge distribution of a molecule or crystal[4]. Zyss [8] drew this link when considering a charge distribution described as a function of distance and angular position, $F(r,\theta)$. A general distribution may be expanded as a sum of *rotational harmonics* in a Fourier decomposition:

$$F(r,\theta) = \sum_{j=0}^{\infty} a_j(r) \ \cos(j\theta + \varphi_j(r)) \qquad (5)$$

where $a_j(r)$ and $\varphi_j(r)$ are *r*-dependent constants for the particular *j*-order expansion terms. The rotational harmonics (from which NLO response may independently arise) have *j*-fold symmetry and have 2^j multipole character [9c]. This can be seen from radial plots of each of the terms of Eq (5) as shown in Refs [7,8]. The component of the angular decomposition with three-fold symmetry corresponds to an octupolar (2^3) charge distribution.

Note, however, that a purely octupolar material need not necessarily possess only an octupole moment [9c,12a]. Figure One shows representative types.
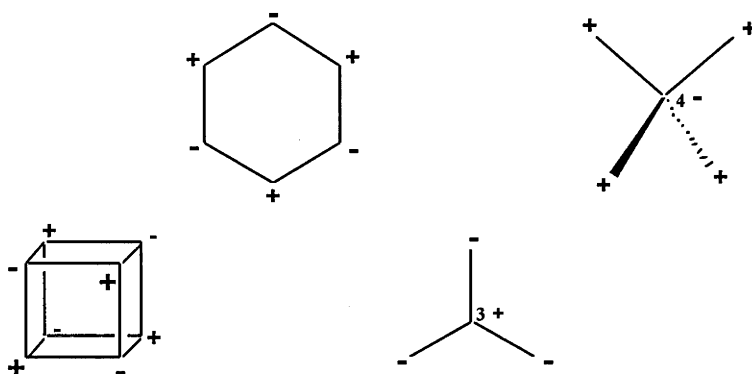
Figure One: Examples of charge distributions conforming to the definition of *octupolar* structures.

---

[4]   Robinson [12b] showed this via determination of the third-order perturbation energy of a nonlinearly polarised material.

Materials with purely octupolar structures do show second-order NLO responses. It has been demonstrated that the nonlinear response from such molecules can be of the same order of magnitude as traditionally studied one-dimensional "dipolar" donor-acceptor molecules:

- The example of 1,3,5-trinitro-2,4,6-triaminobenzene has been studied both experimentally [6a] and theoretically [6b] in order to compute β.
- The hyperpolarisabilities of $C(CN)_3^-$ [6d] and tetrahedral organometallic SnR_4 compounds [6c] were measured with a view to establishing that their second-order NLO responses were large enough to have device-application potential.
- Early studies of the NLO response of triiodide complexes are described in a later section.
- Other examples are summarised in the review of Zyss [7].

Thus, classes of molecular structures based on three-fold symmetry elements have a legitimate place in the increasingly important search for molecules with sizeable second-order NLO response.

Theoretical Prediction of β for Dipolar and Octupolar Molecules

The second-order hyperpolarisability, β, of a molecule may be estimated via a perturbation treatment [5a]. The polarisation, μ, of a perturbed molecule is:

$$\mu = -e\boldsymbol{r} \tag{6a}$$

$$\begin{aligned} \mu_{nm} &= -e\int \psi_n^* \boldsymbol{r}\, \psi_m\; d\tau \\ &= -e\langle n\,|\boldsymbol{r}|\,m\rangle \\ &= -e\,\boldsymbol{r}_{nm} \end{aligned} \tag{6b}$$

where Q is the number of electronic states (labelled n), e is the electron charge. $\boldsymbol{r}$ is the sum of position vectors for all electrons.

The wavefunction of the perturbed molecule may be approximated (to second-order in a static applied field, F) by the expansion:

$$\left| n \right\rangle = \left| n^{(0)} \right\rangle + \left| n^{(1)} \right\rangle + \left| n^{(2)} \right\rangle + \ldots.$$

$$\left| n^{(1)} \right\rangle = -eF \sum_{n \neq m} \left| m^{(0)} \right\rangle \frac{\left\langle m^{(0)} \left| \boldsymbol{r} \right| n^{(0)} \right\rangle}{\mathrm{E}_{mn}}$$

$$\left| n^{(2)} \right\rangle = -e^2 F^2 \sum_{n \neq m} \left| m^{(0)} \right\rangle \frac{\left\langle m^{(0)} \left| \boldsymbol{r} \right| n^{(0)} \right\rangle \left\langle n^{(0)} \left| \boldsymbol{r} \right| n^{(0)} \right\rangle}{\mathrm{E}_{mn}^{\,2}} \qquad (7)$$

$$+ e^2 F^2 \sum_{n \neq m} \sum_{n \neq p} \left| p^{(0)} \right\rangle \frac{\left\langle p^{(0)} \left| \boldsymbol{r} \right| m^{(0)} \right\rangle \left\langle m^{(0)} \left| \boldsymbol{r} \right| n^{(0)} \right\rangle}{\mathrm{E}_{pn} \mathrm{E}_{mn}}$$

where $\mathrm{E}_{mn} = \mathrm{E}_m - \mathrm{E}_n$

which invokes the particular excited states m and p. E denotes the energies of these states. Integration yields terms proportional to F and F^2. According to Eq (1), the coefficient of F^2 is the first hyperpolarisability tensor β:

$$\beta = 3e^2 \sum_{n=1}^{Q} \left\{ \sum_{n \neq m} \sum_{n \neq p} \frac{\boldsymbol{r}_{nm} \boldsymbol{r}_{mp} \boldsymbol{r}_{pn}}{\mathrm{E}_{pn} \mathrm{E}_{mn}} - \boldsymbol{r}_{nn} \sum_{n \neq m} \frac{\boldsymbol{r}_{nm}^2}{\mathrm{E}_{mn}^{\,2}} \right\} \qquad (8)$$

The expression (8) shows that excitations to and between all states should be considered. For conjugated organic molecules of the 'dipolar' type, there may be a dominant transition from the ground state to a single excited state which involves significant internal movement of charge. In such a case, the molecule can be approximated by a two-level system [1,2,5b] and the denominators in Eq (8) can then be considered equal. This can then be modified to an expression utilising the oscillator strength and optical transition frequencies, ω_{eg}:

$$\beta \left(-2\omega; \omega, \omega \right) \cong \frac{3e^2}{2\hbar m} \frac{\omega_{eg} f \, \Delta\mu}{(\omega_{eg}^2 - \omega^2)(\omega_{eg}^2 - 4\omega^2)} \qquad (9)$$

where f is the oscillator strength for this dominant transition and $\Delta\mu$ is the difference between ground and excited state dipole moments. Omitted from the denominator of this expression are 'damping terms' to account for electronic absorption by the molecule. Eq (9) is useful in showing the dependence of β on the exciting frequency, ω. From the ω_{eg} terms in the denominator, it is evident that when ω is close to a one-photon resonance $(\omega_{eg}^2 - \omega^2)$ or a two-photon resonance $(\omega_{eg}^2 - 4\omega^2)$, the hyperpolarisability may become large (infinite were it not for some damping factor).

Such a two-state model is inadequate for description of a purely octupolar system because the $\Delta\mu$ factor is necessarily zero for such symmetries. An expression needs to be derived from Eq (8) invoking at least three states [9a]. Such a three-level model is consistent with the fact that 'octupolar' groups - D_{3h}, D_3, etc, all have doubly degenerate "E"-type excited states given by symmetry. Thus:

$$\beta = 3e^3 \frac{\boldsymbol{r}_{nm}\boldsymbol{r}_{mp}\boldsymbol{r}_{pn}}{2\mathrm{E}_{nm}\mathrm{E}_{np}} \qquad (10)$$

where n represents the ground state and m and p two degenerate excited states. At optical frequency this becomes:

$$\beta\left(-2\omega;\omega,\omega\right) \cong \frac{3\left|\mu_{nm}\right|^2 \mu_{mm}}{2\,\hbar^4 \mathrm{E}_{nm}^2} \frac{\mathrm{E}_{nm}^2}{(\omega_{nm}^2 - \omega^2)(\omega_{nm}^2 - 4\omega^2)} \qquad (11)$$

using the notation of Zyss *et al* [7], in which the μ terms are the transition dipole moments between the various states, $\mu_{nm} = -e\boldsymbol{r}_{nm}$.   The frequency symbols, ω_{nm}, follow the same logic as for Eq (9).

One may better consider the coupling occurring between such states with *circularly* polarised ($\sigma+$ or $\sigma-$) light [9a] rather than the coupling between g and u states through a vector field (using linearly polarised light) as in the case of a two-level dipolar system.

Materials from Octupolar Molecules

From the point of view of construction of materials with high second-order NLO response, there is significant advantage in using architectures with a zero or small dipole moment. This is because noncentrosymmetric stacking is less likely to be energetically unfavorable as is the case with dipolar molecules[5]. This issue of aiming for sizeable quadratic NLO response from 'zero-μ' or small-μ molecular materials has been extensively studied by Zyss and coworkers[6].

---

[5]   Due to coulombic repulsion, an array of dipoles stacked with all μ aligned in the same direction (*ie*, noncentrosymmetrically) is of significantly higher energy than if stacked in a head-to-tail fashion.

[6]   This theme is present in early work [9d] as well as in more recent studies [6a-b,9a-c].

Mixed dipolar-octupolar systems are those molecules/materials having both vector and septor parts to their decomposed β tensor. These have potential as NLO materials as they often have only small dipole moments. The RI_3 molecules studied here are examples of molecules possessing a small permanent μ and a non-zero octupole moment.

Two important points arise from the formalism outlined earlier:

- The second-order NLO response from both dipolar and octupolar 'architectures' can be deduced from the β tensor of mixed molecules.
- These 'dipolar' and 'octupolar' NLO responses can be separately distinguished in the $\chi^{(2)}$ of crystals of mixed dipolar-octupolar molecules.

Scalar Invariants

Once obtained, the groupings of tensor elements comprising the components of the irreducible parts can be presented more simply as the 'scalar invariants' for that particular irreducible part. These are simply worked out as the square root of the sum of squares of all the constituent components of the irreducible part [10a].

The specific combination of elements for β_{vector} and β_{septor} for each crystal symmetry group has been derived by Jerphagnon [10a]. For the case of the fully symmetric $\chi^{(2)}$ tensor for SHG in the 'mixed' R3m (C_{3v}) symmetry group pertinent in this study, the vector and septor parts of the hyperpolarisability tensor are:

$$\beta_{vector} = \sqrt{\frac{3}{5}(\beta_{333} + 2\beta_{311})} \qquad (12a)$$

$$\beta_{septor} = \sqrt{\frac{2}{5}(3\beta_{311} - \beta_{333})^2 + 4\beta_{111}^2} \qquad (12b)$$

Both parts of the decomposed tensor must be considered when comparing NLO coefficients for materials of different symmetry.

3. CHARGE TRANSFER COMPLEXES

It is necessary to first define this group of materials more precisely as the term "complex" is used widely in chemistry to refer to many systems of interacting chemical species. It is complexes occurring between neutral molecules and which form stoichiometric crystalline compounds that are of concern in this work.

Not considered here are complexes between metal ions and various ligands which form the traditional areas of inorganic and organometallic chemistry. The occurrence of charge transfer (CT) interactions is well established in this field[9] and much research into the NLO properties of such complexes has been described[10]. Also of great significance and activity in NLO research (though not included here) is the area of molecularly-doped systems which may involve CT interactions. These include electrically-poled dye-doped polymers[11]. The interaction between dopant molecules and polymer substituents may be of the CT type if they include electron donor and acceptor species.

Crystalline materials comprised of two different molecular species have been described since at least the first decade of this century[12]. These materials are also called "adducts" or "solid solvates". The number of known examples is now very large and the subject has been dealt with in texts [13]. Examples for which NLO properties have been examined are complexes of cyclodextrin and *para*-nitroaniline (pNA) [15a] and complexes between pNA and other organic donor/acceptor molecules [15b]. These complexes are related to binary molecular systems which do not necessarily form stoichiometric crystals. There has been some interest in these latter materials for second order NLO.

---

[9]   as demonstrated, for example, by strong LMCT (Ligand to Metal Charge transfer) or MLCT bands in absorption spectra of many of these compounds.

[10]   See for example, the article by S. Marder: pp115-164 in "*Inorganic Materials*" eds D.W. Bruce and D. O'Hare, (J.Wiley and Sons, 1992).
       See also: I.R. Whittal, A.M McDonagh, M.G. Humphrey and M.J. Samoc, Organometallic complexes in nonlinear optics I: Second-order nonlinearities. *Adv.Organometallic Chem.*, **42** in-press (1997)

[11]   The large amount of work concerning NLO of doped-polymer systems is evidenced by numerous such reports from symposia proceedings such as listed in Refs [3]. See also Chapter 7 in [2]. Examples of second-order NLO response from poled, molecularly-doped sol-gel glasses are given in Refs [17].

[12]   See, for example, the article by Dehn and Connor [16] (which does not, however, address the interaction between the constituent molecules). Foster's book [13] and Mullikan's works [14] also contain references to early studies of these materials.

As an example, nonlinear optical coefficients were determined for nonstoichiometric co-crystallised (pNA) and meta-nitroaniline (mNA) [15c].

The nature of the weak bonding interaction which causes the adduct formation has been investigated. It is discussed using the term (intermolecular) charge transfer (CT) which occurs between electron donor (D) and acceptor (A) components. In the description of Mulliken [14], an overall ground state wavefunction for the complex is considered as a linear combination of wavefunctions correponding to the free D and A molecules with an appropriate amount of the wavefunction for the completely ionic D$^+$-A$^-$ pair:

$$\Psi_{g,(D \cdot A)} = a\ \Psi_{(D,\ A)} + b\ \Psi_{(D^+ - A^-)}$$

(13)

where $a \approx 1$ and $b \ll 1$. An identical expression exists for the wavefunction of the (first) excited state except that the proportion, b, of the ionic wavefunction is much higher and:

$$b \propto \upsilon / (E_{\text{separated}} - E_{\text{ionic pair}})$$

where υ is the overlap integral between the interacting donor and acceptor orbitals and the denominator contains the difference in energy between the wavefunction of the ionic pair and that of the separated molecules. The square of the b coefficient indicates the amount of charge transferred. If this is large, the dipole moment difference, $\Delta\mu$, between the two states is also likely to be large and according to the two-state model outlined earlier at Eq (7), the hyperpolarisability, β, is be expected to be of significant size.

In general, the lowest energy electronic transition in these complexes is that between the highest occupied state of the donor and the lowest unoccupied state of the acceptor and so the spectroscopic transition corresponds to further charge-transfer which explains the increase in b/a (Figure Two).

                                    ————— Donor LUMO

          Acceptor LUMO
                                    CT transition

                                    ————— Donor HOMO

          Acceptor HOMO
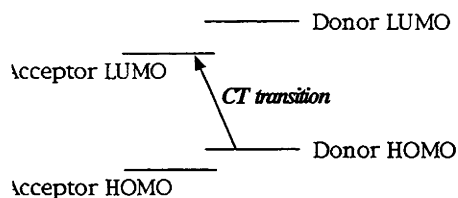
Figure Two: Schematic energy level diagram for a charge-transfer complex. The levels may be blue or red shifted with respect to the levels in the parent donor and acceptor compounds.

The "charge-transfer" classification for this type of attractive interaction is well established in chemical terminology. It usually refers to an intermediate situation in which attractive forces are stronger than ubiquitous electrostatic forces existing between the donor and acceptor species, yet are much weaker than if full ionic or covalent bonding occurs and that each component loses its identity. Whether a molecule is a strong donor or acceptor lies ultimately in the electronegativity of the atoms and depends on the current bonding.

Table One lists several examples of molecules of both electron donor and electron acceptor character, as well as those which are able to act as both.

Table One

DONORS	BOTH	ACCEPTORS
quinoline (n)	octa-sulfur	iodine
dioxane (n)	pyridine (n-donor)	many main group
sulfur dioxide (n)		halides
trimethylamine (n)		carbon tetrachloride
anthracene (π)		trinitrobenzene (π)
azulene (π)		tetracyanoethylene
phenol (π)		(TCNE)

*   largely taken from Foster [13] and the work of Mullikan [14].

Primary evidence for the existence of a CT complex-forming "bond"[13] comes from X-ray structural data which can show rather accurately the distance between adjacent atoms. If this is shorter than that predicted by considering the sum of van der Waals radii of the two atoms (as if they were non-interacting), such an interaction is deemed to exist. Typical shortenings are of the order of 10-15%. A spectroscopic transition associated with the CT interaction is often not observed as it may be obscured by stronger transitions from the interacting donor and acceptor molecules [13].

Complexes between two interacting (organic or inorganic) molecules offer several favorable features for nonlinear optics:

(i)   in crystal matrices of 'complexes', molecules known to have large molecular optical nonlinearities but which form centrosymmetric self-molecular crystals may be favorably aligned for second order NLO response.

(ii)   the incorporation of "NLO-phore" molecules into a matrix may lead to a significant enhancement of NLO response due to local field effects as is discussed later.

Finding CT partner molecules forming good matrices is, of course, difficult. Nevertheless, a large number of potential donor and acceptor partners exists from which those forming noncentrosymmetric matrices may be sought. Zyss [7,8,9c] suggests that to seek crystallisation of octupolar molecules in (CT) host lattices offers promise for producing structures with high second-order NLO responses.

---

[13] On this point, it is interesting to note the comment of Kjekshus and Rakke;
"At present, it is impossible to obtain a direct experimental answer to the important question whether there is or is not bonding between two given atoms. The estimation of bonding is thus confined to deductions from the atomic arrangement and accordingly depends on empirical knowledge."
A. Kjekshus and T. Rakke, The valence concept. *Structure and Bonding*, **Vol 19** (1974)

The Materials

1. GENERAL PROPERTIES

The particular complexes studied in this work are "adducts" of the trigonal-nonplanar molecular triiodides, RI_3, with the octa-sulfur molecule, S_8. They are designated RI_3*3S_8 which indicates the 1:3 stoichiometry between the two components. The complexes have been known for decades: Auger first described AsI_3*3S_8 and SbI_3*3S_8 in 1908 [18a]. The crystal structures of CHI_3*3S_8 and AsI_3*3S_8 were first examined by Hertel in 1932 [18b] and solved in 1938 by West [18c]. The latter study includes refractive index measurements. CHI_3*3S_8 and SbI_3*3S_8 were further examined by Bjorvatten in 1962/3 [37].

The members of the RI_3*3S_8 group (R= As, CH, Sb) resemble each other fairly closely. They crystallise in the same space group (R3m) with three RI_3*3S_8 units in the hexagonal unit cell which has very similar cell dimensions across the series (Table Two). The crystal morphologies manifested by each compound differ only slightly. Views of the hexagonal unit cell looking down the trigonal (c/z) and b axes are shown in Figure Three. An important and unusual feature of this structure is that the C_{3v} point symmetry of the RI_3 molecule is preserved in this crystal lattice. This is an attractive condition from the NLO point of view since it means all tensor components of microscopic nonlinearity (hyperpolarisabilities) are fully projected on to the macroscopic crystal frame[14].

Table Two

	a & b	c	Volume
CHI_3*3S_8 [37a]	24.32	4.440	2274.3 $Å^3$
AsI_3*3S_8	24.739	4.412	2338.5 $Å^3$
SbI_3*3S_8 [37b]	24.817	4.428	2361.8 $Å^3$

Bond distances and angles are given in Chapter Three. The X-ray structure of AsI_3*3S_8 was done in the course of this work. See Appendix One.

---

[14]   This condition simplifies the extrapolation of a molecular NLO-tensor from a crystal-susceptibility tensor and vice versa.
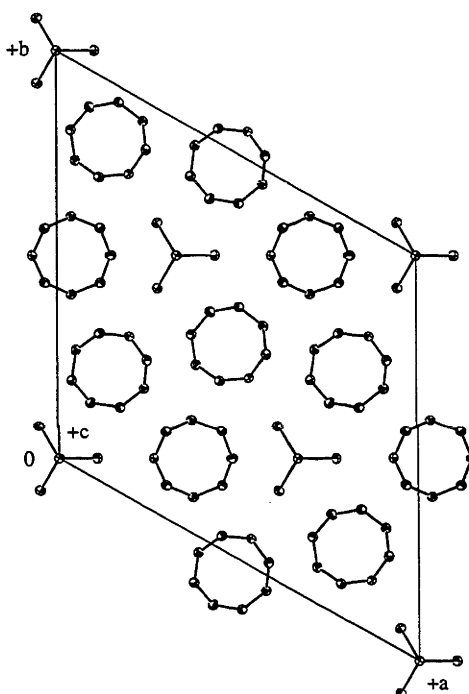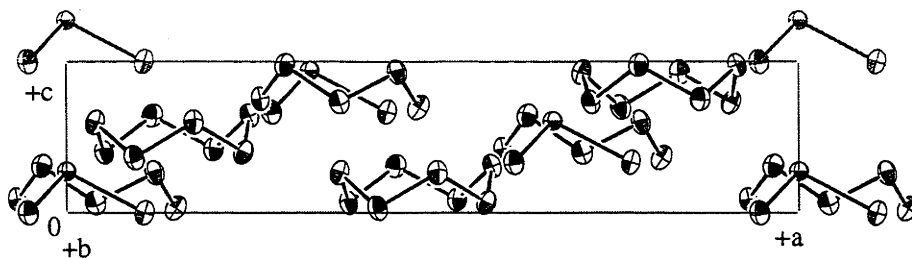
Figure Three: Unit Cell diagrams for the $RI_3 \cdot 3S_8$ crystal structure. The top image regards the cell from along the b axis. The coloured atoms are iodine atoms. The lower picture is a view looking down the crystal c axis.

S---I distances in the complexes are seen to be shorter than the sum of the iodine and sulfur atomic radii (respectively; 1.85Å & 2.15Å). The sulfur-iodine distance is: 3.50Å in $CHI_3 \cdot 3S_8$, 3.571Å in $AsI_3 \cdot 3S_8$, and 3.602Å in $SbI_3 \cdot 3S_8$ all of which are considerably ($\approx$11%) shorter than the 4.0Å "non-interacting" separation thus providing strong evidence for a weak intermolecular CT "bond". As well as this S---I bond shortening, the R---I bond is seen to become longer

when RI_3 is incorporated in the adduct. This effect is small in these complexes. A slight warping of the S_8 ring is also observed with the donor sulfur atom 'pulled away' from the rest of the ring. This is discussed further in Chapter Five.

Crystals of each of these materials form with ease from CS_2 solution at room temperature. They are not particularly robust, however, with each exhibiting low decomposition temperatures of between 100 and 120°C. Accordingly, optical damage thresholds are also low. It was suggested [26] that the antimony adduct may be more thermodynamically stable than the other RI_3*3S_8 though the assertion has never been tested. The PI_3*3S_8 member of the series has been reported [18]. Attempts made during this study to synthesise crystals of this compound were, however, unsuccessful.

The optical properties of the crystals belonging to the RI_3*3S_8 series are also very closely matched. Crystals are uniaxial negative with the unique (n_e or n_3) axis of the indicatrix parallel to the crystal z (and molecular threefold) axis. They all have rather high refractive indices and show large bi-refringences. Important differences do however exist in the absorption behaviour of each compound. This information is summarised in Table Three.

Table Three

	Absorption Edge*	n_o (633nm)	n_e (633nm)	Colour
CHI_3*3S_8	451nm	2.235	1.789	pale yellow
AsI_3*3S_8	504nm	2.283	1.853	orange yellow
SbI_3*3S_8	476nm	2.281	1.901	deep yellow

*   as determined in this work by diffuse reflectance spectra (see Appendix Two). The absorption edge is taken as the wavelength of half-height of absorption onset. Such spectra are unsatisfactory for examination of the presence of absorption bands due to the CT bond -as Löhr [19a] also found. This is due to the strength of absorption in the blue/UV.
         The sources for refractive indices of these compounds are given in Chapter Two.

As indicated earlier, these can be described as mixed 'dipolar-octupolar' materials. The dipole moment of the RI_3 molecule lies parallel to the trigonal crystal z axis. The octupole moment tensor for molecules of this (C_{3v}) symmetry has a major component lying in the plane of the three iodine atoms (which is therefore in the crystal x-y plane).

*2 . THE CHARGE-TRANSFER INTERACTION IN RI$_3$*3S$_8$*

X-ray structural evidence supports the existence of moderately strong charge-transfer interactions between RI$_3$ and S$_8$ molecules, accounting for the formation of a stable crystalline adduct. Other experimental evidence from these and other complexes has also been important in confirming the presence of such an interaction between these compounds - and in determining the donor/acceptor nature of the component molecules:

•   Löhr *etal* [19a], in a nmr solution study of iodomethane complexes with organic ammonium halides, showed that CHI$_3$ was acting as an electron acceptor. This was established from the increase in nuclear shielding seen in the ^{1}H nmr spectra of complexed iodoform as compared to uncomplexed. [13]C nmr showed an unexpected deshielding of carbon nuclear spin however, this is attributed to the dominating effect of the geometry change induced on CHI$_3$ by the complexation. It was also tentatively suggested that certain very low frequency modes seen in the Raman spectra of crystalline samples of these complexes might be due to stretching of the CT bond to the iodine atom of CHI$_3$.

•   Green and Martin [19b] also found evidence for a weak charge-transfer bond between halide donors (from an ammonium salt) and the iodine in CHI$_3$ from the increased proton shielding in the ^{1}H nmr spectrum of complexed iodoform. In the infra-red spectrum, enhancement of the complexed iodoform C--I symmetric stretch absorption at ~400cm^{-1} was attributed to an interaction between the halide donor and the iodine atom.

•   The finding by McCusker and Columba Curran [19c] that trigonal RX$_3$ metal halides (R = As, Sb) manifest significantly larger dipole moments in the solvent dioxane[15], was presented as strong evidence that these molecules coordinate with this solvent molecule, however, the nature of the donor-acceptor interaction was not discussed.

•   As suggested in Table One, in the RI$_3$*3S$_8$ complexes the RI$_3$ molecule acts as an electron acceptor and the octa-sulfur molecule as a donor. Some

---

[15]   For example, μ for SbBr$_3$ is twice as large in dioxane (5.01D) as in CS$_2$ (2.47D). For AsI$_3$, it increases from 0.96D in CS$_2$ to 1.83D in dioxane.

justification for this categorisation is to be found in the structure of the complexes. It is known that divalent sulfur compounds of the type; R-S-R, (such as thioethers) may interact through the sulfur atom with both electron acceptors and electron donors. As pictured in Figure Four, acceptors come toward the sulfur atom perpendicularly with respect to the R-S-R plane as this is a region of higher electron density due to the orientation of the filled 'lone-pair' p-type orbital of sulfur.
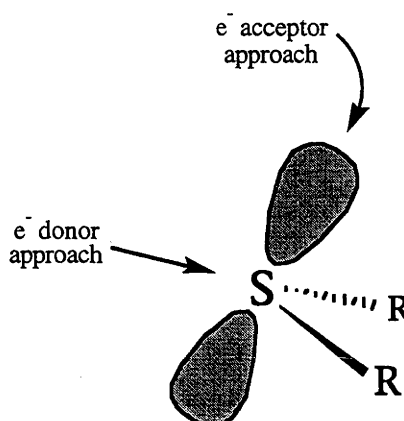
Figure Four

Donors avoid this region and thus approach the S atom in a parallel sense to the R-S-R plane. The crystal structure of these complexes shows that the iodine-sulfur 'bond' forms an angle with the R-S-R plane (where for S_8, R=S) which is closer to 90° than 180°. This is evident if one inspects the unit cell diagram for these complexes looking along the b axis (Figure Three). In $AsI_3 \cdot 3S_8$, for example, it is 71.1°. This indicates that AsI_3 is an acceptor in this interaction. Such an electrostatic argument also explains the co-linearity observed between the CT "bond" and the R-I bond of the RI_3 molecule. Small deviations from a 180° approach may be due to packing energy considerations [13,14].

• Raman spectra measured in this work [Appendix Three] showed that the frequency of the symmetric A_1 R--I stretching mode increases upon complexation. This is indicative of the bond becoming stiffer when it forms the S_8 adduct. The Raman scattering intensities from these experiments suggest that the bond-polarisability-derivative, $\partial \alpha / \partial r$, of this same mode is smaller for the complex. This can be related to a decrease in the R--I 'bond covalency parameter' when the CT complex forms [22].

- Mössbauer experiments [20a&b] on the RI_3*3S_8 adducts and their parent RI_3 compounds have also indicated that the degree of covalent character of the R--I sigma bond increases when the adduct with S_8 is formed.

With such evidence for the existence of a weak charge transfer attraction, it is instructive to now look at some models which explain the findings just described:

Firstly, a representative molecular orbital (MO) picture of the bonding scheme of the RI_3 system is depicted in Figure Five, using AsI_3 as an example.
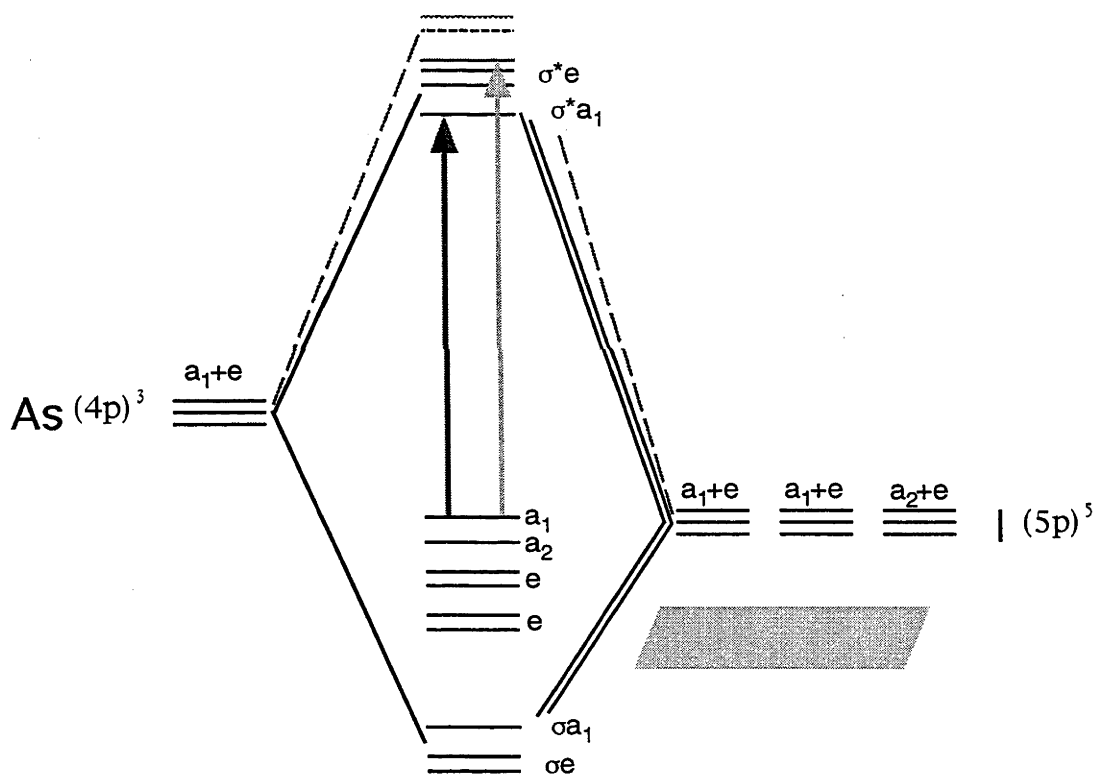
Figure Five: The molecular orbital description of bonding in AsI_3. The HOMO-LUMO gap is shown with the darker arrow. The lighter arrow indicates transitions to states which have been shifted to higher energy. This is a possible explanation for the blue-shift of this transition which occurs in the S_8 complex.

The relative orbital energies and degeneracies for this molecule can be qualitatively deduced or given from ab initio calculations (such as those described in Chapter Three). Semi-empirical 'Xα' calculations carried out for a study by

Grodzicki *et al* [21a] also give the same result. That the *e* states are of lower energy than the *a* states is a consequence of repulsive inter-iodine interactions.

The energy gap corresponding to the lowest spectral transition is from the highest occupied non-bonding "a_1" MO to the lowest energy unoccupied σ^* anti-bonding MOs as indicated by the arrow in the diagram. This is consistent with conclusions reached by Ito *et al* [21b] from their study of CHI_3 spectra in different solvents.

If sulfur lone-pair orbitals lie higher in energy than the bonding σ MOs of AsI_3 (in the energy region indicated by the shaded band in the diagram) the formation of the AsI_3*3S_8 adduct might then be the result of weak σ bonding between I and S, which would then slightly lower the AsI_3 σ orbitals and raise the energy of the corresponding $\sigma*$ orbital (shown dashed in Figure Five). This would explain the blue shift seen upon complexation. The resulting lower energy of the bonding orbitals would also mean a stiffer bond and thus account for the observed shift to higher energy of the Raman active 'R-I' vibration.

Alternatively, these phenomena may all be explained using qualitative electrostatic arguments: The observed blue-shift of the absorption spectrum and the Raman spectrum frequency increase which are both seen upon adduct formation are accounted for if the R-I bond is strengthened when extra electron density is received by the iodine atom. In the formalism of Long and Plane [22], the resulting increasing ionicity of the bond is more energy stabilising than the destabilisation from the concomitant reduction in the (Pauling) covalency parameter, 'σ'.

Previous Relevant Studies on Crystal Complexes

1.   NLO MEASUREMENTS ON RI$_3$ ADDUCTS

Several studies of the nonlinear optical properties of certain addition complexes of the nonplanar trihalides have been reported:

Samoc *et al* [23] performed electro-optic (EO) experiments on crystals of CHI_3*3S_8 and $CHI_3*3C_9H_7N$ (the adduct with quinoline -Qn) in order to determine values of the Pockels coefficients, r_{ij}, governing this phenomenon. These are listed in Table Four. These results were tentatively correlated to estimations of second harmonic generation (SHG) efficiency made using the powder technique[16] with $\omega=1064nm$. The bulk NLO properties of CHI_3*3S_8 were compared to those of *m*-nitroaniline which is a well studied organic compound with a fairly high $\chi^{(2)}$ [29]. Apart from being a convenient reference material, this compound represented the traditional, well-studied class of dipolar, conjugated molecules in which a high NLO response stems from intramolecular charge transfer between donor and acceptor functional groups through a polarisable π-electron system. That the iodoform complex appeared to have the (slightly) stronger response supported the idea that this *class* of materials may exhibit significant optical nonlinearities and thus have potential for future device applications.

Subsequent work from the same laboratories reported similar measurements on 1:3 iodoform-quinoline (CHI_3*3Qn) and the related 1:1 iodoform-hexamethylenetetramine CT complexes [24a,b] . These exhibit lower and higher NLO responses, respectively, than that of CHI_3*3S_8. The link between this response and density of CHI_3 molecules in these solid iodoform complexes was made, suggesting that the NLO response is mainly due to this molecule.

The other important conclusion drawn from these studies was that the magnitude of the crystal NLO response in these very similar iodoform-complexes can be greatly changed by altering the donor species with which the CHI_3 adduct is formed. Possible reasons for this were suggested. They included:

*   that an (attractive) electronic interaction between the donor and acceptor molecules might explain the $\chi^{(2)}$ differences. Presumably, bulk NLO susceptibility would scale with strength of this interaction.

---

16   See description of this method in Chapter Two.

- that differing *local field factors* apply at the iodoform molecule due to the different matrix of donor molecules. These factors describe how the field at the molecule is changed from the applied field due to the 'reaction field' set up in the polarisable medium. Permanent local fields will also be present in the adduct lattices and these will also differ between complexes - perhaps explaining the observed NLO response differences.

In further work on these materials [25], Samoc *et al* accurately measured the NLO susceptibilities for the SHG process in the two iodoform complexes CHI_3*3S_8 and CHI_3*3Qn. The $\chi^{(2)}$ coefficients were evaluated from SHG fringes measured using a fringe technique similar to that explained in Chapter Two. They also re-determined electro-optic coefficients for CHI_3*3S_8 and CHI_3*3Qn using two independent experimental methods. Comparison of the EO and SHG susceptibilities confirmed the earlier hypothesis that the origin of the nonlinearity is mostly electronic in that they were found to be similar in magnitude.

By invoking the 'oriented-gas' model[17], these susceptibility elements could be converted to 'effective' hyperpolarisability tensor elements for the molecule as it exists in the crystal. This uses the assumption that local-field factors, f, from the 'Anisotropic Lorentz Approximation' (ALA) apply (these are simply determined from measured refractive indices, n: $f=(n^2+2)/3$ -see Chapter Four for a detailed explanation). These derived *microscopic* NLO response coefficients for both the octa-sulfur and quinoline adducts were seen to be of similar size. For the macroscopic susceptibility elements, however, much greater differences were seen. This was especially so for the in-I_3-plane $\chi_{11}^{(2)}$ elements. This was taken to indicate that there is a large difference in the local field at CHI_3 when the applied field is in the plane of the iodine atoms depending on whether the complexing partner is S_8 or quinoline. It is not possible to directly relate this to specific structural differences although it is consistent with the sizes of ALA-derived f's. This finding also strengthens the idea that CHI_3 is mostly responsible for this NLO response.

Similar studies [26] were performed on another isomorphous complex of this type, SbI_3*3S_8. Thus, the triiodide acceptor part of the complex was now modified with respect to the iodoform-sulfur complex. Qualitative powder SHG measurements were performed as well as quantitative susceptibility

---

[17]   This model presumes for molecular solids that the solid is composed -as the name suggests- of an array of non-interacting individual molecules. Thus no intermolecular forces or fields are taken into consideration, however, this is often reasonable for organic molecular crystals. See, for example, Refs [39&1].

determinations using the Maker fringe technique. Molecular hyperpolarisabilities were extracted as for the CHI_3*3S_8 study using the oriented-gas model and ALA local field factors.

The results of the experiments performed on CHI_3*3S_8, CHI_3*3Qn and SbI_3*3S_8 are summarised in Table Four.

Table Four

	CHI_3*3Qn [25]	CHI_3*3S_8 [25]	SbI_3*3S_8 [26]
d_{11}	8.1	19.1	8.1
d_{31}	2.5*	5.0*	7.5
d_{33}	2.0	2.6	11.3
r_{12}	≈ 1.9	≈ 4.0	

The bulk NLO coefficients are given[18] as "d_{ij}" values which are used in most experimental studies. Second order susceptibility is given by; $\chi_{ijk}^{(2)} = 2d_{ijk}$.

An asterix indicates that these values were extrapolated from electro-optic measurements performed at 633nm and are thus likely to be over-estimates due to the frequency dependence of the d_{ij} coefficients.
Units of coefficients are $10^{-12}mV^{-1}$ (pm/V). d_{33} for *m*-nitroaniline (mNA) is $20 \times 10^{-12}mV^{-1}$.

Comparison of the NLO coefficients for both the SbI_3 and CHI_3 octa-sulfur adducts is especially interesting. It is seen that the relative sizes of these elements are quite different for the two complexes. The coefficient d_{11}, describing NLO response in the plane of the iodine atoms, is the largest component in CHI_3*3S_8. For the SbI_3 complex, however, the dominant element is d_{33} (describing NLO response parallel to the dipole moment) although the d_{11} component is still of significant magnitude.

Topic Detail

Rigorously, for comparing NLO response from the different charge distributions among molecules of different symmetry, it is necessary to compare not the individual tensor elements but the invariants of the NLO tensor which are obtained from its decomposition into irreducible parts as was described earlier. The invariants of beta for SHG in 3m symmetry were shown in that section.

This is however only absolutely necessary for *intra*-tensor element comparisons. The problem here has been set out as a question framed in terms of $\chi_{33}^{(2)}$ and $\chi_{11}^{(2)}$ of

---

[18] The shortened notation which applies when $\omega_1=\omega_2$ is such that for $d_{2\omega;\omega,\omega}$;
$$d_{111} = d_{11} \text{ etc and}$$
$$d_{132} = d_{123} = d_{14}$$
$$d_{131} = d_{113} = d_{15}$$
$$d_{121} = d_{112} = d_{16}$$

For C_{3v} symmetry, three non-zero, independent tensor elements exist: d_{11}, d_{33} and d_{31} (presuming the Kleinman symmetry condition to be valid and using the convention that one of the mirror planes is perpendicular to the *y* axis).

all three complexes which have identical symmetry. It remains relevant to compare the simple, intra-tensor beta element *ratios* between these isomorphous materials. In addition, determination of invariants involves 311 elements. There is an inherently larger uncertainty in these quantities due to their small size and the sometimes different measurement technique involved to obtain them. This uncertainty carries through as larger error limits for the scalar invariants. Though there is a very small dependence of β_{septor} on β_{311}, this element has a large bearing on β_{vector} and so the error in each invariant is also expected to be different. Use of the simple ratio is also conceptually more accessible.

For these reasons, it is preferred to mostly discuss tensor structure differences through the simple ratio of the elements.

A reason for this large difference is not immediately apparent. One suggestion made in the Ref [26] study was based on the fact that SbI_3 has a larger permanent dipole moment than CHI_3. It was proposed that the larger static electric field from such a dipole moment induces a β_{33} component in the easily polarisable octa-sulfur molecule which contributes to SHG polarised in the z direction only, thus augmenting d_{33}. This proposal has not been tested.

These authors also demonstrated an additive relationship between the linear susceptibility of RI_3 and S_8 parent molecular crystals and the $\chi^{(1)}$ of RI_3*3S_8 crystals. This aspect was discussed in the context of the significant difference noted between the $\chi^{(2)}$ structures for the SbI_3 and CHI_3 adducts. The calculation of these quantities involves use of the Clausius-Mossotti relation and thus the same assumptions are made as for assuming relevance of Lorentz local field factors. This indicates that very strong intermolecular interactions are not present.

These results motivated theoretical studies in which microscopic NLO coefficients for the RI_3 molecules were calculated. Karna and Dupuis [27] had performed ab initio calculations to determine polarisabilities and hyperpolarisabilities of iodoform (and other haloform molecules). The predicted hyperpolarisabilities were far from experimentally derived β - though the ratios $\beta_{vector}/\beta_{septor}$ (see Eqs (12)) did concur with those from experiment. The $\beta_{vector}/\beta_{septor}$ ratio for SbI_3*3S_8 was calculated [26], however, this indicated a large discrepancy between such predicted and measured ratios. This result is discussed in Chapter Five.

Stähelin and Zschokke-Gränacher [28] performed Hyper-Rayleigh Scattering experiments on the iodoform molecule in order to study the octupolar contribution to SHG (β_{11}). Two different solvents were used -one polar and the other nonpolar. A significant difference was observed in the total SH intensity generated from the two solutions: the more efficient SHG being with the polar solvent. Solution values for β_{11} of CHI_3 were extracted using measured

depolarisation ratios in combination with calculated β tensor element ratios given from the work of Karna *et al* [27a]. The solution hyperpolarisabilities also showed a large solvent dependence although reasons for this were not discussed. The solution β_{11} result was compared to that obtained earlier for iodoform in the sulfur adduct to show that this NLO coefficient can be changed readily by surroundings.

Finally, Fünfschilling *et al* made an important point when noting the differences in absolute size of second order NLO response in iodoform complexes [24a]. They raised the possibility that (different) NLO properties of the *donor* molecule may contribute to observed differences in the overall magnitude of $\chi^{(2)}$ elements for the adducts. This issue is important later in the thesis.

As evident from these studies, the NLO susceptibilities of these types of crystalline complexes show quite different anisotropies depending on the inter-related issues of chemical composition and crystal environment. Questions are raised about which factors are important in 'shaping' $\chi^{(2)}$ anisotropy. These are of fundamental and practical interest since they concern the understanding of potentially useful classes of NLO active materials -particularly molecular crystals.

2.   *THEORETICAL STUDIES OF $\chi^{(2)}$ IN MOLECULAR CRYSTALS*

The subject of accurate prediction of $\chi^{(2)}$ and other electric properties of molecular crystals has long been hampered by limitations in the knowledge of the electric fields existing at the microscopic level. The simple and long-used Lorentz approximation mentioned earlier for relating applied field to the 'local' field is known to be inadequate and this has been demonstrated in the work of Munn with respect to more thorough methods [30].

It is essential to know accurately how different the electric fields are in a crystal in order to estimate crystal NLO properties from the molecular hyperpolarisability. Important concepts and aspects of research in this area are now introduced:

*   In dielectric media, a depolarising electric field is set up in 'reaction' to an *applied* electric (optical) field due to bulk polarisation of the medium. This results in a different average field (called the *macroscopic* field) existing within the crystal.

*   On a smaller scale, *local* fields are different again due to the field contributions at a molecule from induced dipoles at/on surrounding polarised molecules.

This phenomenon is ubiquitous and must be accounted for if field-induced effects of the material are being studied.

- As well as these, *permanent* fields exist in molecular crystals due to the presence of the permanent multipole moments of the molecules.

- So-called *'non-local'* effects also exist within molecular crystals. These are effects at a molecule (or between molecules) that arise in response to a field applied at another point (molecule) in the cell. They are also ubiquitous but may be very much smaller than local field effects and can often be ignored.

- Another useful concept in this area is that of *effective* hyper/polarisabilities which refer to the response of a molecule as it exists in its crystal environment.

Both permanent and induced fields may affect NLO response as measured in the bulk via: (i) induced molecular geometry changes and

(ii) through modification of molecular charge distribution and thus of the hyperpolarisability itself.

The large body of work by Munn *etal* has relied on rigorous accounting for electric fields in the crystal at the molecular scale: this has been included in studies of the polarisabilities of certain molecules as they exist in their homomolecular crystals [30,32a-d] and in the examination of the size of their local field factors. The alternative to use of Lorentz local-field factors, f, is use of the local-field-factor *tensor*, d [31]. The method for its determination involves explicit electric field calculation at certain lattice points - these fields arising from induced dipoles on other lattice points. The detailed description of this is found in Refs [33] where the problem of slow convergence of lattice dipole sums is overcome using the 'Ewald method' involving summation over real and reciprocal lattices.

Several organic molecular crystals have been the subject of theoretical $\chi^{(2)}$ determination using computed free-molecule hyperpolarisabilities and crystal structure and refractive indices as source data. Such $\chi^{(2)}$ predictions have been attempted for only a small number of structures. One of the first examples was for *meta*-nitroaniline [34]. The method of these investigations is described in Chapter Four, and further examples are discussed in Chapter Five.

The way in which the shape of the molecule is approximated, and the correct specification of sub-molecular (atomic) positions in the lattice, are very important. This is evident from the development of the sub-molecule treatment [32b&d] and

from studies using the sub-molecule approach, for example Ref [34]. Other interesting theoretical investigations have been made on this topic. For example, it has been noted that the effect of molecular elongation on the local field tensor can be significant in certain length ranges [35]. It was predicted that for a given molecular polarisability, the local field factor decreases rapidly with molecular elongation before reaching a region where d stays effectively constant as molecular length increases.

Munn *et al* [31] have considered effects of permanent-internal-fields on (NLO) susceptibilities of molecular crystals. This issue is of relevance in this study since RI_3 molecules are polar, and a mechanism whereby the vector part of $\chi^{(2)}$ in these crystals is enhanced by this μ, has been proposed [26]. Such fields are part of the general description of the influence of environmental factors on local fields and may be incorporated into this theory [31b]. This effect can be considerable [31b,36a] and is further discussed in Chapter Five where such internal fields are estimated. Also of pertinence is the issue of non-local responses in hetero-molecular crystals [31b] since inter-molecular charge transfer interactions are a means by which such effects can occur. They may therefore be important in the adduct crystals of interest here. In the investigation described in Ref [36b], the non-local effect was a proposed change in the 'effective' polarisabilities of the constituent molecules of two charge transfer complexes occurring because of field induced charge-transfer (FICT) between the molecules. The authors of [36b] were interested in determining the extent of the polarisability changes due to FICT in several anthracene CT-complexes. In practise, however, the problem was complicated by other factors. The theoretical basis for predicting the size of a non-local response [36c] has yet to be successfully tested on a real system.

It is apparent that linear and nonlinear responses of molecules in molecular crystals are considerably more complicated than for the case of the isolated molecule. The RI_3*3S_8 system is a particularly useful system in this regard because of its especially tractable structure.

Explaining the Anisotropy Question

The anisotropies of the second-order NLO susceptibility tensor, $\chi^{(2)}$, for both the CHI_3*3S_8 and SbI_3*3S_8 adducts are notably different as has been described in the previous section. This thesis examines these differences further and aims to provide an explanation for them.

1.   HYPOTHESES

Four hypotheses can be put forward to explain $\chi^{(2)}$ tensor anisotropy differences between CHI_3*3S_8 and SbI_3*3S_8:

HYPOTHESIS ONE: β ANISOTROPY DIFFERENCES

This proposes that $\chi^{(2)}$ anisotropy differences are *entirely* due to the inherent hyperpolarisability differences between the various RI_3 molecules.

Evidence from previous NLO studies [24,25] indicates that the major source of nonlinear optical response in these adducts is at the RI_3 molecule. The chemical nature[19] and polarisable electron distributions in CHI_3 and SbI_3 vary greatly due to differing molecular geometries and numbers of electrons (and their binding potentials) in the two molecules. Thus it seems plausible to suggest that significant β differences exist between such different molecules and that these might completely dominate the appearance of the $\chi^{(2)}$ tensor.

HYPOTHESIS TWO: LOCAL-FIELD DIFFERENCES

This states that while the RI_3 hyperpolarisabilities are important in their contribution to the overall NLO susceptibility, that due to slightly differing environments offered by each of the isomorphous adduct lattices, the $\chi^{(2)}$ anisotropy is significantly governed by the resultant local field factors -to differing extents for each complex.

The manner in which the macroscopic field is modified depends on the densities and the relative positions of both the octa-sulfur and triiodide molecules in the adduct crystal. Appreciable geometry differences of RI_3 molecules are depicted in Figure Six. Looking at the variant shapes of CHI_3

---

[19]   Consider the very different positions of carbon and antimony on the periodic table.

and SbI_3, the lattices of sulfur molecules in each of the adducts are expected to be different. Accordingly, the anisotropy of the *local-field factors* will be different in these two complexes. This could explain the variation seen in the anisotropies of the $\chi^{(2)}$ tensors for these materials.

Both RI_3 and S_8 are rather polarisable molecules which leads to large local field factors. This may mean that relative differences in local fields between the adduct lattices are also larger. This explanation only considers differing local field factors accounting for fields set up in reaction to applied fields on the crystal. The possible influence of different permanent internal electric fields is discussed in Chapter Five.

HYPOTHESIS THREE: RESONANCE ENHANCEMENT EFFECTS
This suggests that the amount of *resonance enhancement* occurring for the SHG process is different for each $\chi^{(2)}$ tensor element in each $RI_3 \cdot 3S_8$ adduct.

If this occurs, it will do so in addition to the previous two mechanisms which will remain of great importance in determining the anisotropy of $\chi^{(2)}$. This effect may, however, obscure the natural (non-resonant) anisotropy given by the hyperpolarisability and the crystal lattice.

The transition responsible for the absorption edge falling close to the 532 nm Nd:YAG second harmonic (presumably the $n \rightarrow \sigma^*$ transition) is polarisation sensitive (Appendix Two). It is anticipated that $\chi^{(2)}$ tensor elements corresponding to the applied field being in the direction where 1064nm 2-photon absorption is strongest (the ab plane) will be preferentially enhanced. This variation will be not be the same for different RI_3 molecules, and so such a mechanism might contribute to the observed $\chi^{(2)}$ differences. Such differences may be due to different influences of the charge-transfer on the electron density of the complex molecules.

HYPOTHESIS FOUR: CONTRIBUTIONS FROM SULFUR
The final hypothesis invokes the possibility that there may be some second-order NLO response of the octa-sulfur molecule. This could add to the RI_3 NLO response in such a way to give the total measured $\chi^{(2)}$ tensor of the adduct crystal (or at least its anisotropy). This is possible due to the

noncentrosymmetric geometry of S_8 - the undistorted molecule belongs to the D_{4d} point group permitting a non-zero β_{123} element at non-zero frequencies. It is, however distorted in the adduct and this may allow other non-zero elements. This is further discussed in Chapters Three and Five. If important, this mechanism would also occur in addition to the first two considerations (at least).

These explanations are not mutually incompatible and each can be expected to contribute to some degree. Experiments and theoretical estimations aiming to demonstrate which of these factors is dominant in explaining the $\chi^{(2)}$ tensor differences between $CHI_3 \cdot 3S_8$ and $SbI_3 \cdot 3S_8$ have been the major tasks of this project.

2. METHODOLOGY

This thesis aims to establish which of the four explanations described in the previous section contribute to $\chi^{(2)}$ anisotropy differences in the $RI_3 \cdot 3S_8$ series of complexes.

As the first step towards this goal, it was deemed useful to quantify the second-order NLO behaviour of the third isomorphous member of this group of compounds; $AsI_3 \cdot 3S_8$. Examination of the NLO properties of a closely related series of CT complexes (R = CH, As, Sb) will then be possible (an improvement on the situation where only two 'isolated' members were available). Correlations between the observed NLO response and the electronic and geometric structure of the adduct are more likely to become evident. Subsequent analyses apply to all three complexes.

It might be anticipated from the positions of the R atoms on the periodic table (note the difference in metallic character between C and Sb), as well as from inspection of physical properties of each of the various triiodide compounds, that the NLO properties of $AsI_3 \cdot 3S_8$ lie somewhere between those of the other two adducts. Table Five lists some properties of the solid RI_3 compounds and Figure Six shows scale models of the free RI_3 molecules.

32

Table Five

	Absorption Edge	Refractive indices: n_o, n_e*	Band Gap (eV) #	Melting Point	Density (gcm^{-3})
CHI$_3$	473nm	2.11 1.76	~3.65	123°C	4.01
AsI$_3$	566nm	2.59 2.23	2.47	141°C	4.69
SbI$_3$	584nm	2.78 2.36	2.41	170°C	4.85

Quantities in the last three columns for AsI$_3$ and SbI$_3$ come from entries in [*Landölt Börnstein Series III*, Teil 17f, p280-4]. Absorption edges are taken from diffuse reflectance spectra measured in this work [Appendix Two].

* Refractive indices determined at 633nm for CHI$_3$ [26], at 656nm for AsI$_3$ and at 671 nm for SbI$_3$. [both listed in *Landölt Börnstein Series II*, Teil 8, 2-236]

\# For CHI$_3$ this was measured at room temperature [38]. The others were determined at 90K. Melting point and density of CHI$_3$ were taken from the CRC Handbook, ed 70.

It could be expected that differences in the anisotropy of refractive indices of the three adducts could be useful since there is a relationship between n and the linear susceptibility: $n^2 = \chi^{(1)} + 1$. This is not the case, however, as these properties are a convolution of microscopic response (polarisability of constituent molecules) and the macroscopic structure (molecular orientations and local field factors).

Actions which can be taken to resolve the question are:

First: one can inspect and compare computed isolated-molecule RI$_3$ hyperpolarisabilities which give an idea of the absolute size and anisotropy of the molecular NLO response. If the isolated RI$_3$ hyperpolarisabilities were to vary only slightly across the series, Hypothesis One is unlikely to be the reason behind the large $\chi^{(2)}$ differences in these complexes.

If there are significant differences in the β tensors of these molecules, Hypothesis One may be valid and the operation of other factors must be shown separately.

Secondly: examination of the free-molecule β anisotropy with respect to the observed crystal $\chi^{(2)}$ anisotropy is instructive. Differences necessarily exist between β and $\chi^{(2)}$ anisotropies due to the local field issues discussed earlier, *i.e.*, reaction and permanent local electric fields in condensed media may anisotropically modify an applied electric field at a molecule in a non-cubic, polarisable lattice. This is in addition to field-induced effects which may occur and

change geometry and hyperpolarisability[20]. If the difference between the microscopic and macroscopic NLO coefficient anisotropies are very similar for each RI_3 / RI_3*3S_8 pair, this would suggest that the second explanation invoking very different local field factors within the different adduct crystals is *not* appropriate.

The **Third** part of this methodology is centred around the hypothetical process of placing an isolated molecule of known hyperpolarisability in a molecular crystal lattice and the NLO susceptibility of this crystal being predicted. Various models of the 'NLO-phore' in the crystal lattice can be used to try to best account for the local fields. One may then compare these 'constructed' NLO susceptibilities with measured $\chi^{(2)}$ values. By doing this, it is possible to gauge the importance of the first two explanations, *i.e.*, to what extent inherent RI_3 β differences and different local field factors account for the $\chi^{(2)}$ differences *together*. If a good agreement can be achieved using a particular model, this would indicate that the First and Second Hypotheses *in combination* are of principal importance in explaining the observed $\chi^{(2)}$ anisotropy phenomenon.

The extent of the match in absolute size and anisotropy between measured and predicted nonlinear susceptibilities of these adduct crystals will depend on the local field model used in the construction of $\chi^{(2)}$. The agreement of $\chi^{(2)}$ from particular models with the experimental $\chi^{(2)}$ is also informative suggesting which local field model for these adducts is appropriate.

Four: The above method of second-order susceptibility construction from RI_3 hyperpolarisabilities can be extended so that the microscopic NLO response of the S_8 molecule is incorporated. This addresses Hypothesis Four in that if these RI_3*3S_8 NLO susceptibilities are in better agreement with measured $\chi^{(2)}$ than for when S_8 hyperpolarisability is not considered, this would indicate that different contributions to $\chi^{(2)}$ from S_8 hyperpolarisability do modify in some way the $\chi^{(2)}$ anisotropies of the complexes.

Five: Information regarding resonance enhancement for Hypothesis Three requires data on the differing electronic resonances for different field directions for the different adducts. One is specifically interested in the absorption at 532nm and 1064nm of the octa-sulfur adduct crystals both parallel (direction 3) and

---

[20]   These direct-field effects (geometry and polarisability changes) may in turn change the way in which the applied electric field is modified at the molecule site. Thus the local-field subject is quite complicated.

perpendicular (direction 1) to the uniaxial axis. From the difference in absorbance in the 1 and 3 crystal directions, it can be inferred if $\chi_{11}^{(2)}$ or $\chi_{33}^{(2)}$ should experience the largest enhancement. This can be done for each complex to indicate how much correction should be applied to the constructed $\chi^{(2)}$ elements for each RI_3*3S_8.

Six: Inspection of the local-field-factor tensors which are calculated in the course of constructing $\chi^{(2)}$ elements is also informative. These measure the extent of the applied field enhancement along the two unique adduct crystal directions. Differences in these factors for the each of the adducts can indicate if augmentation of particular elements -which occurs in the process of estimating $\chi^{(2)}$ from β- is different for any of the complexes. This provides evidence about the importance of local-field-factor variation suggested in Hypothesis Two.

3. TECHNIQUES

♦   It is necessary to obtain free-molecule hyperpolarisabilities 'β_g'. The elements of β_g were calculated at an ab initio level using established computational chemistry techniques. These yield β tensor elements for a hypothetical gas-phase molecule in the complete absence of other bonding interactions or any environmental effects. Experimentally, such hyperpolarisabilities might be measured in a gas-phase EFISH experiment - although no directly equivalent experiment exists since this measures only the vector part of the hyperpolarisability at optical frequency and the calculations are performed at zero frequency. It is recognised that absolute values of such computed quantities are not free from error, however, trends should be preserved. The computational techniques employed for calculating molecular hyperpolarisabilities of both RI_3 and S_8 molecules are discussed in Chapter Three. These were Hartree-Fock (SCF) methods run with various basis set sizes and the perturbation Møller-Plesset (MP) method by which electron correlation is taken into account to a certain degree.

It is presumed that although absolute magnitudes of the hyperpolarisabilities are probably underestimated, the error in the relative sizes between computed elements is much smaller.

♦   Measurements of NLO susceptibilities were made using two experimental techniques. One was the method whereby SH intensity generated from a crystal sample is compared with that induced in a reference material of known nonlinearity. The other method was that of measurement of the magnitude of the electro-optic (Pockels) effect in these crystals. This is described in detail in Chapter Two.

♦   The determination of various adduct $\chi^{(2)}$ predictions from isolated RI_3 hyperpolarisabilities is a major aspect of this thesis. A model describing the manner in which the 'NLO-phore' entity exists within the medium is always used in deriving NLO susceptibility values from a free-molecule β tensor. This naturally affects how local fields are accounted for. Several models are available and three are used in this work. Detailed descriptions of the models are provided in Chapter Four. In summary they are:

- Using a continuum model of the dielectric medium -in which the NLO active molecule resides in a spherical cavity- Anisotropic Lorentz Approximation (ALA) local field factors are determined in a simple but approximate manner.

- A more realistic approach is to treat the medium as an assembly of (sub)lattices of polarisable entities. A cell is defined which contains the 'NLO-phore' molecule and 'submolecular' points are chosen appropriately to describe the molecule/s in question. The procedure determines the field using normal electrostatic relations at every specified point in the cell due to each "lattice" of every other type of point -and each of these determinations is done self consistently. The field is averaged over submolecular points to yield the 'Lorentz-Factor-Tensor' (LFT) for the cell. A local-field-factor-*tensor* for the molecule in its specific crystalline lattice can be determined using the LFT and linear susceptibility or polarisability data. This method is more accurate in that local fields are calculated explicitly and one has control over how one specifies the polarisable lattice points (according to chemical intuition for example). To a first approximation, the complex structure is considered to be comprised of $RI_3(S_8)_3$ supermolecules where the S_8 ring was approximated by a single submolecule.

  - Further improvement of this approach is realised by refining the specification of the molecules in the unit cell. Grouping as supermolecules can be problematic when considering unit cells containing more than one type of molecule (as is shown in Chapter Five). The RI_3*3S_8 unit cell is thus specified as distinct RI_3 molecules and S_8 molecules, with submolecules at each atomic position. This results in one (averaged) Lorentz Factor tensor for sulfur molecules and a separate one for the triiodide molecules.

Chapter Four explains the theory and procedure in detail and leads to four sets of coefficients constructed for the RI_3*3S_8 complexes; ($\chi^{(2)}_{ALA}$, $\chi^{(2)}_{SUPER}$, $\chi^{(2)}_{FULL}$ and $\chi^{(2)}_{COMPOSITE}$). The absolute sizes and anisotropies of these predicted coefficients are discussed with respect to the experimental $\chi^{(2)}$ tensors. This comparison follows the third part of the methodology principles outlined above, *i.e.*, a good theory-experiment agreement of $\chi^{(2)}$ anisotropies would indicate that the First *and* Second Hypotheses are of most importance and that the particular model used represents the adduct crystal well. These comparisons occur in Chapter Five.

◆   To address the question of whether an NLO response from the sulfur molecule is contributing to the adduct NLO susceptibility, the crystal lattice is specified as two completely defined (in submolecules) molecular components, as described above. Once the Lorentz-Factor tensor for this full structure is known, it is a relatively straightforward extension to incorporate computed β from both RI_3 and S_8 to predict an adduct bulk susceptibility. Details of $\chi^{(2)}$ calculation using this '*LFT-Composite*' method are given in Chapter Four. Agreement of NLO susceptibilities predicted in this way with measured $\chi^{(2)}$ will suggest the importance of the S_8 NLO response to adduct $\chi^{(2)}$.

Other aspects about the optical nonlinearity of S_8 in these adducts are discussed in Chapter Five. Distorted ring geometries appear to lead to enhanced computed hyperpolarisabilities for the S_8 molecule.

◆   Information about electronic resonances in these materials was obtained from absorption data collected on each complex. Ideally, polarised single crystal absorption spectra should be used and this was done for one adduct. Useful information can still be drawn from 'average' powder reflectance spectra.

4.   A POSSIBLE ALTERNATIVE

The methodology described in this section takes computed hyperpolarisabilities of the isolated RI_3 molecules and uses them in the construction of crystal NLO susceptibility values based on knowledge of the crystal structure and the linear susceptibility of the bulk material. In principle, the reverse operation could also be used to yield information about reasons for $\chi^{(2)}$ anisotropy. If an effective hyperpolarisability can be determined for a complexed RI_3 unit, this could be

compared with β computed for the isolated non-complexed RI_3 molecule. A similar methodology to that just outlined would apply; agreement between these β would indicate that inherent hyperpolarisability and local field factor differences largely explain differing $\chi^{(2)}$ anisotropies.

There are certain problems in taking this approach. Deriving molecular polarisabilities and hyperpolarisabilities from macroscopic NLO measurements on molecular crystals is complicated by the fact that there is no unique way in which to do this. A small crystal NLO response may be due to molecules with large responses aligned within a cell in such a way that their net induced nonlinear oscillations largely cancel. This is especially problematic for a hetero-molecular crystal since it is considerably more difficult to estimate the relative in-crystal polarisabilities (so the local field factor tensors can be properly derived) and hyperpolarisabilities of different molecules present in the unit cell. In homo-molecular crystals, on the other hand, setting α to be the same for each molecule in the unit cell has more justification.

5.   THE CHARGE-TRANSFER INTERACTION

The question of the effect of the Charge Transfer interaction on NLO response exhibited by the crystal is interesting and pertinent. This is because it is very likely that it has an impact on the hyperpolarisability of the 'NLO-phore' molecule/s of the complex.

A charge-transfer interaction can be seen to fall under the category of *non-local* effects. This is considered in Chapter Five although the problem of how much this may affect the bulk NLO susceptibility does not become theoretically tractable. An experiment was undertaken to show directly whether or not large differences exist between the CT 'bond' strength between iodine and sulfur in each of the complexes. A Raman spectroscopic method was employed in which the scattering intensities from the R-I bond stretch were related to bond covalency changes induced by the S_8 complexation. In this way, one could see if S_8 complexation had a similar impact on each RI_3 molecule.
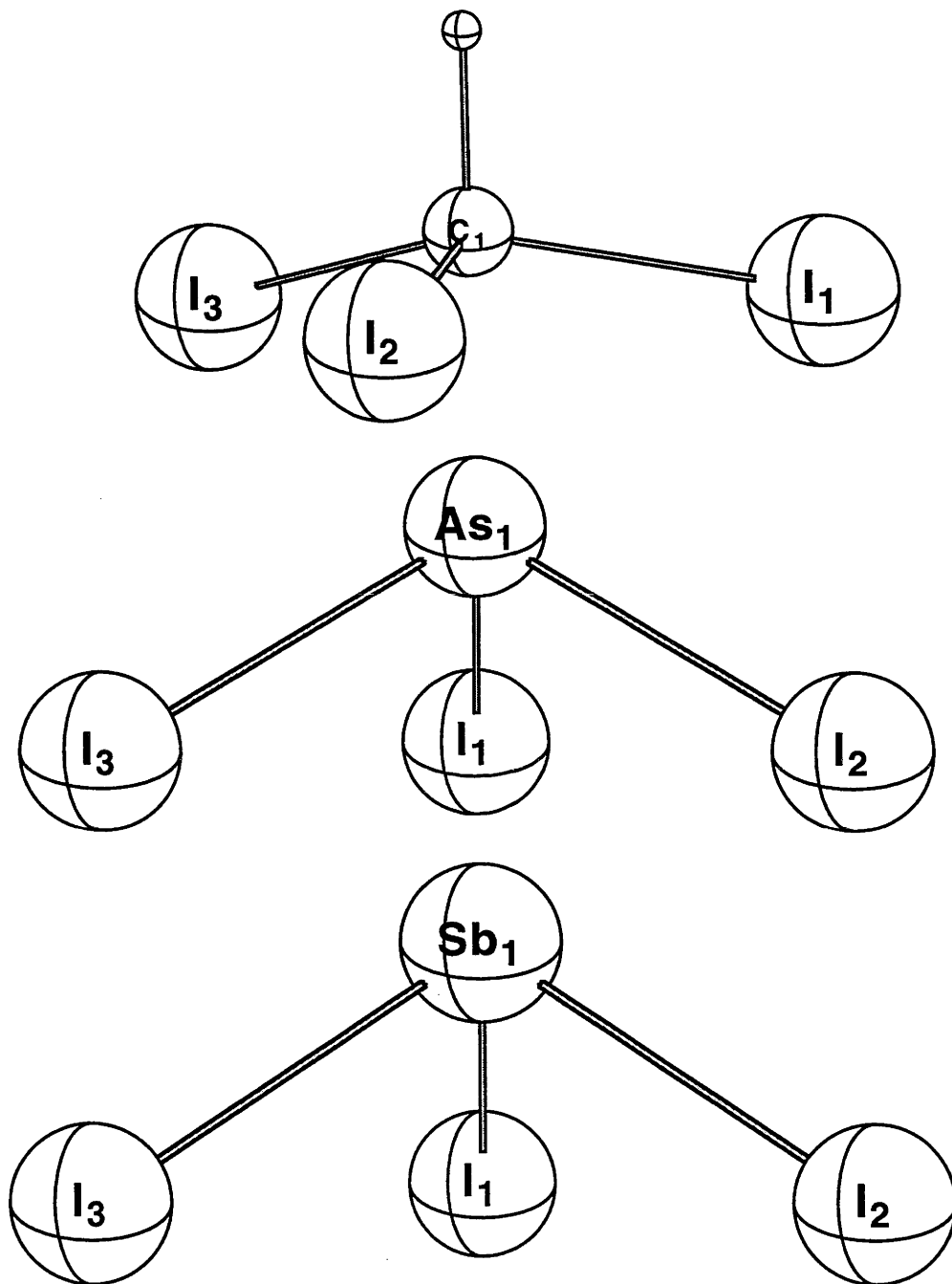
Figure Six: Scale pictures of the RI_3 molecules (gas-phase geometries)   (i) CHI_3 (ii) AsI_3 (iii) SbI_3.

REFERENCES

1.   J. Zyss and D. S. Chemla in; *Nonlinear Optical Properties of Organic Molecules and Crystals.*   eds D.S. Chemla and J. Zyss, (Academic Press, 1987).

2.   P.N. Prasad and D. J. Williams, *Introduction to Nonlinear Optical Effects in Molecules and Polymers.* (J. Wiley and Sons, New York, 1991)

3a.   *Nonlinear optical properties of organic and polymeric materials.* ed D.J. Williams, ACS Symposium Series 233, (American Chemical Society, 1983);

3b.   *Materials for Nonlinear Optics: Chemical perspectives.* eds S. Marder, J. Sohn and J. Stucky, ACS Symposium Series 455, (American Chemical Society, 1991);

3c.   *Nonlinear Optical Properties of Organic Materials III.* SPIE Vol. 1337 (1990);

3d.   *Nonlinear Optics of Organics and Semiconductors.* ed T. Kobayashi, (Springer-Verlag, 1988);

3e.   *Organic Materials for Nonlinear Optics III.* eds G.J. Ashwell and D. Bloor, (Royal Society of Chemistry, 1993)

4a.   C.J.F. Böttcher, *Theory of Electric Polarisation* Vol. 1 (Elsevier, 1973);

4b.   A.D. Buckingham, Molecular quadrupole moments. *Quart.Rev.*, **13**, 183 (1959);

4c.   D.E. Stogryn and A.P. Stogryn, Molecular multipole moments. *Mol.Phys.*, **11**, 371 (1966)

5a.   B.J. Orr and J.F. Ward, Perturbation theory of the non-linear optical polarisation of an isolated system. *Mol.Phys.*, **20**, 513 (1971);

5b.   D. Beratan, Electronic hyperpolarisability and chemical structure. in [3b]

6a.   I. Ledoux, J. Zyss, J.S. Siegel, J. Brienne and J.-M. Lehn, Second-harmonic generation from non-dipolar non-centrosymmetric aromatic charge-transfer molecules. *Chem.Phys.Lett.*, **172**, 440 (1990);

6b.   J.L. Brédas, F. Meyers, B.M. Pierce and J. Zyss, On the second order polarisability of conjugated π-electron molecules with octupolar symmetry: the case of triaminotrinitrobenzene. *J.Am.Chem.Soc.*, **114**, 4928 (1992);

6c.   M. Lequan, C. Branger, J. Simon, T. Thami, E. Chauchard and A. Persoons, First hyperpolarisability of organotin compounds with T_d symmetry. *Adv.Mater.*, **6**, 851 (1994);

6d.   T. Verbiest, K. Clays, A. Persoons, F. Meyers and J.L. Brédas, Determination of the hyperpolarisability of an octupolar molecular ion by hyper-Rayleigh scattering. *Optics Letters*, **18**, 525 (1993)

7.   J. Zyss, and I. Ledoux, Nonlinear Optics in multipolar media: Theory and experiments. *Chem.Rev.*, **94**, 77 (1994)

8.   J. Zyss, Octupolar organic systems in quadratic nonlinear optics: molecules and materials. *Nonlinear Optics,* **1**, 1 (1991)

9a.   M. Joffre, D.Yaron, R.J. Silbey and J. Zyss, Second-order optical nonlinearity in octupolar aromatic systems. *J.Chem.Phys.*, **97**, 5607 (1992);

9b.   J. Zyss, C. Dhenaut, T. Chauvan and I. Ledoux, Quadratic nonlinear susceptibility of octupolar chiral ions. *Chem.Phys.Lett.*, **206**, 409 (1993);

9c.   J. Zyss, Molecular engineering implications of rotational invariance in quadratic nonlinear optics: from dipolar to octupolar molecules and materials. *J.Chem.Phys.*, **98**, 6583 (1993);

9d.   J. Zyss, D.S. Chemla and J.F. Nicoud Demonstration of efficient nonlinear optical crystals with vanishing molecular dipole moment: Second

harmonic generation in 3-methyl-4-nitropyridine-1-oxide. *J.Chem.Phys.*, **74**, 4800 (1981)

10a.　J. Jerphagnon, Invariants of the third rank cartesian tensor: optical nonlinear susceptibilities. *Phys.Rev.B*, **2**, 1091 (1970);

10b.　D.S. Chemla, J.L. Oudar and J. Jerphagnon, Origin of the second-order optical susceptibilities of crystalline substituted benzene. *Phys.Rev.B*, **12**, 4534 (1975);

10c.　J. Jerphagnon, D.S. Chemla and R. Bonneville, The description of the physical properties of condensed matter using irreducible tensors. *Adv.Phys.*, **27**, 609 (1978)

11a.　J.A.R. Coope, R.F. Snider and F.R. McCourt, Irreducible cartesian tensors. *J.Chem.Phys.*, **43**, 2269 (1965);

11b.　H. J. Juretschke, *Crystal Physics* pp, 29-41 (W. A. Benjamin Inc., 1974)

12a.　S.K. Kurtz in F.T. Arecchi and E.O. Schulz-Dubois (Eds), *Laser Handbook*, Vol1, (North Holland; Amsterdam, 1972);

12b.　F.N.H. Robinson, Nonlinear Optical Coefficients. *Bell.Syst.Tech.J.*, **46**, 913 (1967)

13.　R. Foster, *Organic Charge-Transfer Complexes* (Academic Press, 1969)

14a.　R.S. Mulliken and W.B Person, Electron donor-acceptor complexes and charge-transfer spectra. in *Physical Chemistry; an advanced treatise.* ed D. Henderson, **Vol 3** (Academic Press, New York, 1969);

14b.　R.S. Mulliken, Molecular Complexes and their spectra, VI. Some problems and new developments. *Rec.Trav.Chim.Pays Bas*, **75**, 845 (1956)

15a.　S. Tomaru, S. Zembutsu, M. Kawachi and M. Kobayashi, Second harmonic generation in inclusion complexes. *Chem.Comm.*, 1207 (1984);

15b.　K. Wakita, N. Sonoda, T. Shimizu and S. Kaida, Second harmonic generation in binary systems of π-conjugated compounds. in [3c];

15c.　R.V. Vizgert, B.L. Davydov, S.G. Kotovshchikov and M.P. Starodubtseva, Generation of the second harmonic of a neodymium laser in powders of noncentrosymmetric organic compounds. *Sov.J.Quantum Electron.*, **12**, 214 (1982)

16.　W.M. Dehn and R.B. Connor, the action of iodoform on organic bases. *J.Am.Chem.Soc.*, **34**, 1409 (1912)

17a.　Y. Hosoya, S. Muto and Y. Kurokawa, Second harmonic generation of N-(4-nitrophenyl)-L-prolinol-doped alumina film prepared by a sol-gel process. *Thin Solid Films*, **256**, 4 (1995);

17b.　K. Izawa, N. and O. Sugihara, Stable and large second harmonic generation in sol-gel-processed poled silica waveguides doped with organic azo dye. *Jap.J.App.Phys.*, **32** 807 (1993);

17b.　Y. Zhang, P. Prasad and R. Burzynski, Second-order nonlinear optical properties of N-(4-nitrophenyl)-(s)-prolinol-doped sol-gel-processed materials. *Chem.Mat.*, **4**, 851 (1992)

18a.　V. Auger, *Compt.Rend.Acad.Sci.Paris*, 146 478 (1908);

18b.　E. Hertel, Die struktur der Schwefel-Jodidverbindungen, 1. Die Schwefel verbindungen der trijodide. *Z.Physik.Chem.*, **A15**, 51 (1932);

18c.　C. D. West, Sulfur-iodide crystals $PJ_3 \cdot 3S_8$: structure unit and optical properties. *Z.Krist.*, **94**, 459 (1937)

19a.　H.G. Löhr, A. Engel, H.P. Josel, F. Vögtle, W. Schuh and H. Puff, Three-dimensional linkage by electron donor-acceptor interactions: Complexes of organic ammonium halides with triiodomethane. *J.Org.Chem.*, **49**, 1621 (1984);

19b. R.D. Green and J.S. Martin, Anion-molecule complexes in solution. I. Nuclear magnetic resonance and infrared studies of halide ion-trihalomethane association. *J.Am.Chem.Soc.*, **90**, 3659 (1968);

19c. P.A. McCusker and B. Columba-Curran, Electric moments of inorganic halides in dioxane I. *J.Am.Chem.Soc.*, **64**, 614 (1942)

20a. H. Sakai, [129]I Mössbauer effects in the triiodides of group Vb elements and their molecular complexes with sulfur. *J.Sci.Hiroshima Univ.Ser.A*, **36**, 47 (1972);

20b. S. Ogawa, Nuclear quadrupole resonances in arsenic and antimony trihalides and sulfur addition compounds. *J.Phys.Soc.Jap.*, **13**, 618 (1958)

21a. M. Grodzicki, H. Walther and S. Elbel, The electronic structures of the GroupV series ER_3 (E=N→Sb; R=H,Hal). An intercomparison of photoelectron spectra and SCC-Xα calculations. *Z.Naturforsch.*, **39b**, 1319 (1984);

21b. M. Ito, P.C. Huang and E. Kosower, Electronic absorption spectra of iodo-and bromomethanes. *Trans.Farad.Soc.*, **57**, 1662 (1961)

22a. T.V. Long and R.A. Plane, Calculation of absolute Raman intensities of A_1 modes of molecules and ions from a delta-function potential model. *J.Chem.Phys.*, **43**, 457 (1965);

22b. D.A. Long, Intensities in Raman Spectra I. A Bond Polarisability Theory. *Proc.Roy.Soc..*, **A217**, 203 (1953)

23a. A. Samoc, M. Samoc, J. Fünfschilling and I. Zschokke-Gränacher, Nonlinear and electrooptical properties of complexes of iodoform. *Mat.Science* (Wroclaw), **10**, 231 (1984);

23b. A. Samoc, M. Samoc, J. Fünfschilling and I. Zschokke-Gränacher, The linear Pockels effect in crystals of the iodoform-sulfur complex. *Chem.Phys.Lett.*, **114**, 423 (1985);

23c. A. Samoc, M. Samoc, J. Sworakowski, J. Fünfschilling, M. Staehelin and I. Zschokke-Gränacher, Electrooptic effect in crystals of the iodoform-quinoline 1:3 complex. *Mat.Science* (Wroclaw), **13**, 223 (1987)

24a. J. Fünfschilling, M. Ruggiero, M. Staehelin and I. Zschokke-Gränacher, Nonlinear optical properties of iodoform complexes. *Z.Phys.B*, **68**, 305 (1987);

24b. D. Kohler, M. Staehelin, T. Enderle, J. Fünfschilling, and I. Zschokke-Gränacher, Second-order nonlinearities of molecular complexes. *Helv.Phys.Acta*, **62**, 912 (1989)

25. A. Samoc, M. Samoc, D. Kohler, M. Stähelin, J. Fünfschilling and I. Zschokke-Gränacher, Linear and second-order optical properties of the trigonal adducts of triiodomethane with sulfur and quinoline. *Mol.Cryst.Liq.Cryst.Sci.Tech. Section B: Nonlinear Optics*, **2**, 13 (1992)

26. A. Samoc, M. Samoc, P. Prasad and A. Krajewska-Cizio, Second harmonic generation in the crystalline complex antimony triiodide-sulfur. *J.Opt.Soc.Am.B*, **9**, 1819 (1992)

27a. S.P. Karna and M. Dupuis, Frequency-dependent hyperpolarisabilities of haloforms from ab initio SCF calculations. *Chem.Phys.Lett.*, **171**, 201 (1990);

27b. S.P. Karna, M. Dupuis, E. Perrin and P.N. Prasad, Theoretical and experimental studies of optical nonlinearities of haloforms CHX_3, X=F, Cl, Br, I. *J.Chem.Phys.*, **92**, 7418 (1990)

28. M. Staehelin and I. Zschokke-Gränacher, Hyper-Rayleigh scattering: A versatile tool for the characterisation of molecular hyperpolarisabilities. *Nonlinear Optics*, **9**, 241 (1995)

29. J.F. Nicoud and R.J. Twieg in Volume Two of [1]

30. J.H. Meyling, P.J. Bounds and R.W Munn, Breakdown of the anisotropic Lorentz approximation in *p*-terphenyl. *Chem.Phys.Lett.*, **51**, 234 (1977)

31a. M. Hurst and R.W. Munn, Theory of molecular opto-electronics I -macroscopic and microscopic response. *J.Mol.Electron.*, **2**, 35 (1986);
31b. M. Hurst and R.W. Munn, Theory of molecular opto-electronics II -environmental effects on molecular response. *J.Mol.Electron.*, **2**, 43 (1986);
31c. R.W. Munn, Theory of molecular opto-electronics: from the molecule to the crystal. *J.Mol.Electron.*, **4**, 31 (1988);
31d. R.W. Munn, Delocalisation and dimensionality effects on local electric fields in molecular materials. *Synth.Metals*, **64**, 117 (1994);
31e. R.W. Munn, Electric dipole interactions in molecular crystals. *Mol.Phys.*, **64**, 1 (1988)

32a. P.G. Cummins, D.A. Dunmur and R.W. Munn, The effective molecular polarisability and local electric field in molecular crystals. *Chem.Phys.Lett.*, **22**, 519 (1973);
32b. P.J. Bounds and R.W. Munn, Effective molecular polarisabilities in some aromatic hydrocarbon crystals. *Chem.Phys.*, **24**, 343 (1977);
32c. R.W. Munn and S.M. Bourne, The polarisability of iodoform in the crystal. *Chem.Phys.Lett.*, **75**, 403 (1980);
32d. T. Luty, On the effective molecular polarisability in molecular crystals. *Chem.Phys.Lett.*, **44**, 335 (1976)

33a. D.A. Dunmur, The local electric field in anisotropic molecular crystals. *Mol.Phys.*, **23**, 109 (1972);
33b. P.G. Cummins, D.A. Dunmur, R.W. Munn and R.J. Newham, Applications of thhe Ewald Method I -calculation of multipole lattice sums. *Acta Cryst.*, **A32**, 847 (1976)

34. M. Hurst and R.W. Munn, Theory of molecular opto-electronics IV -prediction of $\chi^{(2)}$ for *meta*-nitroaniline. *J.Mol.Electron.*, **2**, 139 (1986)

35. M. Hurst and R.W. Munn, Theory of molecular opto-electronics III -effect of molecular elongation. *J.Mol.Electron.*, **2**, 101 (1986);

36a. D.G. Bounds, A. Hinchliffe, R.W. Munn and R.J. Newham, The dipole moment of HCN in the crystal. *Chem.Phys.Lett.*, **29**, 600 (1974);
36b. R.W. Munn, R.J. Phillips and C.J. Eckhardt, Dielectric theory of weak charge-transfer crystals I -effective polarisabilities. *Chem.Phys.*, **135**, 1 (1989);
36c. R.W. Munn, and T. Luty, Effective and non-local polarisability response in molecular assemblies. *Chem.Phys.*, **81**, 41 (1983)

37a. T. Bjorvatten, Crystal structure of the 1:3 addition compound iodoform-sulfur ($CHI_3 \cdot 3S_8$). *Acta Chem.Scand.*, **16**, 749 (1962);
37b. T. Bjorvatten, O. Hassel and A. Lindheim, Crystal structure of the addition compound $SbI_3 \cdot 3S_8$. *Acta Chem.Scand.*, **17**, 689 (1963)

38. A.Samoc, M. Samoc, J. Sworakowski, I. Koropecky and S. Nespurek, Photoconductivity of crystalline iodoform. *Mol.Cryst.Liq.Cryst.*, **78**, 1 (1981)

39a. J. Zyss and J.L. Oudar, Relations between microscopic and macroscopic lowest-order optical nonlinearities of molecular crystals with one- or two-dimensional units. *Phys.Rev.A*, **26**, 2028 (1982);
39b. J.L. Oudar and J. Zyss, Structural dependence of nonlinear optical properties of methyl-(2,4-dinitrophenyl)-aminopropanoate crystals. *Phys.Rev.A*, **26**, 2016 (1982)

CHAPTER TWO

In Chapter One, the objective of determining second-order NLO susceptibility tensor components in the AsI_3*3S_8 adduct was proposed. The RI_3 part in this complex has physical properties in between those of CHI_3 and SbI_3 and it is anticipated that 'intermediate' NLO properties of AsI_3*3S_8 may assist in explaining why $\chi^{(2)}$ tensor anisotropy is so different in the series of RI_3*3S_8 materials.

This chapter deals with the determination of these coefficients in the arsenic complex. This was accomplished using two methods:
- The first was the technique whereby Second Harmonic intensity generated in a sample of interest is compared to that in a reference crystal. The particular method used is called the Maker Fringe Technique.
- The second method employed measurement of the magnitude of the linear electro-optic effect (Pockels Effect).

The adducts SbI_3*3S_8 and CHI_3*3S_8 have previously been examined using these techniques with fundamental radiation at $\sim 1\mu m$ for the first technique and at 633nm for the electro-optic experiment. It is appropriate, therefore, to study the NLO properties of AsI_3*3S_8 in the same way.

This chapter explains both of these techniques in some detail and describes aspects of the experiments as performed in this work. Results are presented and examined in the context of the hypotheses proposed in Chapter One.

The Maker Fringe Technique

1.   *BACKGROUND*

The Maker Fringe Technique is a method by which bulk nonlinear optical susceptibilities of materials may be determined through measurement of the magnitude of their *harmonic light generation* response. A coherent (laser) light source acts as the exciting field. Second and Third harmonic generation in materials may be studied in this way.

The first such experiment was performed by P.D. Maker and co-workers in 1961 [1a] when they passed a ruby laser beam (@694nm) through a quartz slab and measured the fluctuating intensity of the second harmonic radiation (@347nm) generated as the sample was rotated around an axis perpendicular to the beam propagation direction. The intensity fringes were given Maker's name and it was recognised that there was great potential for this experiment to be used as a method for the accurate determination of nonlinear optical coefficients of suitable solid samples.

Used as a measurement technique, the experiment is nearly always performed in a comparative sense -absolute determinations of nonlinear susceptibilities are very difficult and have been done only for a few materials. With the interest in this study in second-order NLO coefficients, description of the method specifically deals with the measurement of *second* harmonic generation (SHG) from solid samples[1].

The experiment performed in this work is essentially identical to that of Maker and is sketched in Figure One.   A 'fundamental' laser beam is directed through the noncentrosymmetric sample (crystal) of interest.   The intensity of second harmonic light generated after passage through the material is recorded as a function of sample rotation and compared to the intensity generated in a well known second-order NLO substance such as crystalline quartz or KDP (potassium dihydrogenphosphate) measured in identical conditions.

---

[1] Third harmonic generation -including from liquids and gases- is used routinely in third-order hyperpolarisability 'γ' or third-order susceptibility '$\chi^{(3)}$' measurements but is somewhat complicated by the need to account for THG from the sample cell and air [1b].

The technique is appropriate for this study in that it allows quantitative determination of individual tensor components of the nonlinear susceptibility. The accuracy in $\chi^{(2)}$ attainable with this method can be around 5% [2,3] with optimum sample quality. Measurement of different $\chi^{(2)}$ tensor elements is possible due to the control one has over fundamental and SH beam polarisation and over crystal orientation (Figure Three illustrates this). Such determinations are not possible with qualitative powder measurements (which are described on page 61).
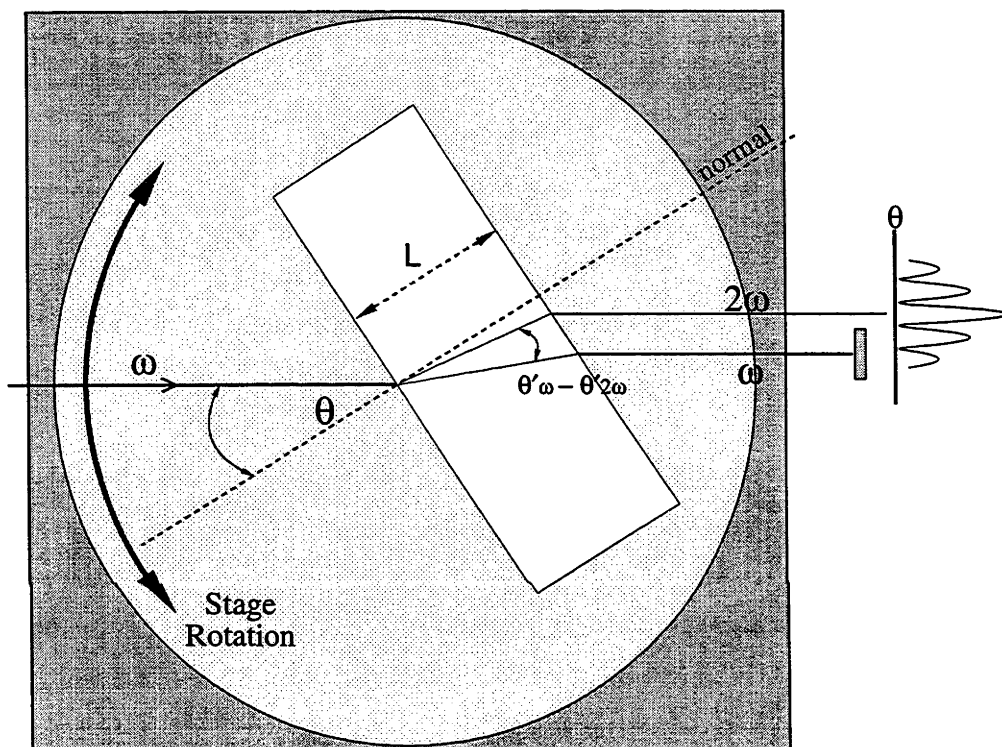
Figure One: Close-up schematic of the Maker Fringe Experiment. Lateral displacement between ω and 2ω (called the 'walkoff') is shown greatly exaggerated. The point where the beam enters the sample coincides with the axis of stage rotation. See text for further explanation.

2. THEORY: Why does Second Harmonic intensity oscillate with sample rotation?

In strong E-M fields, appreciable amounts of second harmonic radiation may be induced from where the fundamental beam (of frequency ω) first impinges upon a noncentrosymmetric medium. The SH light comes from the component of induced electric polarisation which oscillates at 2ω -which is sometimes referred to as the *bound wave* because it is driven by the fundamental wave providing the energy. The 2ω oscillating polarisation therefore remains associated (or bound) with the fundamental throughout its propagation in the nonlinear medium. Hence,

the bound wave travels with a 'phase velocity' c/n_ω as it passes through the material. The induced 2ω polarisation constructively radiates a 2ω light field in the forward direction. This beam is referred to as the *free wave* since it propagates through the medium on its own -experiencing the $n_{2\omega}$ refractive index.

So there are two 2ω polarisation waves now oscillating in the material, each with different phase velocities, c/n_ω and $c/n_{2\omega}$. Due to inherent dispersion in all materials, the indices n_ω and $n_{2\omega}$ will -in general- be different. The condition where $n_\omega \neq n_{2\omega}$ is called the 'non-phase-matched' situation. Starting from an in-phase situation, this means that the phase fronts of these two waves become progressively more out of step until after a certain distance they are completely out of phase. The free wave is then destructively interfering with the SH field being generated by the bound wave at that point and thus goes to zero intensity. Further on, the intensity of the free harmonic wave builds up due to a constructively interfering situation between the bound and free waves. Second harmonic intensity is at a maximum when bound and free waves are again exactly in phase.

Thus, the SH beam leaving the crystal has an intensity determined by where the exit plane of the crystal falls in this cycle. The effective thickness can be continuously changed by rotating the crystal around an axis perpendicular to that of the fundamental laser beam (Figure One). The move through the constructive/destructive interference cycle at the exit face is then seen as the so-called Maker fringes. A 'fringe' pattern of SH intensity is measured as a function of angle of inclination from normal incidence.

An equivalent explanation for the occurrence fringes describes the interacting fields as they propagate through the material. A set of "coupled amplitude equations" arise which describe the progression of the electric field amplitudes of each beam with propagation distance and with respect to each other's change in amplitude. The development of these are outlined here (based in general on a $\omega_1 + \omega_2 = \omega_3$ process -for SHG, $\omega + \omega = 2\omega$) as they are the basis for developing an expression for $I_{2\omega}$ (the second harmonic intensity leaving the sample).

Following Zernike [4], one starts with the wave equation, Eq (1), and considers the derivation for the nonlinear, 2ω frequency only (each frequency must be treated separately). The 2ω electric field vector, E_3, of the free wave and the 2ω electronic polarisation vector, P_3, can act as source terms in:

$$\nabla^2 E = \frac{\varepsilon}{c^2}\frac{\partial^2 E}{\partial t^2} - \frac{4\pi}{c^2}\frac{\partial^2 P}{\partial t^2} \qquad (1)$$

To derive the coupled equations, expressions for each term in Eq (1) are found by using the relation that the nonlinear polarisation generated in the material is given by:

$$P_3 = \chi^{(2)} : E_1\, E_2 \qquad (2)$$

where the third rank $\chi^{(2)}$ tensor is the bulk second-order nonlinear susceptibility of the material and E_1 and E_2 are the electric field amplitudes of the fundamental beam/s.

We now consider only one dimension, z, for the sake of tractability and take each of the electric fields as being of the following form which invokes the 'slowly varying envelope' (SVE) approximation:

$$E_j(z,\,t) = \; E_j(z)\, e^{-i(\omega_j t - k_j z)} + \text{c.c.} \qquad (3)$$

in which $E(z,\,t)$ is considered to be separable into a time-invariant envelope $E_0(z)$ and a wave part described by the exponential term. k_j is the wave vector in the z direction in the material and equals $2\pi/\lambda_j$ where λ_j is the wavelength in the NLO medium.

Using Eq (3) as the appropriate function, the $\dfrac{\partial^2 E_3}{\partial t^2}$ term of Eq (1) is:

$$\frac{\partial^2 E_3(z,\,t)}{\partial t^2} = -\omega_3^2\, E_3(z)\, e^{-i(\omega_3 t - k_3 z)} \qquad (4)$$

In the one dimensional treatment, the $\nabla^2 E$ term of Eq (1) is given by $\dfrac{\partial^2 E_3(z,\,t)}{\partial z^2}$.

Again using the form of Eq (3) for the electric field:

$$\frac{\partial^2 E_3(z,\,t)}{\partial z^2} = \frac{\partial^2 E_3(z)}{\partial z^2}e^{-i(\omega_3 t - k_3 z)} + 2ik_3\frac{\partial E_3(z)}{\partial z}e^{-i(\omega_3 t - k_3 z)} - k_3^2 E_3(z)\, e^{-i(\omega_3 t - k_3 z)}$$

The physical situation in the experiment is such that the field gradient with distance is much larger then the change in this gradient with respect to propagation extent through the sample. This is another expression of the SVE

approximation: $\dfrac{\partial E_{(z)}}{\partial z} >> \dfrac{\partial^2 E_{(z)}}{\partial z^2}$. Thus, the first term of the RHS of this expression can be disregarded, leading to:

$$\frac{\partial^2 E_{3(z,\,t)}}{\partial z^2} = -\left[k_3^2 E_{3(z)} - 2ik_3 \frac{\partial E_{3(z)}}{\partial z} \right] e^{-i\left(\omega_3 t - k_3 z\right)} \tag{5}$$

Finally, substituting (3) into (2), the nonlinear polarisation is:

$$P_3 = 2\chi^{(2)} E_{1(z)}\, E_{2(z)}\; e^{-i\left[(\omega_1 + \omega_2)t - (k_1 + k_2)z\right]}$$

which when differentiated twice with respect to time (as appears in Eq (1)), gives:

$$\frac{\partial^2 P_3}{\partial t^2} = -\left(\omega_1 + \omega_2\right)^2\, 2\chi^{(2)} E_{1(z)}\, E_{2(z)}\; e^{-i\left[(\omega_1 + \omega_2)t - (k_1 + k_2)z\right]} \tag{6}$$

Substituting Expressions (4), (5) and (6) into Eq (1) and rearranging to give an expression for $\dfrac{\partial E_{3(z)}}{\partial z}$ one obtains:

$$2ik_3 \frac{\partial E_{3(z)}}{\partial z} e^{-i\left(\omega_3 t - k_3 z\right)} = -\left(\omega_1 + \omega_2\right)^2 \frac{4\pi}{c^2}\, 2\chi^{(2)} E_{1(z)}\, E_{2(z)}\; e^{-i\left((\omega_1 + \omega_2)t - (k_1 + k_2)z\right)} \tag{7}$$

and after setting $\omega_1 + \omega_2 = \omega_3$ for the sum-frequency process:

$$\frac{\partial E_{3(z)}}{\partial z} = -i\frac{4\pi}{c^2} \frac{\omega_3^2}{k_3}\, \chi^{(2)} E_{1(z)}\, E_{2(z)}\; e^{i(k_1 + k_2 - k_3)z} \tag{8}$$

Analogous coupled amplitude equations may be derived for E_1 and E_2. These describe the electric field amplitude of a particular beam with respect to that of the other beams as they propagate through the NLO medium.

Exact solutions to these equations are complicated to derive. Assume, however, that E_3 remains small, that E_1 and E_2 are equal (as for SHG) and constant (no depletion of pump beams) and that the interaction occurs in a medium of thickness, L. Eq (8) may then be integrated over the distance, L, (the z direction) to give:

$$E_3 = \frac{4\pi\omega_3^2}{k_3 c^2 \Delta k} \; \chi^{(2)} \; E_1^2 \left(e^{i\,\Delta k\,L} - 1 \right) \tag{9}$$

where, for the second harmonic generation process, Δk is the mismatch in phase between the ω and 2ω wavevectors:

$$\Delta k = (k_1 + k_2 - k_3) = (2k_\omega - k_{2\omega})$$

To obtain an expression for the intensity of this radiation, one uses the relation:

$$I = \frac{c\,n}{2\pi} \; E\,E^* \tag{10}$$

and after multiplying E_3 of Eq (9) by its complex conjugate, expressing in trigonometric form and converting angular frequency and wavevectors, one obtains:

$$I_3 \frac{2\pi}{n_3 c} = \left(\frac{-8\pi^2}{n_3 \lambda_3 \Delta k} \right)^2 (\chi^{(2)})^2 \; I_1^2 \left(\frac{2\pi}{n_1 c} \right)^2 \; 4\sin^2(\frac{\Delta k\,L}{2}) \tag{11}$$

Eq (11) can be rearranged and expressed as an equation for the second harmonic intensity, $I_{2\omega}$:

$$I_{2\omega} = G \frac{1}{n_\omega^2 n_{2\omega}} \frac{1}{(\Delta k)^2} (\chi^{(2)})^2 \; I_\omega^2 \; \sin^2(\frac{\Delta k\,L}{2}) \tag{12a}$$

where G is a collected constant term $\dfrac{512\pi^5}{A\lambda_{2\omega}^2 c}$.

Jerphagnon and Kurtz [4] derived a similar expression using a different approach: the appropriate solutions of the wave equation (1) were taken for the $E_{2\omega}$ of both the bound and free waves in the NLO medium. The sum of these was used to determine the SH intensity. Omitting transmission and reflection factors for the moment their result was:

$$I_{2\omega} = G \; \frac{1}{(n_\omega^2 - n_{2\omega}^2)^2} (\chi^{(2)})^2 \; I_\omega^2 \; \sin^2(\frac{\Delta k\,L}{2}) \tag{12b}$$

where G is the collected constant term $\dfrac{128\pi^3}{Ac}$.

Inspection of Eqs (12) shows that for a constant Δk ($\neq 0$) for an experiment, the intensity of the generated SH beam oscillates due to the $\sin^2(const \times L)$ functional dependence it has on sample thickness. From this expression, one can also see that for a given sample thickness, there is a $\left\{\dfrac{\sin(const \times \Delta k)}{\Delta k}\right\}^2$ 'phase-matching' dependence of $I_{2\omega}$ on Δk.

Any technique by which sample thickness, L, of the NLO medium can be changed during an SHG experiment must show that the second harmonic intensity witnessed at the output face is an oscillating function of L. This follows from both of the descriptions just offered.

To illustrate that this is the case for the measured patterns, an example of a Maker Fringe pattern (measured on the setup assembled during this project) is shown in Figure Two in which the sample was a thin plate crystal of potassium hydrogen phthalate[2].

Second Harmonic Intensity (Arb Units)

-40.0   -24.0   -8.00   8.00   24.0   40.0

Stage Rotation (Degrees from Normal Incidence)
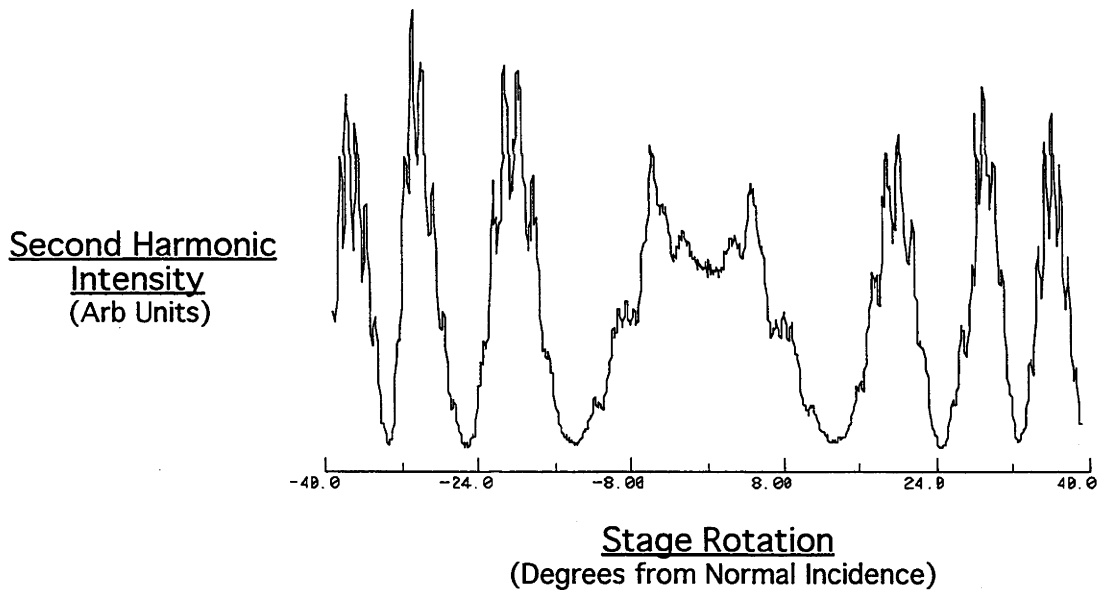
Figure Two: A pattern of second harmonic intensity 'Maker Fringes' generated in a single crystal of potassium hydrogen phthalate (measured in this work). The features evident on the main peaks are extra interference fringes arising from the 'etalon effect' whereby multi-internal reflections interfere inside the plane parallel crystal.

The oscillatory nature of the pattern is clear and a resemblance of this (and other patterns shown later) to a parent $\sin^2(const \times L)$ functional form is evident.

---

2   Crystals of this compound were easily grown from aqueous solution.

The term given to the internal distance between the destructively and constructively interfering conditions is the *coherence length* l_c. This is dependent on the magnitude of the wave-vector mismatch Δk between the ω and 2ω beams -and thus on the difference between n_ω and $n_{2\omega}$. Wave vector mismatch, Δk, is equal to:

$$
\begin{aligned}
\Delta k &= 2k_\omega - k_{2\omega} \\
&= 2n_\omega \frac{\omega}{c} \cos\theta'_\omega - n_{2\omega} \frac{2\omega}{c} \cos\theta'_{2\omega} \\
&= \frac{2\omega}{c}\left[n_\omega \cos\theta'_\omega - n_{2\omega} \cos\theta'_{2\omega} \right] \\
&= \frac{4\pi}{\lambda}\Delta n \qquad \textit{at normal incidence}
\end{aligned}
$$

and since l_c is the distance over which a phase shift of π occurs between the fundamental and second harmonic beams:

$$
\begin{aligned}
l_c \times \Delta k &= \pi \\
l_c &= \frac{\lambda}{4(n_\omega \cos\theta'_\omega - n_{2\omega} \cos\theta'_{2\omega})} \\
l_c &= \frac{\lambda}{4\Delta n} \qquad \textit{at normal incidence}
\end{aligned}
\qquad (13)
$$

Over this distance the power in the SH beam goes from zero to its maximum (or vice versa). Thus, the angle difference between two minima or two maxima of a fringe pattern represents a change in optical pathlength of $2 \times l_c$.

Second Harmonic intensity leaving the crystal is given by Eq (12). This can be expressed in another form invoking the coherence length:

$$
I_{2\omega} = H \frac{1}{n_\omega^2 n_{2\omega}} (\chi^{(2)})^2 \, I_\omega^2 \left(\frac{l_c}{L}\right)^2 \sin^2(\frac{\pi L}{2l_c}) \qquad (14)
$$

This expression is a little more useful since it is more convenient to deal with coherence lengths than phase mismatch. Again, I_ω is the fundamental power, $\chi^{(2)}$ is the bulk second order NLO susceptibility, L is the crystal thickness and H is the factor $\dfrac{1024\pi^3}{\lambda_3^2 c}$. Equations (12) and (14) do not include transmission correction factors to account for reflection losses. These are given in the next section.

The variable in the Maker Fringe experiment is L although in certain experimental arrangements, both L and Δn may be dependent on rotation angle. This means that l_c will change as the sample is rotated leading to a more complex functional dependence. One can see from Eq (14) that given that L is the only variable, the quantities determining the *shape* of the fringe pattern are:

• the dispersion of the material (between the particular ω and 2ω concerned) since this determines the coherence length,

• and the thickness of the sample.

The frequency dependence of l_c is not an issue here as only one fundamental wavelength was used.

3. APPLICATION: *How are fringe patterns used to measure NLO coefficients?*

In this technique, one measures second harmonic fringes from the sample and from a reference material of known NLO susceptibility. The procedure requires that conditions of fundamental beam power, shape, mode structure be identical for both measurements. Therefore reference and sample Maker-fringe pattern collection is performed either concurrently or immediately pre/proceeding the other.

In this case, 2ω power extrapolated to normal incidence ($\theta=0$) in both materials can be compared. From Eq (14) it can be seen that:

$$I_{2\omega} \propto I_{\omega}^2 (\chi^{(2)})^2\, l_c^2 \qquad (15)$$

which is adapted to give:

$$d_{Sample} \Big/ d_{Reference} = \left(\frac{I_{2\omega,Sample}}{I_{2\omega,Reference}} \right)^{\frac{1}{2}} \frac{l_{c,Reference}}{l_{c,Sample}} \frac{\eta_{Sample}}{\eta_{Reference}} \qquad (16)$$

where the NLO susceptibility, $\chi^{(2)}$, is replaced by the alternative coefficient, d, more usually encountered in experimental work. They are related via:

$$d = \frac{1}{2} \times \chi^{(2)}.$$

Correction factors 'η' have been included in Eq (16) to account for reflection losses:

$$\eta(0) = \frac{(n_\omega{'} + 1)^2 (n_{2\omega} + 1)}{n_\omega^2 n_{2\omega}} \quad \text{in which the } \frac{1}{n_\omega^2 n_{2\omega}} \text{ term from}$$

Eq (12) is included but consideration of the multiple reflections[3] is neglected.

All quantities in Eq (16) apply to the case where the fundamental beam is at normal incidence (the experiment is usually setup on the premise that the light is polarised along one crystallographic axis - in most useful experimental geometries, this is only exactly true at normal incidence).

Equation (16) may be used as it stands or rearranged specifically for this experiment to give:

$$d_{Adduct} = \frac{d_{ADP} \times l_{c,ADP}}{l_{c,Adduct}} \left(\frac{I_{2\omega,Adduct}}{I_{2\omega,ADP}} \right)^{\frac{1}{2}} \frac{1 - R_{\omega,ADP}}{1 - R_{\omega,Adduct}} \left(\frac{1 - R_{2\omega,ADP}}{1 - R_{\omega,Adduct}} \right)^{\frac{1}{2}}$$

$$\times \left(\frac{n_{\omega,Adduct}^2 \, n_{2\omega,Adduct}}{n_{\omega,ADP}^2 \, n_{2\omega,ADP}} \right)^{\frac{1}{2}} \quad (17)$$

where ADP refers to the reference material (see later) and sample properties are labelled as "Adduct" for these experiments. This was how Samoc *et al* [8] performed the comparison to get d in their work on $SbI_3{*}3S_8$. Here, η are expressed as standard Fresnel reflection factors:

$$R = [(n-1)/(n+1)]^2.$$

For the determination of d, two quantities need to be evaluated - the *coherence length* as well as the *SH intensity*, both extrapolated to normal incidence.

---

[3] The factor worked out by Jerphagnon and Kurtz applicable to their intensity

expression is:
$$\eta(0) = \frac{(n_\omega + 1)^3 (n_{2\omega} + 1)^3 (n_\omega + n_{2\omega})}{n_{2\omega} R(0)} \quad .$$

This factor [2] is the reciprocal of the combination of Fresnel transmission factors; $T_\omega^4(0)$

$T_{2\omega}(0)$ multiplied by the $\dfrac{1}{(n_\omega + n_{2\omega})^2}$ factor in Eq (12b). $R(0)$ is a multiple reflection

correction factor determined by Jerphagnon and Kurtz [2]

$$R(0) = 1 + \left(\frac{n_{2\omega} - 1}{n_{2\omega} + 1} \right)^2 \left(\frac{n_\omega - 1}{n_\omega + 1} \right)^4 \bigg/ \left(1 - \left(\frac{n_{2\omega} - 1}{n_{2\omega} + 1} \right)^4 \right) \left(1 - \left(\frac{n_\omega - 1}{n_\omega + 1} \right)^8 \right)$$

at normal incidence.

For the value of $I_{2\omega}$, one simply extrapolates the 'envelope' in which the fringes lie to normal incidence and uses this value - being careful that the scale and all other conditions are the same as for the reference measurement. It is possible to fit a theoretical envelope function however this is not usually necessary as values extrapolated by eye are sufficiently accurate.

Obtaining the value for l_c at normal incidence is more involved as it must be sufficiently accurate. It can be taken directly from the fringe pattern[4] or one may measure n_ω & $n_{2\omega}$ (or gauge them from an accurate dispersion formula if this is available) and calculate l_c directly from these indices. These methods however, are not always sufficiently accurate (usually because of errors in the determination of refractive indices of small crystals).

To circumvent this problem, one recalls that it is the dispersion of the material and the thickness of the sample that determine the fringe spacing. The fringe pattern is thus fitted to a function as in Eq (15) by refining values of Δn ($n_{2\omega} - n_\omega$) and the crystal thickness. The relevant Δn values thus yielded (Δn_e or Δn_o) can be used for calculation[5] of l_c at normal incidence.

Experimental geometries in which refractive index is constant with sample rotation are desirable since l_c remains constant during the experiment and fringe fitting requires fewer parameters. Depending on the crystal symmetry, control of crystal orientation and of beam and analyser polarisations may enable these arrangements to be selected. It is also by control of these factors that various tensor elements may be measured. See Figure Three for the relevant experimental geometries for each tensor element.

---

[4] A measure of l_c can be obtained from the fringe pattern by determining the thickness change, Δt, that the angle between the maxima and zero of a fringe represents;

$$l_c = \Delta t = \left(\frac{L}{\cos \theta_1'} - \frac{L}{\cos \theta_2'} \right) 1 \Big/ n$$

where symbols have the same meanings as in Figure One. In the example shown in Figure Three, this is ~15.5µm which is a typical value in such a low-dispersion material.

[5] The situation as described is complicated by crystal-optic factors. Second harmonic intensity is an oscillating function largely because thickness changes with angle of rotation. But coherence length may also change as the sample is rotated because of different refractive index contributions of other crystal axes which become important when beams propagate with greater components along other axes of the crystal (consider changing propagation direction with respect to the indicatrix). This can be seen as a bunching up of the fringes or asymmetry of the fringe pattern around $\theta=0$. There may also be a problem with the (slightly) different ω & 2ω beam paths - called "walkoff". This phenomenon can greatly reduce $I_{2\omega}$ but is generally only a problem for thick samples at large angles of incidence. These effects are expected to be very small in experiments described here, as they are performed in the preferred 'thin crystal' limit.
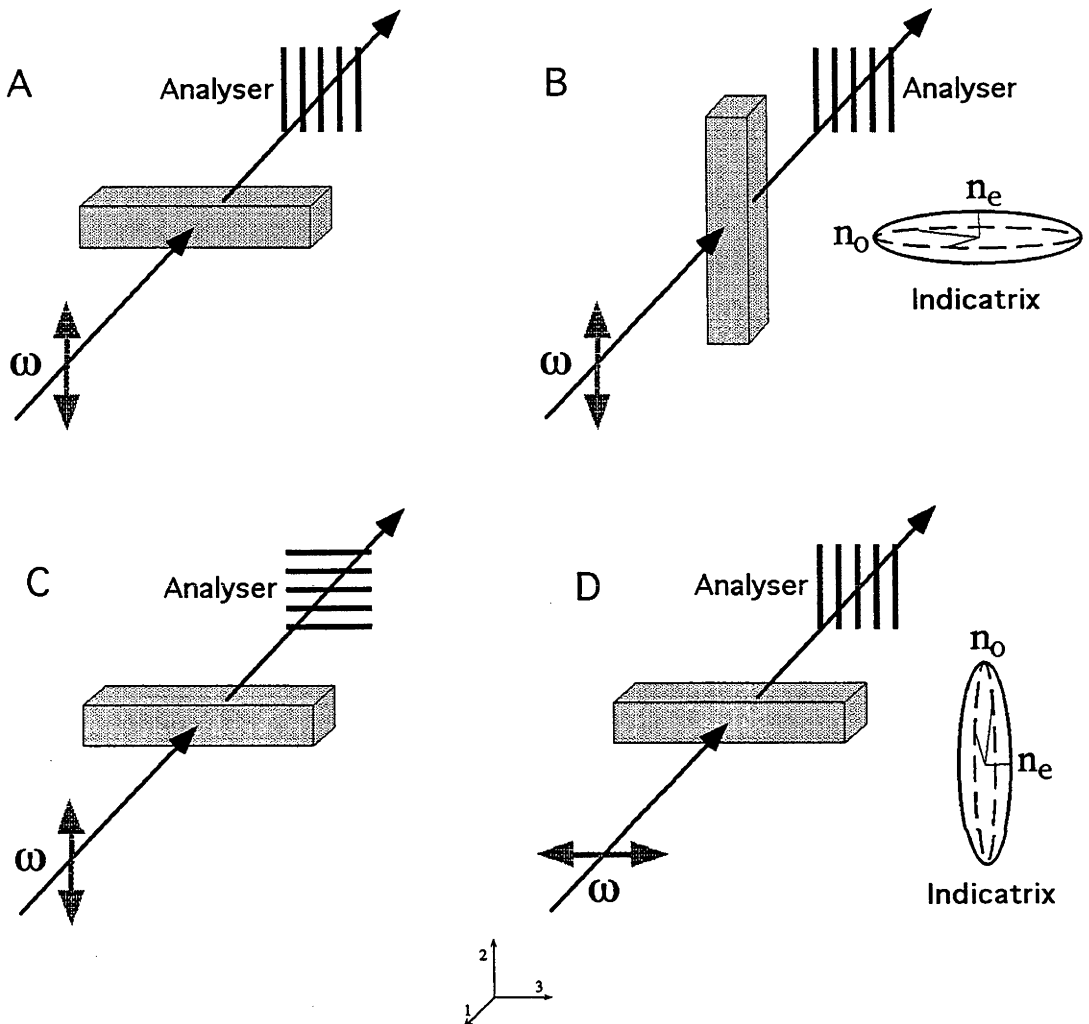
Figure Three: Diagrams illustrating the experimental geometries employed for various tensor element determinations for the uniaxial crystals examined in this study. In all diagrams, the rotation axis is parallel to the length of the page. A: geometry for d_{111}, B: that for d_{333}, C: that for d_{311} (unsuccessful),   D: a non-preferred geometry for d_{311} in that n is not constant with extent of rotation. The coordinate system is shown for the horizontally drawn crystals.

Once an l_c value (or average value from fits of fringe patterns from several samples) is established, this may be used along with I_ω and the reference sample parameters in Eq (16) in order to extract a value for the particular $\chi^{(2)}$ (or d) component which was governing the SHG for the given experimental geometry. Values for the reference parameters needed are taken from reference material measurements made *under identical experimental conditions*.

4 .   EXPERIMENTAL

Reference Crystal Samples

Reference and $RI_3{*}3S_8$ crystal samples needed to be prepared. For a reference material, attempts at making a thin quartz slab of suitable optical quality were abandoned due to polishing difficulties and since it was not possible to determine the exact cut of the particular crystal block.

A large crystal of ammonium dihydrogenphosphate (ADP) was grown from an aqueous solution immersed in a temperature controlled bath which was slowly cooled over a period of some days. For the symmetry of ADP -point group 42m, nonzero elements of the nonlinear susceptibility tensor $\chi^{(2)}$ are: $d_{14}=d_{25}$ and d_{36}. Since 'Kleinman conditions'[6] are closely fulfilled in the conditions for these experiments, all three elements are in fact equal and thus only one coefficient, d_{36}, needs to be measured and quoted. To probe this element in the Maker Fringe experiment, the geometry shown on the left of Figure Four is required.
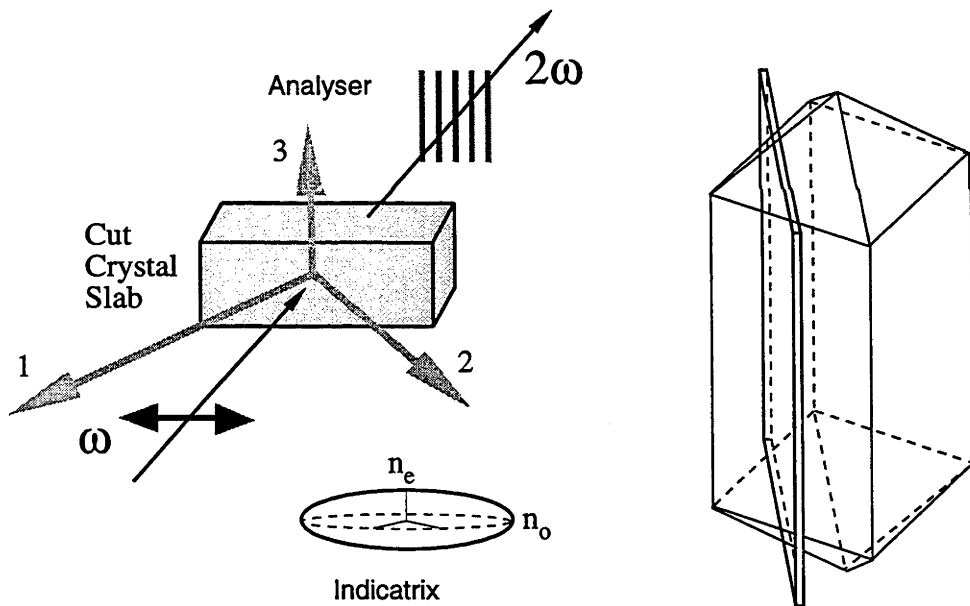
Figure Four: Left: experimental geometry required for fringe pattern measurement in ADP.
Right: the cut taken from a naturally grown ADP crystal.

Unfortunately, tetragonal crystals of ADP develop (010) and (100) faces. Hence it was necessary to cut and polish (110) faces at 45^0 to the natural faces for the

6 These are that there is zero dispersion exhibited by the sample between both fundamental and second harmonic wavelengths. This permits full permutation of tensor indices [4,8].

crystals to be used as SHG references. This is indicated on the right of Figure Four. The crystal cutting was done using a thin diamond saw and the slabs were polished to sub-micron level on both sides by a professional petrographic laboratory. The value of d_{36} for ADP[7] is 0.76pmV^{-1} and the coherence length (calculated from highly accurate dispersion formula [6]) is 10.6μm for ω=1064nm.

Adduct Samples

In order to obtain useful fringe patterns with this technique, samples of the complexes used in the measurements must be crystal specimens: (i) of high internal optical quality, (ii) having faces of high flatness and (iii) possessing highly parallel opposing faces. This is necessary so that wavefront phase is not distorted and that the thickness change with angle can be accurately known. Crystal dimensions needed to be of the order of 1mm (alignment was very difficult if the face area was too small) though the thickness was not of concern. These requirements presented some challenge for finding appropriate crystal growth conditions.

The RI$_3$ and S$_8$ components of the adduct were separately dissolved in CS$_2$, the solutions mixed, filtered and the solvent allowed to slowly evaporate. The CS$_2$ used was first washed with an aqueous solution of Na$_2$S$_2$O$_3$ so that S$_2$O$_3^{2-}$ was available in the crystal growth solution to scavenge I$_2$ formed from any photochemical decomposition of RI$_3$. Large crystals and crystalline aggregates of the adduct readily formed, however, they were mostly of low quality due to the presence of opaque inclusions which rendered the crystal unsuitable. Small crystals grew in a seemingly high quality manner, but in a needlelike fashion and were not suitable because the face areas are too small.

An improvement was made by growing crystals in round-bottom test-tubes placed in a refrigerator (dark and ~4°C). When the solution was close to saturation (distinguished by its dark colour) one or two seed crystals were added. Encouraging growth outward and away from (rather than along) the vessel walls by using a test-tube seemed to enable two opposite faces of high quality to develop more easily. With these conditions, the temperature and evaporation rate for crystal growth yielded several good crystals for Maker-fringe measurements each batch.

---

7 derived from [5] -also listed in Landölt-Börnstein III/11 Sect6.

Equipment

An experimental arrangement suitable for the quantitative measurement of Maker Fringe patterns needed to be specially constructed. The set-up assembled for this study is schematically shown in Figure Five.

The fundamental light source was the 1064nm output of a Quantel Nd^{3+}:YAG laser running at a 10Hz repetition rate and with a pulse width of ~10 ns. Beam profile was periodically checked by the appearance of burn patterns on IR sensitive paper - though for this laser, these were never highly uniform. Beam polarisation was controlled by adjustment of one of the quarter-wave plates mounted just before the exit aperture, inside the laser housing. The degree of polarisation was very high, as determined by passing the beam through a Glan Thomson polariser.

Beam intensity was attenuated by passing it through a series of ND filters. The beam was then preliminarily aligned for appropriate height and levelness with a prism on an adjustable mount.

The rotating stage mechanism was built in-house and consisted of a SlowSyn HS25 Stepper motor (200 steps/rev) coupled to a 30:1 reduction gearbox which then turned a worm/wormwheel mechanism housed within a sturdy aluminium block. The stage surface was fixed to the wormwheel and rotated exactly in the horizontal plane. A vertical holding unit was firmly securable to the floor of the stage such that the centre of the aperture lined up exactly with the rotation axis of the stage. The holder could slide back on the stage to compensate for crystal thickness. After all gearings, the motor-to-stage step size was 3.564×10^{-3} degrees/step.
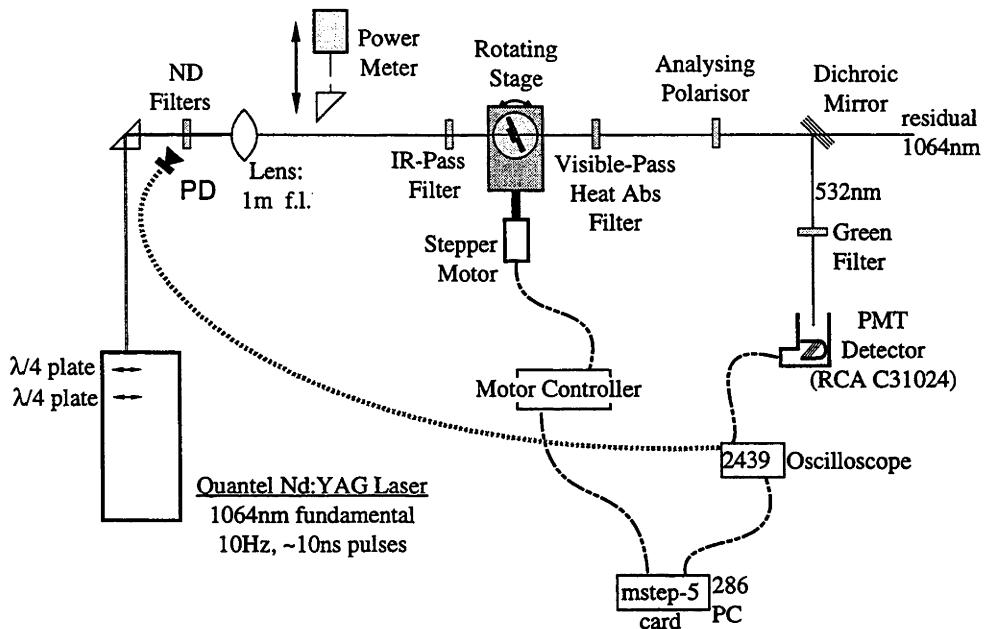
Figure Five: Schematic of the experimental arrangement used for the measurement of Maker Fringe patterns.

The focussing lens (1m focal length) was placed in the beam on an xy adjustable platform and then the stage unit was positioned carefully such that the beam passed through the stage rotation axis. Exact positioning of the beam with respect to this axis was very important or else the beam position on the crystal moves with rotation and thickness change with angle is not precisely known. This was achieved by fine lateral adjustment of the lens position after the stage unit was securely fixed. The arrangement was also such that the beam waist of the lens falls at the rotation axis though this aspect is not as critical as the beam position.

The fundamental laser power was typically 1.2 - 1.5 mW and the spot size was estimated to be 60-90μm in diameter from observing burn patterns on damaged crystals.

An IR pass filter was introduced just before the sample holder to remove the small amounts of green light present in the beam from surface SHG from earlier optical elements. A heat absorbing visible-pass filter was mounted just behind the stage unit. An analysing polariser - which was simply a polaroid sheet in an rotatable collar - was installed behind this. The two elements before the photo-multiplier tube (PMT) were for further filtering. First, a dichroic mirror reflecting 532nm and passing infra-red and finally, a green filter was fixed in front of the PMT housing which was positioned at 90° to the mirror.

The measurement system was a synchronised move-collect-store sequence of actions coordinated by a Metrabyte 'Mstep' card equipped personal-computer running custom software written for this experiment. Bi-directional move commands were sent to the stage motor via a controller unit which converted the ttl signal from the card to a suitable pulse train for moving the motor. Detection of the second harmonic was achieved with a sensitive photomultiplier tube (RCA C31024) operated at 1800V. It was found that the relatively great position-insensitivity of this PMT was most beneficial to the experiment since there are small displacements of the signal beam during stage rotation which for other PMTs resulted in an extra intensity change being recorded as this signal-beam shift occurred.

Signals were processed by a digital storage oscilloscope (Tektronix 2439) and averaged over 128 laser pulses (a photodiode signal from the ND filter reflection acted as both a reference channel for laser power and as the scope trigger). The computer saved reference and signal values from both channels before sending the next move command to the stage.

Procedure

Qualitative SHG powder measurements[8] were performed prior to the more accurate methods to follow. Finely crushed (ungraded) powders between glass slides were positioned in the Nd:YAG fundamental beam. The amount of second harmonic light generated was detected by eye. No difference between the substantial amounts of green light generated from AsI_3*3S_8 and SbI_3*3S_8 could be seen. Both of these complexes showed more SHG than CHI_3*3S_8. This was repeated on different powder samples with the same result.

For the MF experiment, suitable single crystals of the adducts were carefully mounted on microscope cover-slips with an adhesive taking care that none remained between the cover-slip and the clear part of the crystal being examined. This was due to indications that the glue burnt in the laser beam and it also slightly dissolved the crystal surface. The cover-slip was clamped in the holder unit such that the crystal was in the appropriate orientation for the

---

[8] This was developed by Kurtz and Perry [7] as a semi-quantitative method for the rapid assessment of potential second order NLO materials: powdered samples of the substance of interest are placed in an IR fundamental beam and the amount of visible second harmonic light generated is measured. This is compared with that generated from a reference material -usually urea. By using a series of powders graded by size, one can predict if the material is phase-matchable.

particular d_{ij} element being measured. The preferred geometries discussed earlier were employed in these measurements (Figure Three).

The unit was then fixed to the rotating stage and set at approximately normal incidence while the cover-slip was carefully manipulated so that the laser beam passed through a high quality region of the crystal. Due to the generally small area of perfect optical quality on/in the crystal, angle scans were mostly measured in one direction only - thus avoiding interference from crystal edges[9]. Full information is obtainable from such a half pattern. Some full patterns were collected. This improves the confidence in the extrapolated $I_{2\omega}(0)$ slightly.

Scan parameters (step size, step length and shots averaged) were entered and the scan initiated. The computer automatically drove the stage to the starting stage angle and began collecting. The laser was run for some time to ensure output intensity had stabilised.

Analysis

Maker Fringe patterns, once collected, need to be analysed in order to extract the relevant parameters and conduct the comparison with the reference sample to determine the d_{ij} coefficient.

Data was treated using VAX-based software in which patterns were displayed and axes corrections and conversions were performed. It proved easiest to obtain extrapolated SH intensities at normal incidence ($I_{2\omega}(0)$), by selecting the intensity envelope intercept at zero degrees by eye and using a manually controlled cursor to select and record the value.

Coherence length information is contained in the spacing of fringes. One could calculate l_c given sufficiently accurately known values of refractive indices -see Eq (13) and the example shown for potassium hydrogen phthalate in Figure Two. For the case of $RI_3 \cdot 3S_8$ fringes, however, n are not determinable to the accuracy required for reliable l_c calculation.

Thus, for analysis of the patterns to yield l_c values a fitting procedure was employed in which the refractive indices and the dispersion (between 1064nm and 532nm) were variables for the fit. Three main factors affect the shape of the fringe pattern:

---

[9] This practice is also employed in measuring Third-Harmonic fringes from liquid samples [1b], polymer films [*eg* 9a] and in measuring SHG from LB films [*eg* 9b].

- The material *dispersion* between the fundamental and SH indices ($n_{2\omega}-n_{\omega}$). This most strongly influences fringe spacing as one can see by this and the $1/_{(\Delta k 2)}$ factors appearing in Eqs (12).

- The *absolute* value of the refractive indices affects breadth of the fringe peaks since (due to Snell's law), an increased n means a smaller increase of internal angle occurs as external angle is increased. Hence, for a full fringe to be seen, a larger range of external angle needs to be scanned.

- Crystal thickness, *L*, also affects the width of fringe peaks since the optical path-length difference which is represented by a small angle change is given

  by $\quad t = \dfrac{L(\cos\theta_1' - \cos\theta_2')}{n\,\cos\theta_1'\cos\theta_2'}\quad$ so that thicker samples mean that

  there is a greater *t* with rotation and so more coherence lengths are passed-through in the experiment. This is seen as a pattern with more fringes, each of which are narrower than for thin samples.

The latter two effects on the pattern shape are the same and so the pattern can actually be fitted with the dispersion and the absolute refractive index. These were incrementally adjusted from input values. The routine was performed by an existing, custom[10] PC-based fringe fitting program. It fits dispersion first, then absolute index. A single fit is not unique and it was found that there is a relationship between the magnitude of the $n_{2\omega}$ and n_{ω} indices determined by the fitting procedure and the dispersion it yields. Each pattern was fitted several times, each with slightly different input values to give a small range of index-dispersion values.

For each fit, the dispersion value was plotted against its $n_{2\omega}$ value to give reasonable straight line plots. An example of an assembly of these plots is shown in Figure Eight. An average Δn at the actual value of the refractive index was taken which gives a more reliable value for l_c than a single fit would offer. Coherence lengths are simply calculated from the relation: $l_c = \lambda/4\Delta n$ (for normal incidence). The Δn vs $n_{2\omega}$ plots for all the fringe patterns fitted fell close to each other, indicating a good degree of consistency in these determinations of l_c.

---

[10] written by MJS

5.   RESULTS

Numerous crystal samples of both the iodoform and AsI_3 adducts were measured successfully in both the d_{11} and d_{33} geometries. These were analysed in the manner just described. A fringe pattern so measured from a crystal of CHI_3*3S_8 is shown in Figure Six. All attempts, however, at measuring fringe patterns in the d_{31} experimental geometry were in vain for both materials as the SH signal generated was extremely low for the several crystals on which this was tried. It is believed that as well as this coefficient being very small, the coherence length for this geometry[11] is very short. Both these factors prevent a pattern developing above the noise.
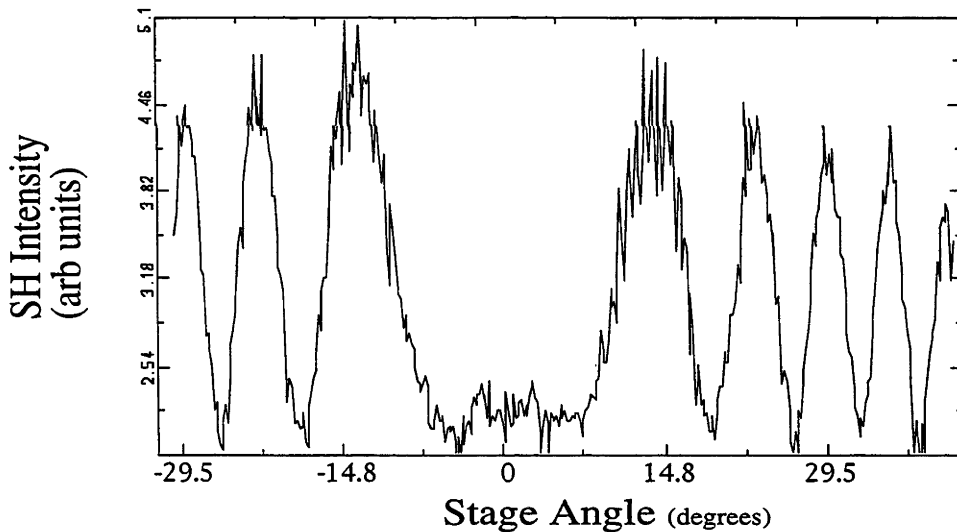
Figure Six: Maker Fringe pattern generated from a 0.43mm thick CH_3*3S_8 crystal. Experimental geometry was such that harmonic generation is governed by the d_{11} susceptibility component.

---

[11] since Δk for d_{31} is given by $|n_{3,2\omega}-n_{1,\omega}|$ which at ≈ 0.3 is fairly large, leading to a predicted l_c of $\approx 0.9\mu m$. This is a consequence of the birefringence being larger than dispersion in these crystals.

Nearly all fringe patterns (both full and half) measured for both components for both substances were able to be fitted in the manner described earlier. The very close match between calculated and measured patterns, after the fitting routine has been applied, is illustrated in Figure Seven with a typical result - in this case with d_{33} fringes from AsI_3*3S_8.
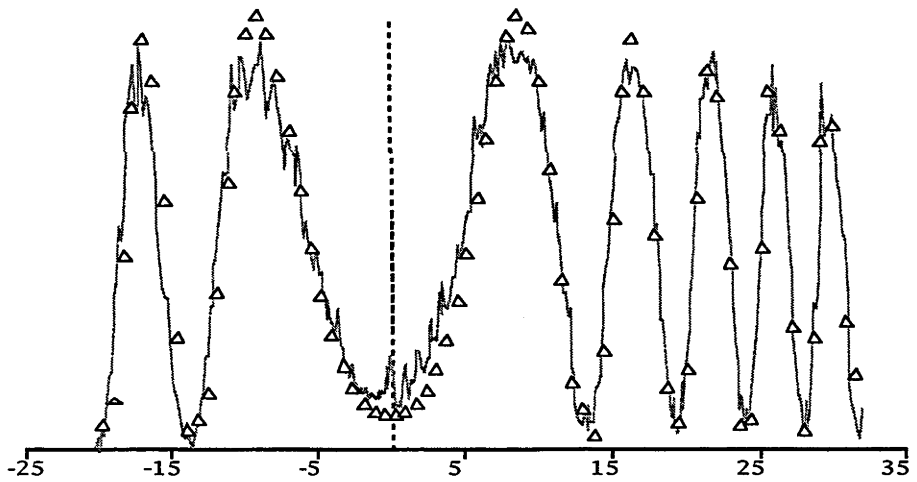
Figure Seven: Maker Fringe pattern generated from a 0.92mm thick AsI_3*3S_8 crystal. Experimental geometry was such that harmonic generation is governed by the d_{33} susceptibility component. The result of the least-square fit is shown with triangles.

An example of Δn versus n_{max} plots obtained from the multiple fits of several d_{33}-AsI$_3$*3S$_8$ fringe patterns is shown in Figure Eight. With knowledge of the actual appropriate refractive index (n_o or n_e for the 2ω beam), dispersion values can be read from the intercept that the actual index makes with the straight line fit. This is evident in the Figure.
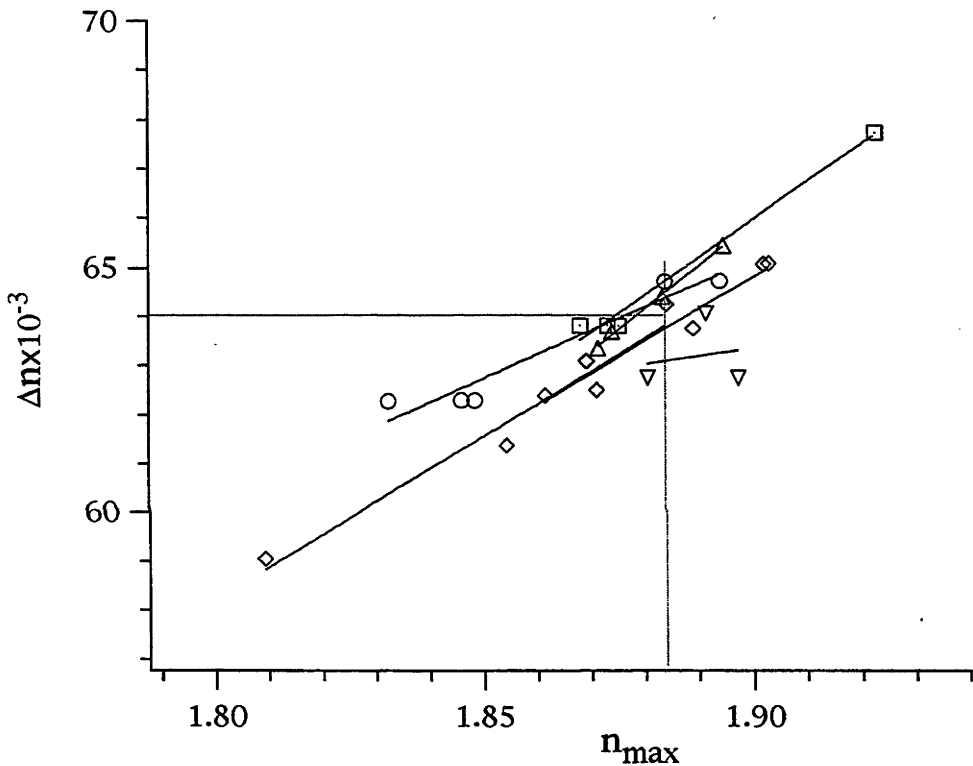
Figure Eight: Plot of fitted dispersion values (Δn) vs fitted $n_{2\omega}$ for d_{33} fringes measured in different AsI$_3$*3S$_8$ crystals as in Figure Seven. Each fringe pattern is represented by one type of point marker.

In this case, $n_{2\omega}$ is known to be ~1.884 for AsI$_3$*3S$_8$. The average of the five dispersion values is 0.064 and this was taken for calculation of $l_c(0)$ [$=^{\lambda}/4\Delta n$].

Other cases were treated identically and Δn values determined for both the d_{33} and d_{22} interaction cases in AsI$_3$*3S$_8$ and in CHI$_3$*3S$_8$ are tabulated in Table One with estimates of the uncertainty in these values.

Table One:

	CHI_3*3S_8 $l_{c,11}$	CHI_3*3S_8 $l_{c,33}$	AsI_3*3S_8 $l_{c,11}$	AsI_3*3S_8 $l_{c,33}$
Δn	0.1186	0.04408	0.12975	0.06455
Δn	0.1196	0.04375	0.13178	0.06380
Δn	0.11785	0.04438	0.13526	0.0644
Δn	0.1179	0.04432	0.13865	0.06342
$<l_c>$	$2.25\pm0.05\mu m$	$6.0\pm0.1\mu m$	$2.0\pm0.1\mu m$	$4.2\pm0.1\mu m$
$\lambda/4\Delta n$	$2.66\mu m$	$8.06\mu m$	$1.96\mu m$	$4.29\mu m$

The average coherence lengths, $<l_c>$, are also shown in the Table and are the values subsequently taken for use in Eq (17) for the d value determination. Coherence lengths predicted directly from measured refractive indices (see Table Two) are also shown in the last row. Error estimates for these coherence length predictions are of the same order as the uncertainty in the refractive index values. This is estimated to be between 2 and 5% - see the next section.

Except for $l_{c,33}$ for CHI_3*3S_8, the agreement between both l_c determinations is reasonable. The poor agreement for CHI_3*3S_8 could be partly due to error in the estimated n_ω. Such errors can arise quite easily from small errors in the Sellmeier formula when making predictions at wavelengths removed from experimental points.

The coherence lengths are seen to be small and of similar magnitude for both materials. They are shorter for AsI_3*3S_8 due to its larger dispersion (along both axes).   These measurements are also consistent with coherence lengths determined for SbI_3*3S_8 (**2.1**μm and **3.6**μm for $l_{c,11}$ and $l_{c,33}$ respectively [10]) which has virtually the same ordinary refractive index but a higher extraordinary refractive index as AsI_3*3S_8.

The dispersion values obtained from fits of fringe patterns measured on several different samples of each complex were quite consistent as can be seen in Figure Eight. Coherence length determination for ADP was very close to the literature value of 10·6μm for these conditions [2].

Extrapolated second harmonic intensity values, $I_{2\omega}$, were unfortunately not so consistent. The principal reason for this is due to differing amounts of scatter from sample to sample as well as between the same crystals run at different times - it was noticed that in both materials, a small amount of surface decomposition occurred after a period of IR laser irradiation. This was enough to reduce perfect optical faces to those which still yielded good fringes, but which received fundamental intensity by a smaller yet unquantifiable amount.

Despite this problem, by measuring half fringe patterns for numerous samples and by using different fundamental beam intensities, it was possible to obtain reliable values for $I_{2\omega}$ from a sufficient number of patterns in each experimental geometry. Since SHG is a second-order NLO phenomenon, it must show a quadratic dependence on fundamental intensity. The $I_{2\omega}$ values from each fringe pattern were thus plotted against the average I_ω reference signal (taken from the PD channel). This was done first for the ADP reference sample (which does not suffer any laser damage). Figure Nine shows the quadratic dependence for SHG on I_ω seen for ADP and for both tensor geometries for $CHI_3 \cdot 3S_8$ and $AsI_3 \cdot 3S_8$.

As would be expected, data points from fringe patterns generated from crystals exhibiting excessive surface scatter are only of *lower* SH intensity than those for good quality samples showing very small amounts of scatter. Additionally, such points did not show a quadratic dependence on I_ω and on these two criteria were rejected. Despite the disappointingly small number of acceptable data points for $I_{2\omega}$ determination (reflecting a major difficulty in performing such measurements in these compounds), a good degree of confidence is associated with those points deemed useful by virtue of the numerous other crystals examined.

The $\dfrac{I_{2\omega,Adduct}}{I_{2\omega,ADP}}$ ratio required in the calculation of d is taken from this plot. The numbers determined for each compound and tensor geometry are tabulated in Table Two along with reflection factors, R, which are also necessary for use in Eq (17).
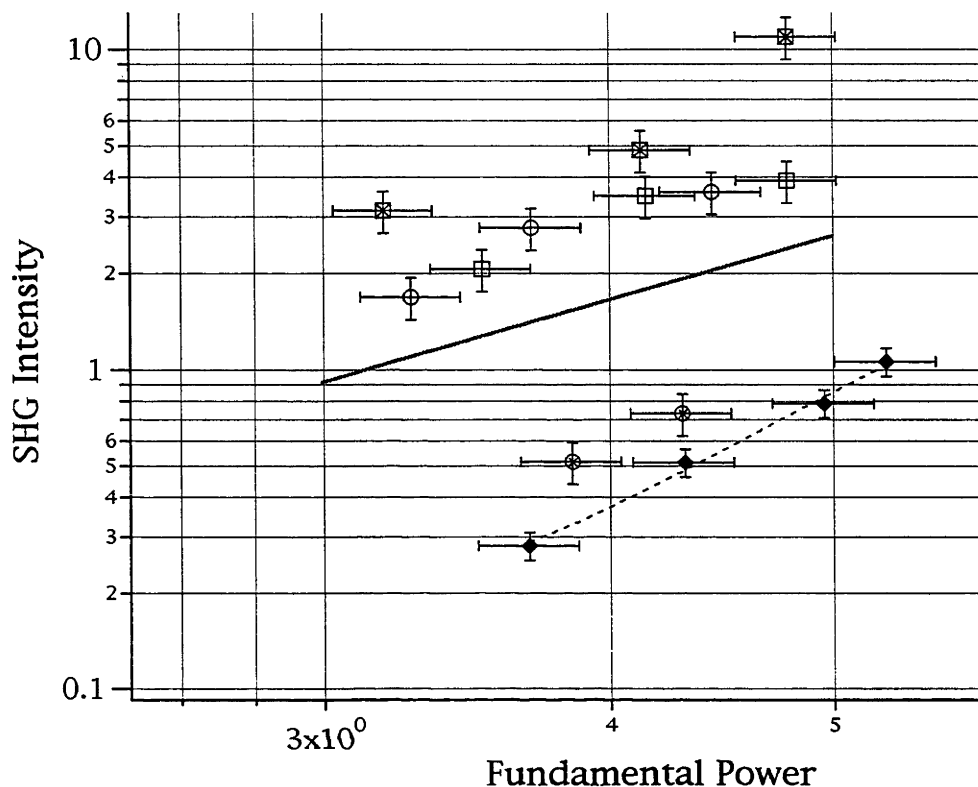
Figure Nine: Second Harmonic Intensity versus Fundamental (1064nm) laser power generated in the different experimental configurations in this work. Both scales are logarithmic in Arbitrary Units. Points rejected on the basis of low SHG and non-quadratic response are not shown on this diagram. The shaded line is the $I_{2\omega} = (I_{\omega})^2$ function.

- ◆   ADP d_{36}.
- ⊠ $AsI_3 \cdot 3S_8$ d_{33},
- ☐ $AsI_3 \cdot 3S_8$ d_{11},
- ⊗ $CHI_3 \cdot 3S_8$ d_{33},
- ○ $CHI_3 \cdot 3S_8$ d_{11}

The error limits indicated in the Figure are: ±15% in $I_{2\omega}$ (±10% for ADP) and ±5% in I_{ω}.

Table Two:

	n_ω	$n_{2\omega}$	R_ω	$R_{2\omega}$	$\dfrac{\text{SAMPLE } I_{2\omega}}{\text{REFERENCE } I_{2\omega}}$
CHI_3*3S_8 for d_{11}	2.1854 (n_o)	2.2855 (n_o)	0.1531	0.1385	8.6, 8.90, 6.87
CHI_3*3S_8 for d_{33}	1.7727 (n_e)	1.8057 (n_e)	0.07766	0.08246	1.51, 1.52
AsI_3*3S_8 for d_{11}	2.209 (n_o)	2.345 (n_o)	0.1419	0.1617	8.2, 8.49, ~5.9
AsI_3*3S_8 for d_{33}	1.820 (n_e)	1.882 (n_e)	0.08455	0.09366	12.08, 15.43, 16.4
SbI_3*3S_8 for d_{11}	2.209 (n_o)	2.332 (n_o)			
SbI_3*3S_8 for d_{33}	1.858 (n_e)	1.931 (n_e)			
$(NH_4)H_2PO_4$	1.50705 (n_o)	1.48189 (n_e)	0.0409	0.0377	

The combined use of the data in Tables One and Two in the comparative formula Equation (17) enabled the following d values to be obtained:

Table Three:

	d pm/V	d pm/V	d pm/V	Lit d
CHI_3*3S_8 d_{11}	20.0	22.2	22.8	19.1 [11]
CHI_3*3S_8 d_{33}	2.3	2.3		2.6
AsI_3*3S_8 d_{11}	21.5	25.1	26.0	-
AsI_3*3S_8 d_{33}	11.6	11.2	9.9	-
SbI_3*3S_8 d_{11}				8.1 [10]
SbI_3*3S_8 d_{33}				11.3
$(NH_4)H_2PO_4$				0.76 [5,6]

It is appropriate at this point to examine the results obtained for these complexes with those of the antimony adduct [10]. It is apparent that AsI_3*3S_8 does have second-order (SHG) NLO properties intermediate to those of the CHI_3 and SbI_3

70

complexes in that the 11 susceptibility component is of similar size to that of CHI_3*3S_8 and the 33 component being the same as that of SbI_3*3S_8.

In that study, a spread in $\dfrac{I_{2\omega, Adduct}}{I_{2\omega, ADP}}$ of about 15% was noted. A similar variance is seen between the few useful such points measured in the experiments reported here.

Of some significance in support of these results is the comparison of susceptibilities measured on CHI_3*3S_8 in these experiments with those measured by Samoc *et al* using the wedge technique and a fundamental of 937nm as reported in [11a]. It can be seen that the agreement is very good. It is expected that the values obtained in that work would have differed slightly due to the different ω employed.

6.   *ERRORS AND UNCERTAINTIES*

Two important correction factors need to be considered along with these measured NLO coefficients. Both corrections are within, but contribute to, a 15-20% accuracy range for this technique:

(i)   The first is that a slightly larger uncertainty exists in the refractive index values for the AsI_3 adduct. The n_e and n_o taken for this complex were determined from a Sellmeier fit of rather old experimental data reported by West [12] and they may carry more uncertainty (particularly for n_ω) than the index values used for CHI_3*3S_8. Due to fairly rapid surface decomposition under laser irradiation, it was not possible to perform accurate refractive index measurements in this study.

A test was made to assess the size of the error. The data of West for CHI_3*3S_8 was fitted to a Sellmeier function exactly as for AsI_3*3S_8. Refractive indices at 532nm and 1064nm were determined from this fit and compared with indices determined from the more recent data of Samoc *et al* [11a]. This showed that n_ω values using West's data were a little smaller by about 1%[12] than those obtained using Samoc's Sellmeier fit and that $n_{2\omega}$ values using West's data were marginally larger than the more recent values.

---

12 This is similar to the uncertainty quoted for the measured refractive indices for SbI_3*3S_8 in Samoc *et al* [10].

If one neglects error in determination of the recent refractive indices and takes them as "correct", there would be a *maximum underestimation* of 2.5% for both d_{11} and d_{33} arsenic adduct susceptibilities which corresponds to upper error limits of ≈ 0.6pm/V in d_{11} and ≈ 0.3 pm/V in d_{33}. For the anisotropy of $\chi^{(2)}$ for this complex, the error introduced with these refractive indices is very small.

(ii)   Absorption of fundamental or second harmonic beams is the other experimental aspect which can affect the measured NLO coefficients. Through the theoretical development by Kurtz and Jerphagnon [3a-c], an expression accounting for the effect of absorption of the fundamental and/or second harmonic has been derived. $I_{2\omega}$ is also proportional to an additional factor not included in Eqs (16) and (17) and this factor may be applied to the determination of d;

$$d_{Corr} \propto e^{(\alpha_\omega + \frac{1}{2}\alpha_{2\omega})\frac{L}{2}}$$

where the α are absorption coefficients in cm^{-1} and L is the thickness of the sample.

Using absorption spectra data reported in Appendix One, it is possible to apply this to the case of d_{11} determination for AsI$_3$*3S$_8$ crystals. Taking $\alpha_\omega = 0$ and $\alpha_{2\omega} \approx 5$ and a crystal of typical thickness of $L = 0.07$cm leads to the correction that this element is $\approx 9\%$ larger than when absorption is not considered. This case is interesting as it is the most absorptive orientation for the most absorptive material yet the predicted underestimation of this element caused by neglect of $\alpha_{2\omega}$ is reassuringly not too large.

In this case, the anisotropy of the d (and $\chi^{(2)}$) tensor is affected. The d_{11} coefficient for AsI$_3$*3S$_8$ listed in Table Three is too small by $\approx 9\%$ yet the d_{33} coefficient is underestimated by only $\approx 2.5\%$. This means that the $\chi_{11}^{(2)}/\chi_{33}^{(2)}$ anisotropy for this complex which is used in Chapter Five is too small by $\approx 3.5\%$. Of course this treatment only takes account of losses of the 2ω signal and not of any *enhancement* of response due to proximity of this resonance. This is discussed in Chapter Five.

Thus, two of the three tensor elements for the bulk second order NLO coefficients have been experimentally determined here for the CHI$_3$*3S$_8$ and AsI$_3$*3S$_8$ charge transfer addition complexes using the Maker Fringe technique. Data on the former adduct was in good agreement with and verifies earlier measurements. The information obtained for AsI$_3$*3S$_8$ is hitherto unreported.

Linear Electro-Optic Effect Measurement

Attempts to determine the size of the NLO susceptibility component, $\chi^{(2)}_{311}$, by measuring second harmonic intensity generated from an appropriately oriented $AsI_3 \cdot 3S_8$ crystal in the Maker Fringe experiment were not successful. An alternative method of 'accessing' this element is through measurements of another second-order NLO phenomenon, the electro-optic or Pockels effect.

1.   EXPLANATION AND THEORY

The Pockels effect is a second-order nonlinear interaction in which a strong *static* electric field, $E_{(0)}$, polarises the medium thereby modifying the optical properties for a probe beam. This optical field may be of low intensity and propagates through a substance experiencing a different dielectric constant. The experimental observable in this method is thus a change in the refractive indices of the material. This may be sensitively measured as a phase change in a beam propagating along appropriate crystal axes and can be done in various ways. The requirement for noncentrosymmetric structures for the manifestation of this effect still holds.

The basis for the explanation of the effect [13a,b] is via description of changes in material optical properties using the index ellipsoid construction or 'indicatrix' for which - n the general case when ellipsoid axes are not coincident with macroscopic axes- the equation is:

$$\frac{x^2}{\varepsilon_{11}} + \frac{y^2}{\varepsilon_{22}} + \frac{z^2}{\varepsilon_{33}} + \frac{2xy}{\varepsilon_{12}} + \frac{2xz}{\varepsilon_{13}} + \frac{2yz}{\varepsilon_{23}} = 1 \tag{18}$$

where x, y and z are the macroscopic cartesian coordinates and $1/\varepsilon_{ij}$ are elements of the dielectric (rank two) tensor of the unperturbed material. The inverse of the ε_{ij} tensor, $[1/\varepsilon_{ij}]$ or $[1/n^2]$ is called the 'impermeability' of the material and is also a second rank tensor. It relates the applied electric field to the dielectric displacement of Maxwell's equations:

$$E_j = D_i \cdot \left[\frac{1}{\varepsilon}\right]_{ij}$$

Upon application of the strong static field, a change is induced in one or more tensor elements of the impermeability. The coefficient relating the size of this change to the inducing field strength is the electro-optic or Pockels coefficient:

$$\Delta\left[\frac{1}{\varepsilon}\right]_{ij} = r_{ijk} \cdot E_k \tag{19}$$

where the indices refer to cartesian axes of the laboratory frame. One can see that definition of this constant in terms of the reciprocal dielectric tensor is convenient in that it facilitates use in the equation for the indicatrix - thus describing the change in optical properties more conceptually.

The Pockels coefficient, r, is a third rank tensor often having certain elements equivalent as determined by the symmetry of the process and of the medium. The uncontracted 3x3x3 tensor has the same structure for each space group as does the second-order nonlinear susceptibility tensor governing second harmonic generation. In the contraction of these tensors however, they differ in that r_{ijk} becomes a 3x6 matrix of r_{ij} elements where i=1-6 and indicates the direction of impermeability change and j is the direction of application of the strong electric field. Conversely, $\chi^{(2)}_{ijk}$ becomes a 6x3 matrix of $\chi^{(2)}_{ijk}$ elements where i =1-3 and indicates the direction of the induced nonlinear polarisation and j =1-6 referring to possible combinations of directions of application of two electric fields. Tabulations of these tensors for the noncentrosymmetric space groups can be found (specifically for r) in Ref [13a] (for example).

The symmetry of the electro-optic medium determine which r are nonvanishing and one can then easily predict which impermeability tensor elements are affected by application of a static field, $E_{(0)}$, in a given direction by using Eq (20). For example, consider the case of a material of 3m symmetry with a strong $E_{(0)}$ applied along the crystal y axis.

$$\Delta\left[\frac{1}{\varepsilon}\right] = \begin{pmatrix} 0 & r_{12} & r_{13} \\ 0 & -r_{12} & r_{13} \\ 0 & 0 & r_{33} \\ 0 & r_{13} & 0 \\ r_{13} & 0 & 0 \\ r_{12} & 0 & 0 \end{pmatrix} \begin{pmatrix} 0 \\ E_2 \\ 0 \end{pmatrix} = \begin{pmatrix} r_{12}E_2 \\ -r_{12}E_2 \\ 0 \\ r_{13}E_2 \\ 0 \\ 0 \end{pmatrix} \tag{20}$$

Substitution of the non-zero impermeability elements on the RHS of Eq (20) into Eq (18) then informs as to which way the indicatrix is changed:

$$x^2\left(\frac{1}{\varepsilon_{11}} + r_{12}E_2\right) + y^2\left(\frac{1}{\varepsilon_{22}} + r_{12}E_2\right) + \frac{z^2}{\varepsilon_{33}} + r_{12}E_2 \; yz = 1$$

indicating that the indicatrix axes lengths are modified along y and x and that rotation of ellipsoid axes has also occurred around the x axis (final term) so that the indicatrix is no longer exactly coincident with crystal axes when the field is applied this way.

Simplifying this expression by rotating coordinates to those of the new indicatrix one has (changing ε_{ij} to relevant refractive indices):

$$x^2\left(\frac{1}{n_o^2} + r_{12}E_2\right) + y^2\left(\frac{1}{n_o^2} - r_{12}E_2 + r_{13}E_2\right) + z^2\left(\frac{1}{n_e^2} - r_{13}E_2\right) = 1$$

from which it is possible to determine expressions for the magnitude of refractive index changes (Δn) for different experimental situations. For example, if the probe beam was propagated along the z axis and polarised parallel to the y axis,

$$\frac{1}{n_y^2} = \left(\frac{1}{n_o^2} - r_{12}E_2 + r_{13}E_2\right)$$

Differentiating n_y with respect to the applied field strength yields:

$$-2n_y^{-3}\,\frac{dn_y}{dE} = -(r_{12} + r_{13})dE_2$$

For small Δn and taking finite differences:

$$\Delta n = -\frac{1}{2}\,n_o^3(r_{12} + r_{13})E_2 \qquad\qquad (21)$$

And so a combination of the r_{12} and r_{13} coefficients would be measured in this particular experiment.

Likewise, expressions can be deduced for other experimental conditions of applied field and optical field directions. One can then see which components of the Pockels coefficient tensor govern the EO effect for each condition, thereby enabling a choice of appropriate experimental arrangement. Preferred geometries are those which involve only the r_{ij} coefficient of interest - unlike in the above example. Of major consideration is which geometries are actually experimentally

achievable.   As shall be seen later, the most favourable geometry may be precluded by some sample or instrumental factor.

In order to measure the size of the coefficient, one could conceivably measure n with the field present and when it is not and calculate the difference, Δn, to use in the appropriate equation. Due to the small differences induced by the static field however, this is not feasible so more sensitive techniques than the classic beam deflection methods are required. Direct determination of Δn by measuring the change of phase in the probe beam when $E_{(0)}$ is applied is ideal and this is how Δn is obtained. The phase shift, $\Delta\Phi$, is related to the difference in refractive index by:

$$\Delta\Phi = \Delta n \; {}^{2\pi L}\!\!\big/\!\!{}_{\lambda} \qquad (22)$$

where L is the optical pathlength (sample thickness at normal incidence) and λ is the wavelength of the optical field (633nm for the HeNe line). Knowing the field strength and refractive indices, r_{ij} is then easily extracted from the appropriate expression such as Eq (21).

There are two main methods for measuring these phase changes accurately [11]. One is an interferometric technique in which a beam passing through the sample is recombined with a pathlength-matched reference beam and a phase change is inferred from shifts in interference fringes upon the recombination of the two beams. This method can be very accurate but is not discussed further here as it was not employed in this work.

The other method is called the 'intensity modulation' technique. This is where the optical or probe field propagates through the birefringent material with components *along two mutually perpendicular directions* , -at least one of which undergoes change in refractive index in its direction when $E_{(0)}$ is applied. These directions are generally selected to be principal axes of the optical indicatrix.

Such a situation is effectively beamsplitting at the front surface and beam recombination at the rear crystal face. With the field off, the two components may experience different indices and thus exhibit a particular 'baseline' phase shift upon recombination. This situation changes when the field is switched on. A new phase shift is observed in the exiting beam which is a superposition of the phase shifts occurring along each axis. The change of the phase shift is manifested as the change of the degree of ellipticity in the exiting polarisation.

This is sensitively measured as an intensity change after passing through an analyser. Figure Ten illustrates this.

In practice, 'dual axis propagation' is simply achieved by polarising the probe beam at 45° to both crystal axes. One then adjusts the baseline polarisation $[E_{(0)} = $ off$]$ condition to circular (or close to circular) which can be done before or after the sample with a $\lambda/4$ plate or by subtle adjustment of the inclination of the crystal sample in the probe beam. With the field off, the intensity passing through the analyser is recorded and denoted I_{DC}. When the field is on, the ellipticity induced in the circularly polarised light results in a small increase or decrease in the signal transmitted through the analyser. This signal is that due to $E_{(0)}$ and is denoted I_F. In this arrangement (where the baseline polarisation is circular) $\Delta\Phi$ is a linear function of the intensity passing through the analyser. $\Delta\Phi$ is then determined from the relation:

$$\sin \Delta\Phi = {I_F}\Big/{I_{DC}} \qquad (23)$$

For $E_{(0)}$ being modulated (*eg* at about 100-1000Hz), I_F is easy to see as the modulation of the transmitted signal. If required, lock-in detection can be used to increase sensitivity for experiments exhibiting very small phase changes.

Finally, the condition of dual axes propagation must be accounted for in the development of the expression for Δn *cf* Eq (21). For example, in the case above for a probe beam propagating along the y axis and polarised at 45° to the x and y axes, the expression for Δn becomes

$$\Delta n = -\tfrac{1}{2}\, n_o^3 \left(r_{12} - \left({n_e}\Big/{n_o} \right)^3 r_{13} \right) E_2 \qquad (24)$$

2.   EXPERIMENTAL ASPECTS

The essential features for the measurement of the strength of this phenomenon with the intensity modulation method are shown schematically in Figure Ten. Of utmost importance is the crystal sample which may have to be cut correctly and also must possess high optical quality (flatness and polish) for the faces through which the optical field propagates.

♦   The optical field was the 632.8nm output beam from a small (4mW) polarised HeNe laser. An actual polarised output is important as the different

polarisations of different modes will lead to unwanted fluctuations during intensity modulation measurements as mode-hops occur. The $E_{(0)}$ field was supplied from a small high-voltage transformer (an automotive coil) driven by an audio-amplifier fed by a WaveTek signal generator through which all control of the field strength and frequency was exercised. The modulation frequency was maintained at ~200Hz and the voltage delivered to the electrodes could be up to 4000V peak-to-peak.
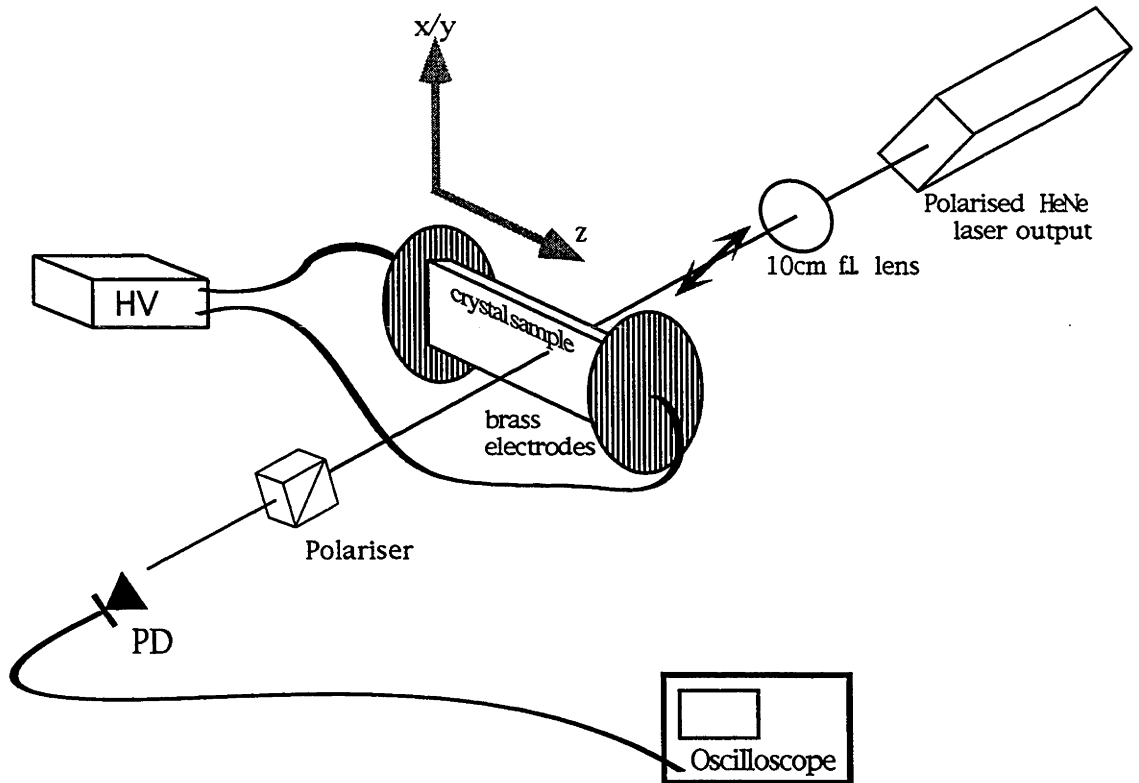
Figure Ten: Diagrammatic representation of experiment for measurement of Pockels coefficients in $RII_3 \cdot 3S_8$ crystals.

♦   A cell was built to securely house the crystal between electrodes. It contained index matching fluid and allowed small adjustment of the crystal orientation with respect to the HeNe beam (to enable baseline phase shift to be manipulated). A teflon cell conforming to these requirements was built in-house. The brass electrodes individually screwed in to the threaded core of the teflon rod and served also to seal the sample chamber for the index-matching fluid. The crystal was appropriately affixed to one of the electrodes, the fluid was then introduced through the open window and a coverslip fixed over this to close it (ensuring no air bubbles remained). This unit could then be placed in a holder,

the high-voltage leads attached and alignment in the HeNe beam undertaken. The analyser was a high quality Glan-laser polariser held in a rotatable mount. Detection was effected using a photodiode, the output of which fed directly to the oscilloscope. The experiment is shown schematically Figure Ten.

♦   The crystal samples of $AsI_3 * 3S_8$ used for these Pockels effect measurements were obtained as for those for Maker Fringe experiments.

♦   Following the methodology outlined earlier, a number of conditions in which the r_{13} element is involved can be deduced by determining the effect on the indicatrix when $E_{(0)}$ is applied along each crystallographic axis[12]. One suitable condition would be for $E_{(0)}$ to be applied along the z axis and the probe field is also directed along the z axis and polarised at 45° to x and y. In such a case, Δn is given by $-\frac{1}{2} n_o^3 r_{13} E_3$. Unfortunately, this particular geometry is impossible to achieve experimentally; crystals do not form natural (001) faces and cutting and optically polishing plane parallel slabs is virtually impossible in these materials. Another 'clean' possibility with $E_{(0)}$ applied along y and the probe field along y at 45° to x and z had to be ruled out as x and y axes are optically indistinguishable in these uniaxial crystals.

The geometry employed therefore is that in which $E_{(0)}$ acts along the z axis. The indicatrix change is then given by:

$$x^2\left(\frac{1}{n_o^2} + r_{13}E_3\right) + y^2\left(\frac{1}{n_o^2} + r_{13}E_3\right) + z^2\left(\frac{1}{n_e^2} - r_{13}E_3\right) = 1$$

With the HeNe beam propagating through the only natural face available (of Miller index 010 or 100 depending on the axis system chosen) and at 45° to z, the index modulation will be:

$$\Delta n = -\frac{1}{2} n_o^3 \left(r_{13} - \left(\frac{n_e}{n_o}\right)^3 r_{33}\right)E_3 \qquad (25)$$

and it is the grouping $\left(r_{13} - \left(n_e/n_o\right)^3 r_{33}\right)$ that is measured.

♦   Fine beam positioning was done by manipulation of the lens in front of the sample. After passage through the sample, the beam was passed through a pinhole to remove most scatter. The analyser was rotated to check for circular polarisation condition (*i.e.*, that there was a minimum of transmitted intensity

---

[12]   This is done as before using Eqs (17, 19) and then simplifying in the manner of obtaining Eq (20).

fluctuation as the analyser was rotated) and the crystal orientation was carefully moved until this was satisfactory. This was checked by eye. It was not possible to achieve perfect circular polarisation background for the experiment using crystal manipulation however, it makes only a small difference if there is some ellipticity already in the background polarisation.

I_{DC} was measured on the scope and the field switched on.   The modulation depth was recorded for a number of field strengths. The process was repeated several times on different parts of the crystal. For each I_F vs $E_{(0)}$ set of measurements at different crystal beam positions, the same set of voltages from the signal generator were used, thus, the actual applied fields are the same in each set.

To help confirm the verity of the signal, the sample was removed and re-loaded in a different orientation - such that $E_{(0)}$ was directed along x (or y). A much larger modulation signal was observed in this experiment. Unfortunately only a limited amount of data was recorded in this orientation -for measuring r_{12}- as the HV transformer failed at this point.

3.   RESULTS

Data is not collected as a 'scanned' measure of the size of $\Delta\Phi$ or Δn with increasing $E_{(0)}$ field strength. In principle, a single measurement for a particular geometry suffices although it is most important to ensure that one is working in the linear response regime and to try to establish that no mechanical or other electronic or optical effects are causing or obfuscating the signal.

Plots of I_F vs $E_{(0)}$ are shown in Figure Eleven. It can be seen that the dependence of I_F on $E_{(0)}$ is linear, though with deviations at low and high field strengths. At low field, I_F becomes increasingly difficult to read from the oscilloscope screen and this may account for deviations here. At high field, some sort of saturation region appears to be reached though the reasons for this are not known. This linearity alone suggests that -at least predominantly- it is the Pockels effect being measured. Mechanical contributions to this 'unclamped measurement' are presumed to be small due to the low modulation frequency used. Furthermore, when the orientation of the sample was changed and the EO effect measured in this new geometry, a change in magnitude of the modulated signal of the predicted size occurred also indicating that in both of these arrangements, it was the Pockels effect that was being observed.
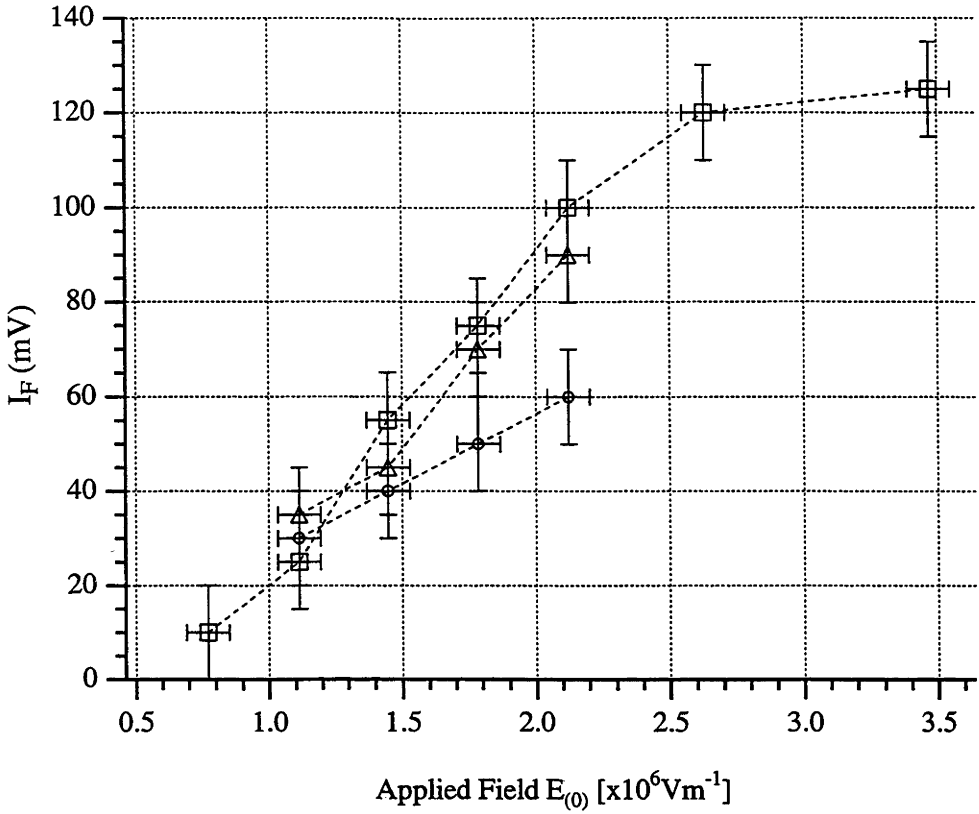
Figure Eleven: Plot of modulated signal intensity measured in the electro-optic effect experiment as a function of applied field strength. Error bars indicate worst-case confidence limits of ±10mV in I_F and ±0.08x10^6Vm^{-1} in $E_{(0)}$.
The three different data sets are measurements from different crystals.

Evaluation of $(r_{13} - (n_e/n_o)^3 r_{33})$ from this data commences with determination of the phase shift $\Delta\Phi$ induced in the beam by the applied electric field using Eq (23). This can be done at any point though it is clearly best to do this within the linear domain of I_F vs $E_{(0)}$. Once a $\Delta\Phi$ value is obtained, it is related to the applied field strength through the expression for Δn from Eq (22):

$$\Phi = \Delta n \, 2\pi L \big/ \lambda = -n_o^3 \left(r_{13} - (n_e/n_o)^3 \, r_{33} \right) E_3 \, \pi L \big/ \lambda \tag{26}$$

Taking a typical case from the graph in Figure Eleven:

> when $E_{(0)}$ (= E_3) = **2.12x10^6 V/m**, $I_F \approx 0.06$V.
> For this measurement, I_{DC} =1200mV. From Eq (23), $\sin\Phi = I_F/I_{DC} = 0.06/1.2$
> $\underline{\Phi \text{ is therefore} \approx 50 \text{ milliradians}}$.

> Taking: λ=632.8x10^{-9}m   L = 1.27x10^{-3}m
> n_e= 1.853 and n_o= 2.283   (determined for 633nm using the earlier dispersion formula), Eq (26) yields:

$$(r_{13} - (n_e/n_o)^3 r_{33}) = 0.30 \text{pmV}^{-1}.$$

This process is repeated on points within each curve and also on those of the other measured E_f vs $E_{(0)}$ plots. In this way, a more reliable average figure for the coefficient is obtained. In doing this, values between 0.28 and 0.34pmV^{-1} were evaluated for ($r_{13} - 0.535r_{33}$). Note that it is quite a small range in which these lie. In further calculations, a value for ($r_{13} - 0.535r_{33}$). of **0.31pmV^{-1}** is used.

It is relevant to compare this figure to the analogous measured electro-optic coefficient for CHI_3*3S_8 [11] in which ($r_{13} - 0.512r_{33}$) was found to be 0.29±0.12pmV^{-1}. In the context of celebrated crystalline electro-optic materials, the particular RI_3*3S_8 response measured here is about one tenth that of large responses of, say KH_2PO_4. It is worth remembering, however, that this grouping of Pockels coefficient components for AsI_3*3S_8 is probably not the largest for the complex. In the iodoform compound, r_{12} was measured as $\approx$4pmV^{-1} [11].

The aim of this experiment was to estimate the $\chi_{31}^{(2)}$ NLO susceptibility component via measurement of the r_{13} electro-optic coefficient. In practice, however, this procedure is problematic:

- Firstly, one cannot experimentally access the r_{13} component alone and must measure a phase change dictated by a *grouping* of components.
- Secondly, one needs to know the size and sign of the r_{33} component if r_{13} is to be extracted from this measured grouping and this is unknown (and so the r_{13} element can conceivably be of any size). It is -in principle- possible to derive r_{33} from the SHG-measured d_{33} component[13] however, this is only strictly possible for dispersionless media and so would be considered to have a large error associated with it for this adduct. There is also uncertainty as to the appropriate numerical coefficient, K, to use in this determination.
- Even if an r_{13} is extracted in this manner, one must again make the assumption of Kleinman conditions [4,8] to derive $d_{13} = d_{31}$ and by doing this the error is further amplified.

It is reasonable to suggest, however, that because d_{33} for AsI_3*3S_8 is larger than that for CHI_3*3S_8, a similar relation applies between the r_{33} coefficients of these complexes. If this is the case, then because the $\{r_{13}-(\approx0.5)r_{33}\}$

---

[13] A relationship exists [14] between the Pockels coefficient and the second order NLO susceptibility:

$$d_{ij} = K\ n_{ii}^2\ n_{jj}^2\ r_{ij}$$

groupings for the two adducts are the same, it follows that the r_{13} coefficient for AsI_3*3S_8 is somewhat larger than that of CHI_3*3S_8.

Summary

Inspection of the experimentally determined NLO susceptibilities as a group reveals that the NLO response of AsI_3*3S_8 is different again to that of the previously measured complexes.   The AsI_3 adduct exhibits strong NLO response in both the xy plane *and* parallel to the z axis. One also observes a decrease in the anisotropy ratios of these two responses across the series CH $\rightarrow$ Sb. In this property too, the arsenic adduct occupies an intermediate position to the other complexes.

The objective of attaining a set of second-order NLO coefficients for the other 'intermediate' charge-transfer addition complex of the RI_3*3S_8 type has been achieved with the data collected on AsI_3*3S_8 as described in this chapter. The lack of a conclusive determination of d_{31} is unfortunate, however, the focus of subsequent analyses is on the anisotropy between '11' and '33' NLO response.

REFERENCES

1a. P.D. Maker, R.W. Terhune, M. Nisenoff and C.M. Savage, Effects of dispersion and focussing on the production of optical harmonics. *Phys.Rev.Lett.*, **8**, 21 (1962);

1b. F. Kajzar and J. Messier, Third harmonic generation in liquids. *Phys.Rev.A*, **32**, 2352 (1985)

2. J. Jerphagnon and S. Kurtz, Maker Fringes: A detailed comparison of theory and experiment for isotropic and uniaxial crystals. *J.App.Phys.*, **41**, 1667 (1970)

3a. S.K. Kurtz in H. Rabin and C.L. Tang (Eds), *Quantum Electronics*, (Academic Press; New York, 1975);

3b. S.K. Kurtz in F.T. Arecchi and E.O. Schulz-Dubois (Eds), *Laser Handbook*, Vol1, (North Holland; Amsterdam, 1972);

3c. D. Chemla and P. Kupecek, Analyse des experiences de génération de second harmonique. *Rev.Phys.App.*, **6**, 31 (1971)

4. F. Zernike and J.E. Midwinter, *Applied Nonlinear Optics*. John Wiley, New York (1973)

5. J. Jerphagnon and S. Kurtz, Accurate relative values for quartz, ammonium dihydrogenphosphate, and potassium dihydrogenphosphate. *Phys.Rev.B*, **1**, 1739 (1970)

6. F. Zernike, Refractive indices of ammonium dihydrogenphosphate and potassium dihydrogenphosphate between 2000Å and 1.5μm. *J.Opt.Soc.Am.*, **54**, 1215 (1964)

7. S.K. Kurtz and T.T. Perry, A powder technique for the evaluation of nonlinear optical materials. *J.App.Phys.*, **39**, 3798 (1968)

8. D.A. Kleinman, A. Ashkin and G.D. Boyd, Second-harmonic generation of light by focussed laser beams. *Phys.Rev.*, **145**, 338 (1966)

9a. C. Talliani *etal* pg 301 in: *Organic Molecules for NonlinearOptics and Photonics*. eds J. Messier, F. Kajzar and P. Prasad, NATO ASI Series E. Vol 194, (Kluwer Academic, 1991);

9b. F. Kajzar *etal* pg 403 in: *Organic Molecules for NonlinearOptics and Photonics*. eds J. Messier, F. Kajzar and P. Prasad, NATO ASI Series E. Vol 194, (Kluwer Academic, 1991)

10. A. Samoc, M. Samoc, P. Prasad and A. Krajewska-Cizio, Second-harmonic generation in the crystalline complex antimony triiodide-sulfur. *J.Opt.Soc.Am.B*, **9**, 1819 (1992)

11a. A. Samoc, M. Samoc, D. Kohler, M. Stähelin, J. Fünfschilling and I. Zschokke-Gränacher, Linear and second order optical properties of the trigonal adducts of triiodomethane with sulfur and quinoline. *Nonlinear Optics*, **2**, 13 (1992);

11b. A. Samoc, M. Samoc, J. Fünfschilling and I. Zschokke-Gränacher, Nonlinear and electrooptical properties of complexes of iodoform. *Mat.Science* (Wroclaw), **10**, 231 (1984);

11c. A. Samoc, M. Samoc, J. Fünfschilling and I. Zschokke-Gränacher, The linear Pockels effect in crystals of the iodoform-sulfur complex. *Chem.Phys.Lett.*, **114**, 423 (1985)

12. C. D. West, Sulfur-iodide crystals RJ$_3$·3S$_8$: structure unit and optical properties. *Z.Krist.*, **94**, 459 (1937)

13a. S.H. Wemple, *Electro-optic materials*. in [3b].

13b. R.W. Boyd, *Nonlinear Optics*. (Academic Press, 1992);

14. J. Zyss and J.L. Oudar, Relations between microscopic and macroscopic lowest-order optical nonlinearities of molecular crystals with one- or two-dimensional units. *Phys.Rev.A*, **26**, 2028 (1982)

CHAPTER THREE

This Chapter describes the computations of molecular first-hyperpolarisability coefficients of the RI_3 molecules on whose sulfur adducts experimental NLO measurements were undertaken.

The rationale behind the pursuit of calculated values of molecular hyperpolarisabilities is that these β are for hypothetical *isolated* molecules. It was proposed in Chapter One that molecular β tensors could be used in conjunction with various models of the local fields in the adduct crystals to 'construct' values of NLO susceptibility for RI_3*3S_8. These can then be compared with the measured $\chi^{(2)}$s of the complexes.

It has been possible to calculate beta-tensor elements for all three tri-iodide molecules at a reasonably high level of theory using *ab initio* quantum chemical methods as available in the Gaussian94® program suite. Performing these calculations also had the benefit of yielding molecular orbital energies and degeneracies. A feature of this work is the computation of hitherto unreported molecular hyperpolarisabilities of the arsenic and tri-iodide molecule.

This chapter commences with a short introduction concerning the calculation of quadratic hyperpolarisability[1]. Previous relevant work is outlined and is followed by description of the computation methods. Results from these are subsequently presented and analysed.

---

[1]   Theoretical prediction of molecular third-order NLO response has been discussed. For example, see Dudis *etal*[1] and Brédas *etal*[2].

Theory: The Computation of β

1.   TYPES OF METHODS

For calculations of reliable first hyperpolarisabilities, the appropriate computational method must have a sufficiently extended set of basis functions in order to accurately describe the outer parts of the electronic charge distribution. The hyperpolarisability is particularly sensitive to these less-tightly bound electronic distributions. β tensors may be computed with *semi-empirical* (SE) and *ab initio* quantum-chemical methods. The review article by Kanis *et al* [6] gives a comparative account of these techniques.

In semi-empirical methods, certain molecular parameters are obtained from experimental data rather than being explicitly calculated. The Hamiltonians are of simpler form, generally only explicitly dealing with valence electrons and containing empirical data for the potential of core electrons. Basis sets may contain fixed atomic orbital exponents. Also, the calculation of the molecular wavefunction and energy judiciously neglects certain integrals between different centres comprising the wavefunction. These choices reduce the number of steps in the calculation but can be detrimental to the accuracy for some molecular properties.

Semi-empirical techniques were used only sparsely in this work. The majority of work involving the calculation of β do so for π-electron organic molecules. It is expected that the parametrisation of such methods is quite inappropriate for the determination of β for sigma-bonded heavy atoms - even if the method is optimised for calculating NLO response. Their usefulness in this regard is discussed in several works [3-7] though the reliability of their computed βs is not established. The simplest SE methods are not relevant to the issue of calculating hyperpolarisabilities in molecules such as RI_3 since they only consider the π electrons of unsaturated organic molecules. Many have been superceded by the increased facility of performing ab initio level calculations.

Ab initio calculations of molecular properties are more rigorous in that they deal with the entire electron distribution of the molecule but, consequently, they are computationally more expensive.

86

2. HARTREE-FOCK METHOD

The most important ab initio computational chemistry procedure is the Self Consistent Field (SCF) or Hartree Fock (HF) method of wavefunction calculation. A hamiltonian describing all electrostatic interactions in the molecule is first devised. For the examination of molecular properties such as optical resonances, hyperpolarisabilities etc, this must contain terms describing the change of energy imposed by an applied external field. Such a Hamiltonian is shown in Eq (1) [6]:

$$H(E) = \sum_{I>J} \frac{Z_I Z_J}{R_{IJ}} - \sum_I Z_I R_{IJ} \cdot F - \sum_i \left(\frac{1}{2} \nabla_i^2 + \sum_I \frac{Z_I}{r_{iI}} + F \cdot r_i \right) + \sum_{i>j} \frac{1}{r_{ij}} \qquad (1)$$

Where Z is nuclear charge, R_{IJ} is internuclear distance, r_{iI} is electron-nucleus distance and r_{ij} inter-electron distance. The first term describes nuclear-nuclear repulsion, the second accounts for (linear) energy change arising from nuclear displacement induced by an applied electric field[2], F. The next term is comprised of electron kinetic energy, electron-nucleus potential, and applied-field effects on the electron and is summed over all electrons. The final term describes electron-electron repulsion. i and j are electron labels and I and J nuclear labels.

An electronic wavefunction for the entire molecular system is composed and is written as a Slater determinant with the elements denoting the products of molecular orbitals, ϕ, and electron spin states, a or b;

$$\Phi = \begin{vmatrix} a_1 \cdot \phi_1 & b_1 \cdot \phi_1 & a_1 \cdot \phi_2 & b_1 \cdot \phi_2 & \cdots & a_1 \cdot \phi_{n/2} & b_1 \cdot \phi_{n/2} \\ a_2 \cdot \phi_1 & b_2 \cdot \phi_1 & a_2 \cdot \phi_2 & b_2 \cdot \phi_2 & \cdots & a_2 \cdot \phi_{n/2} & b_2 \cdot \phi_{n/2} \\ & & & \vdots & & & \\ a_n \cdot \phi_1 & b_n \cdot \phi_1 & a_n \cdot \phi_2 & b_n \cdot \phi_2 & \cdots & a_n \cdot \phi_{n/2} & b_n \cdot \phi_{n/2} \end{vmatrix}$$

where a_n and b_n designate the 'up and down' spins respectively of electron 1, 2 ... n etc. The $a \cdot \phi$ products are sometimes called molecular spin-orbitals. Use of this procedure guarantees the necessary wavefunction antisymmetry with respect to particle exchange. This determinant is generally large with n^2 elements.

The molecular orbitals in turn are considered as being linear combinations of basis functions belonging to the atomic centres.

---

[2] In this chapter only, an applied electric field is denoted by F in order to distinguish it from the energy, E.

$$\phi = \sum_i c_i \psi_i$$

Where ψ is the atomic wavefunction and 'c' is a combination coefficient.

Gaussian-type functions are used as the descriptors for these atomic wavefunctions as they are mathematically straightforward to manipulate - although generally, several such functions (of the form $y = p \, e^{-ar^2}$) are required to describe one atomic orbital basis function, ψ.

Energy is calculated using this starting wavefunction in the time-dependent or time-independent Schrödinger equation. A procedure for obtaining the correct composition of these molecular orbitals uses the 'Roothaan method' [8]. Some starting set of basis function combination coefficients for each MO serves as input and the so-called Roothaan-Hall simultaneous equations are solved. This involves terms for[3];

- the energy of single electrons in the nuclear potential, H_{core},
- the two-electron repulsion interaction for/between each electron
- and factors giving the extent of overlap between one-electron basis functions, ϕ.

In the Roothaan method, the combination coefficient, c, is assigned to a linear combination of these terms for each electron and this is adjusted until a set of c are obtained such that $\dfrac{\partial E}{\partial c}$ is a minimum. The resulting wavefunction has a new set of coefficients which are then treated as input and the process repeated until the change between the new set of input coefficients and old is negligible at which point it is self consistent. The energy of the system should also converge as the SCF calculation proceeds. Self consistency of atomic orbital coefficients as well as energy convergence are used as criteria to establish when wavefunction calculation is complete. 'Restricted' Hartree-Fock (RHF) calculations in which paired orbital occupancy is forced is appropriate for closed-shell systems such as for the molecules of concern here.

In a geometry optimisation, nuclear coordinates are varied and the SCF energy computation is repeated at each geometry in the absence of any field. The energy gradient with respect to molecular atomic positions is calculated and the optimised structure is taken where this is a minimum.

---

[3]   These are each calculated in ab initio procedure but are empirically determined to give agreement with experimental data in semiempirical methods.

3.   *SCF HYPERPOLARISABILITES*

The calculation of hyperpolarisability tensor elements is done in 'single-point' calculations which take a self-consistent/energy-optimised geometry determined in the manner just described. From the well known expression[4]:   (using the Einstein summation convention)

$$\mu_i = \alpha_{ij}F_j + \tfrac{1}{2}\beta_{ijk}F_jF_k + \tfrac{1}{6}\gamma_{ijkl}F_jF_kF_l + ... \qquad (2)$$

the polarisability and hyperpolarisabilities can be expressed as appropriate-order field derivatives of either the energy or the dipole moment of the system:

$$\beta_{ijk} = \frac{\partial^2\mu_i}{\partial F_j\partial F_k} = \frac{\partial^3 E}{\partial F_j\partial F_k\partial F_l} \qquad (3)$$

presuming the Hellmann-Feynman principle to be valid[5]. F is the applied electric field and E is the energy of the molecule. Thus the derivatives in Eq (3) have to be evaluated in order to yield β. Different tensor components are obtained by appropriate substitution of x, y and z for i, j and k in Eq (3). The computation of the derivatives may be done analytically -in which case the technique is referred to as Coupled Perturbed Hartree-Fock- or numerically in which case the term 'finite field' (FF) is used. Both should yield identical results but have different computational efficiency.

In the description above, the NLO coefficient has been considered to describe the *static* molecular response. It is possible to extend the HF method to incorporate the dependence of the response on the frequency of an applied oscillating electric field. Implementation of the time-dependent Hartree-Fock (TDHF) method is not trivial, however, as the time-dependent Schrödinger Equation must be solved. Applied electric fields, F, in the second and fifth terms of the hamiltonian, Eq (1), will have a complex form leading to complex orbitals. Also, in the determination of β using Eq (3), the fields, F, are also of a complex form and the calculation must be done analytically [5,10b]. Unfortunately, however, the TDHF method was not available for this study.

---

[4]   The numerical coefficients, $1/n!$, before successive expansion terms are included in Eq (2) in accordance with nearly all quantum chemical descriptions of the calculation of hyperpolarisabilities. These are frequently omitted in definitions of experimental NLO coefficients. This leads to the necessity of introducing n! multipliers when comparing experimental and theory-derived hyperpolarisabilities.

[5]   This is the principle connecting the change in energy of a system with the change in a particular molecular property.

The basis sets necessary for these calculations are extended compared to those for geometry optimisations. They incorporate 'diffuse functions' which are s and p orbitals that are larger than those existing for a particular atom in its ground state. They enable the more 'diffuse' outer electron distribution reaches to be more accurately accounted for. Similarly, addition of extra functions of higher angular momentum quantum number allows the spatial characteristics of the wavefunction to be better described. These are called 'polarisation' functions. It has been established that the addition of sufficient diffuse and polarisation functions[6] is mandatory for the reasonable evaluation of beta [4,5,7].

For light atoms, all orbitals -including those of core electrons- are described with gaussian basis functions which may be of the 'contracted' type, being linear sets of *primitive* gaussian functions. For calculations involving heavy elements (iodine, antimony and arsenic atoms in this work), the large number of electrons requires use of 'pseudo-potentials' (aslo: effective core potentials)[7] in order to reduce the number of computed integrals. In this approximation, that part of the hamiltonian describing interactions between the core electrons -which play little part in the bonding interactions- and valence electrons is replaced by a single pre-determined potential. These have been determined for each element [22] and are called upon by the Gaussian program when needed.

For all calculations, an appropriate set of basis functions must be chosen. The 6-311G(2d,2p) basis set is widely regarded as a good standard level for reliable geometry determinations of organic molecules (and was used on C, As & H atoms in geometry optimisations in this study). This notation indicates that for this set, each orbital of the core is represented by a single gaussian function formed from the contraction of six Gaussian-type functions, and that the valence orbitals are each represented by a set of three functions ('triple-zeta' basis set), one of which is formed from the contraction of three Gaussian-type orbitals. This basis set was augmented with two d-type polarisation functions for the carbon atom and 2 p-functions for the hydrogen atom. Effective core potentials were used for the heavy atoms (As, Sb and I) with diffuse and/or polarisation functions added to the valence functions.

---

[6]   As quoted in Kanis [6], the basis sets necessary are "discouragingly large".
[7]   This standard method is described in texts such as Levine [10] and described in detail where the potentials are published [19]. Effective core potential use is exemplified in Karna's work [12-14] and by Glukhovtsev *etal* [21].

With respect to choice of basis set employed, van Mourik and van Duijneveldt [13] found in the study of weak hydrogen bonding interactions between the water molecule and several small substituted methane molecules, that singly polarised, double zeta basis sets were of sufficient size to yield satisfactory interaction energies. These are rather dependent on the outer charge distribution as is the hyperpolarisability so this conclusion should be applicable here. This observation is confirmed in these results where it is seen for AsI_3 and CHI_3, little change is seen in β in extending double to triple zeta basis sets.

4.   CONSIDERATION OF ELECTRON CORRELATION

An inherent limitation of the SCF method is the neglect of the effect of electron correlation. This stems directly from the procedure where a single determinant is used to describe the electron distribution in the molecule. The electron distribution is effectively static and so cannot include representation of the tendencies of the electrons to minimise their proximity (or rather, probability of close proximity) apart from the prohibited extreme close proximity of electrons having the same MO and spin. In energy terms, this causes the SCF energy to be an over-estimate (eg, Atkins, Levine [8]). Hyperpolarisabilities are very sensitive to valence electron distribution and hence to electron correlation [5,7].

It is β tensor components of small absolute value which are generally most affected when the calculation method accounts for electron correlation [4]. Consideration of electron correlation has greater importance for molecular systems of small size [5]. This is presumably because the distortions imposed on the electronic wavefunction upon field application are relatively greater in such instances. As an example, β_{xyz} for H_2O_2 was larger by ≈ 6 times and β_{zyy} for H_2O was larger by ≈ 3 times when electron correlation was considered [16].

According to Luo [7a], the correlation effect can be large for both small and larger molecules. Often however [9,16], electron correlation has only a small effect on dominant tensor elements. Also, it is likely that the effects of correlation on β of small molecules are different to those on π-electron charge-transfer organic molecules (eg, *p*-nitroaniline). Significantly, it was concluded [4] that for octupolar

91

molecular systems, there can be dramatic differences in β components and correlation effects are strong and should be incorporated in methods for calculating hyperpolarisabilities.

Computational methods which incorporate electron corelation consideration include density functional techniques, perturbation methods and those in which configuration-interaction is included. This work has made use of hyperpolarisabilities calculated with a perturbation technique[8].

In the computational procedure employed by the Gaussian94 software, an approach using the perturbation energy is taken. The system is considered as *weakly* perturbed by the applied electric field, (for example, following Foresman [8b]).

A Hamiltonian operator describing the polarised molecule can be written as the expansion:

$$H = H^{(0)} + H^{(1)} + H^{(2)} + \cdots \quad = H^{(0)} + \lambda V \qquad (4)$$

where $H^{(n)}$ represents the various orders of perturbation and $H^{(0)}$ the unperturbed system. The coefficient, λ, applies to the perturbation, V, which is the difference between the instantaneous interaction between electrons and the the SCF interaction between electrons in an averaged field.

The wavefunction and energy can be described (to third order) as the Taylor expansions:

$$\Psi = \Psi^{(0)} + \lambda\Psi^{(1)} + \lambda^2\Psi^{(2)} + \lambda^3\Psi^{(3)} + ...$$
$$E = E^{(0)} + \lambda E^{(1)} + \lambda^2 E^{(2)} + \lambda^3 E^{(3)} + ... \qquad (5)$$

which if substituted in the Schrödinger equation gives expressions containing higher order terms of Ψ and E. For example:

$$(H^{(0)} - E^{(0)})\Psi^{(2)} = (E^{(1)} - V)\Psi^{(1)} + E^{(2)}\Psi^{(0)}$$

$$(6)$$

---

8   Density functional methods have not been extensively used for hyperpolarisability calculation. This is discussed in Ref [9b] in a study of the use of such methods in comparison with the Hartree-Fock method for calculating β for certain small molecules. DFT predictions were closer to experimental values.

The particular perturbation method used in this work -called the Møller-Plesset procedure- uses the fact that the 'Hartree-Fock' energy given by the SCF computation is equal to $H^{(0)} + H^{(1)}$. In the second-order treatment where Eq (5) is truncated at the third term, the aim is to calculate $E^{(2)}$, the 'correlation energy'. This can be shown to equal

$$E^{(2)} = \left\langle \Psi^{(0)} \left| V \right| \Psi^{(1)} \right\rangle \tag{7}$$

where $\Psi^{(0)}$ is the known ground state wavefunction and $\Psi^{(1)}$ that of the first-order perturbed system. Eq (7) is expressed as a linear combination of ground and excited-state wavefunctions and the integrals performed to yield $E^{(2)}$. It is this admixture of other states or higher energy configurations which causes an effective correlation consideration since the set of quantum numbers possessed by each of these must, by definition, be different.

The calculation of molecular polarisabilities and hyperpolarisabilities occurs as before by the coupled perturbed Hartree-Fock or finite field evaluation of the derivatives of Eq (3). This second-order treatment is called the MP2 method.

From comparative analyses of calculations on numerous small molecules [4,5,9], the MP2 method is considered a good approach for β calculation[9] in most molecules because it accounts for the majority of correlation effects (~90% of effects on β) yet it is not too expensive in processor time. Agreements with experimental values are good, generally giving very slight underestimates.

---

[9] For α too, good agreement is obtained [14] using MP2 with a 6-31++G(sd,sp) basis set, typically giving numbers only 5% below static experimental values.

Previous Calculations Performed on RI$_3$ and S$_8$ Molecules

1.   PRIOR β CALCULATIONS FOR HALOFORMS

In 1990, Karna *et al* [11] reported their ab initio calculations of molecular polarisability and first and second hyperpolarisabilities for haloform molecules (CHX$_3$). The computed coefficients were determined using the coupled perturbed Hartree-Fock (CPHF) method in the static frequency limit (ω=0) to yield the vector part of beta, β_v, which for isolated molecules belonging to the C$_{3v}$ point group is given by[10]:

$$\beta_v = \beta_{xxz} + \beta_{yyz} + \beta_{zzz}$$

These authors employed the effective core potentials published by Stevens *et al* [20] for the large atoms, bromine and iodine.

These *β* were compared to experimentally derived values of (hyper)polarisability. The authors obtained satisfactory agreement between measured and calculated polarisabilities but very poor correspondence for hyperpolarisabilities (see Table Four). In fact, the calculation underestimated β_v by more than two orders of magnitude. Different simulated conditions to those for the measurements and neglect of electron correlation were proposed as explaining the lack of agreement.

This work was extended by the same group [10a,12] to determine dynamic CHX$_3$ polarisabilities and hyperpolarisabilities at optical frequencies. This used a time-dependent CPHF method and effectively, simulated gas phase Kerr, electro-optic and EFISHG experiments. Properties were calculated at λ=694.3nm and electron correlation was not considered. As in the previous work, it was found that there was poor agreement between the calculated β values and liquid phase EFISHG derived quantities (a discrepancy of about an order of magnitude). They also examined the dispersion of (hyper)polarisability manifested by these haloform molecules. For iodoform, a trend was observed in the computed dispersion with β_v increasing slightly as ω increased[11].

---

[10]   some studies show this multiplied by a factor of 3/5 depending on choice of definition of β_v.

[11]   This incorporated a $\approx$15% increase in the off diagonal elements, $\beta_{xxz} = \beta_{yyz}$ while β_{zzz} was slightly diminished.

These studies are useful for comparison with the NLO calculations on the iodoform molecule which were performed in this study (albeit with the different aim of looking at individual tensor elements). They were one of the first indications that SCF hyperpolarisability calculations -even with reasonable basis sets- may be inadequate for small molecules.

2.   PRIOR AB-INITIO CALCULATIONS FOR SbI_3 AND AsI_3

Sakai and Miyoshi [14a] reported ab initio calculations on AsI_3 and SbI_3 molecules with the intent of examining the influence that two basis set choices had on Hartree-Fock-derived molecular geometries. These sets incorporated model potentials on the calculated structural parameters of these species. The larger of these two basis sets was similar to one of those tried in this work for obtaining an optimised geometry. Agreement with experimental quantities was good although these workers noted a small overestimation discrepancy which was smaller when all electron calculations were performed (AsF_3 and SbF_3). As far as is known, calculated β values for AsI_3 have not been reported.

Breidung and Thiel [14b] reported calculations on the RX_3 (and RX_5) series (where R = P-Bi and X=F-I). In this work, theoretical geometry parameters, vibrational frequencies, force constants, dipole moments were determined among other properties. Some of their results are included in Tables Two and Three.

Samoc *et al* [15] measured and discussed the NLO properties of $SbI_3 \cdot 3S_8$ and reported preliminary *ab initio* calculations of the β tensor elements of SbI_3. The calculations were performed in the same manner as those calculations on iodoform, by using the quantum chemical package 'HONDO'.

3.   OCTUPOLAR MOLECULES

Brédas *et al* performed calculations of β on purely octupolar molecules using several methods [17]. This has some relevance to the present work in that it demonstrates the possibility that optical nonlinearities can be predicted from octupolar charge distributions. This work, however, was performed on aromatic

organic structures in which the origin of the electronic hyperpolarisability is largely attributed to the π-electron system. This is different to the case of RI_3 molecules which require a very different parameterisation involving accurate representation of atomic charge distributions and that of the sigma bonds. Thus the analysis of Brédas for calculations of 1,3,5-triamino-2,4,6-trinitrobenzene are not directly relevant to these molecules. An important conclusion was, however, that inclusion of electron correlation into such calculations is necessary for proper determination of β from octupolar structures.

4.   *OCTASULFUR*

No previous studies involving computed hyperpolarisabilities of the octasulfur molecule have been reported. This is also true for the third-order hyperpolarisability of this molecule.

Methods Used in this Study

Ab initio computed hyperpolarisabilities for both RI_3 and S_8 molecules were sought despite the discouraging results attained by Karna's work and despite the problems of accounting for the unknown dispersion of the resultant βs.

The work conducted in this study follows much of the same method as that of the earlier studies with certain restrictions and improvements as dictated by available computer resources. The computations were performed with the Gaussian94® program package. This has routines for performing calculations with numerous methods of which Hartree-Fock and MP2 were used in this work. Unfortunately, however, there is no means by which to perform *frequency-dependent* hyperpolarisability calculations within the current version of the Gaussian program.

In each case, SCF geometry optimisation calculations were performed before the single point calculations evaluating the hyperpolarisability coefficients. Basis sets can be of a lower level for the first step and those employed are shown in

Tables One to Three in the next section. The calculations were of medium size involving between 83 and 137 basis functions. Polarisation and diffuse functions were included for most calculations. Their usage is indicated by the convention of "+" symbols for diffuse functions and characters in parentheses for polarisation functions.

The 'sp' diffuse and 'd' polarisation functions employed for the arsenic atom were those published by Binning [18a] (sp=0.021, d=0.273, f=0.372; Breidung *et al* [14b] used d=0.35). When using the Pople basis sets, additional functions specified were simply called-up by Gaussian94. For antimony, the value of 0.211 suggested by Huzinaga [18b] was employed as the exponent for a 'd' polarisation function to augment the D95 basis set in SbI_3 calculations (Breidung used 0.25).

An attempt was made to further improve the basis set of Sb by including an 'f' polarisation function as described earlier. As there is no recommended published value for this exponent for antimony, an estimate was obtained by extrapolation of the f-polarisation functions published for other heavy elements. Using the progression of f functions for the fourth-row elements (from Binning and Curtis [18a] & Huzinaga [18b]), an analogous progression was extrapolated for the fifth-row elements on the basis of the published f exponent for iodine (of 0.441) [19]. Thus, a value of 0.411 was obtained for the f exponent that would apply to antimony.

In each calculation, the D95 basis set was used for the iodine atom. In most cases, it was augmented by diffuse and polarisation functions. These were taken from Glukhovtsev *et al* [19]. Calculations using the MP2 method employed SCF determined geometries and a primary SCF calculation to determine the initial wavefunction.

The point group of S_8 is D_{4d} for which a single β element is predicted -β_{xyz}- which vanishes in the zero-frequency condition [24]. Since Gaussian94 only calculates static β, a predicted hyperpolarisability was unobtainable for the undistorted molecule. Ab initio hyperpolarisabilities for the S_8 molecule were calculated using warped molecular geometries as they exist in the adduct crystal. SCF and MP2 methods were used with the 6-311+* basis set.

Semi-empirical frequency dependent β calculations were able to be performed for these S_8 geometries using a time-dependent HF method available in the semi-empirical "MOPAC" program[12]. The method is similar to that used by Karna in the HONDO program and involves semi-empirical calculation of the wavefunction and energy using a certain Hamiltonian (MNDO or AM1). Time-dependent Hartree-Fock calculation of β is then done analytically up to a maximum frequency of 0.5eV in this case (which is still well removed from the fundamental frequency of 1.17eV used in this work). A hyperpolarisability for AsI_3 (using the PM3 Hamiltonian) was also performed, however, the magnitude of the tensor elements appeared to be seriously overestimated.

A geometry optimisation and single point (hyperpolarisability) calculation for iodoform using a density functional method was also performed. The geometry and β tensor element magnitudes thus yielded were almost identical to those achieved using the SCF/MP2 routine (see Tables One and Seven) but they required far greater computational effort and thus were not continued.

Gaussian94 yields hyperpolarisabilities and polarisabilities in atomic units (au). For β, conversion to electrostatic units (esu), one multiplies by 8.6392×10^{-33} and from au to SI units of m^4V^{-1}, the factor is 3.6213×10^{-42} [5]. This does not include the factor of $\frac{1}{2}$ which must often be included if comparing experimental and calculated hyperpolarisabilities (depending on inclusion/exclusion of numerical expansion coefficients in Eq (2)).

---

[12] "*MOPAC 93 Manual*" Fujitsu Limited, 1993. See also [12b] for details of time-dependent Hartree-Fock hyperpolarisability computations.

Results

1.   *RI₃ MOLECULES*

The geometries calculated for iodoform with various basis sets are shown in Table One. The molecular structure parameters as calculated by the RHF method are basically constant with basis set level. Along with the computed energy, the dipole moment is recognised as a primary indicator of the quality of the calculated molecular geometry. It is a property which reflects molecular electronic structure more sensitively than bond lengths and angles and is a quantity for which experimental data is available.

Table One:

BASIS SET &ECP §	C-I (Å)	I-C-I (degrees)	C-H (Å)	Dipole Moment	Energy (hartrees)
D95 (d,p) I DZ (d) WH ECP	2.144	113.1	1.072	0.646D	-71.9073
6-31G(2d,2p) I DZ (d) WH ECP	2.147	112.9	1.0721	0.717D	-71.9088
6-311G(2d,2p) I DZ (d) WH ECP	2.15	112.9	1.0719	0.720D	-71.9139
D95 (d,p) I DZ (2d) St ECP	2.152	113.1	1.0716	0.551D	-72.0337
6-31G(2d,2p) I DZ (2d) St ECP	2.149	112.8	1.0718	0.622D	-72.0370
DFT	2.165	113.1	1.077	0.609D	-72.859
KARNA [10a] [11]	2.150	112.9	1.085	0.79D 0.65D	
Experiment; Gas Phase [22a]	2.120	113.0	1.097	0.86D in benzene [23a] 0.82D in C₆H₁₂ [23b]	
Experiment; in S₈ [22b]	2.10	115.9	-	‡	

§   The first line of these entries is the basis set applied to C and H atoms (polarisation functions for carbon and hydrogen respectively are in parentheses).
        A double zeta treatment for the iodine valence electrons was used in all cases -the different numbers of polarisation functions for this atom are shown in parentheses on the second line.
        The Effective Core Potential [20] used for iodine is indicated on the last line: 'WH' = those published by Wadt and Hay and incorporated into the LANL2DZ basis set of Gaussian, 'St' = those published by Stevens *etal*.
‡   This quantity is estimated to be 1.2-1.3D in the analysis of Chapter Five.

A persistent, small discrepancy between calculated and experimental bond lengths is observed, with the computed carbon-hydrogen bond length too short by ~0.03 Å and the carbon-iodine bond as too long by the same amount. The origin of this error is not clear but it is within the same error limits reported by Karna [10,11] and Glukhovtsev *et al*[19]. The I-C-I angle is in good agreement with the gas-phase experimental value.

The molecular geometry as calculated using the 6-311G(2d,2p) basis set was taken for use in 'single point' calculations in which first hyperpolarisability components were computed. It is evident from these results that agreement between the theory and experiment is slightly better when the Hay-Wadt effective core porential set is used as opposed to the set published by Stevens *et al* The former set was therefore used for the optimisations and the single point calculations.

For consistency, one should use the same 'Wadt and Hay' effective core porentials, for the AsI_3 & SbI_3 molecules as for iodoform. This does not introduce any discrepancies as very good agreement between experimental and computed geometries was achieved for both these species, using both effective core porentials. These values are included in Tables Two and Three.

Table Two:

BASIS SET &ECP §	As-I (Å)	I-As-I (degrees)	Dipole Moment	Energy (hartrees)
'LANL2DZ'	2.679	101.8	1.09D	
As&I=D95 plus d:As=2.0 d:I=.279	2.601	101.5	0.65D	-39.491
As&I=D95 plus d:As=.273 d:I=.279	2.572	101.2	0.74D	-39.530
As=6-311G(d) I=DZ+dexp=.279	2.569	101.3	0.86D	-39.535
SAKAI; As=TZ(d) I=TZ	2.584	101.5	1.30D	
SAKAI; As=TZ(2d) I=TZ(d)	2.579	101.0	0.80D	
BREIDUNG [14b]; DZ(3/21) & d functs	2.567	101.4	0.766D	
Experiment; [22c] in AsI₃ [22d]	2.556 2.591	102.0 ± 0.1 99.67 ± 0.05		
Experiment; [22e] gas phase	2.557	100.2±0.4	0.96D in CS_2 [23c,d]	
Experiment; in S₈ [Appendix One]	2.574	99.7	?	

Table Three:

BASIS SET &ECP §	Sb-I (Å)	I-Sb-I (degrees)	Dipole Moment	Energy (hartrees)
'LANL2DZ'	2.827	99.7	2.866D	-38.7786
Sb&I=D95 plus d:Sb=2.73 d:I=.279	2.736	99.5	2.005D	-38.8491
Sb&I=D95 plus d:Sb=.211 d:I=.279	2.741	99.4	1.960D	-38.8529
SAKAI; Sb=TZ(d) I=TZ	2.750	99.3	2.83D	
SAKAI; Sb=TZ(2d) I=TZ(d)	2.737	99.6	2.07D	
BREIDUNG [14b]; DZ(3/21) & d functs	2.739	99.5	2.057D	
Experiment; [22f] in SbI$_3$	2.868	99.1		
Experiment; [22g] gas phase	2.719	99.1	1.58D in CS$_2$ [23c]	
Experiment; in S$_8$ [22h]	2.747	96.6	?	

In Tables Two and Three; D95 indicates use of the basis set of this name in which a 3/21 contracted gaussian function (double zeta) is applied to all electrons of the system. LANL2DZ represents a calculation using the D95 set but for elements above Z=11. The 'Hay and Wadt' ECPs are employed to treat core electrons. TZ indicates that a triple zeta basis set was used (see [7]).

Unlike the dipole moment and higher multipole moments, the structural properties of the molecule are fairly insensitive to the level and basis set employed. One can also see the close agreement attained with previously calculated properties -especially those of Breidung. Comparison with calculated geometry parameters for other molecules is good, for example, for AsBr$_3$, Binning [18a] recorded theory-experiment discrepencies of: 0.01Å in As-Br, 0.4° in Br-As-Br and 0.38D in the dipole moment. This lends confidence to the subsequent calculations which used these geometries.

For AsI$_3$, the geometry which employed the 6-311G(d) basis set for arsenic was used for the single point calculations (fourth row of Table Two). For SbI$_3$, though acknowledged to be less than ideal, the geometry yielded by the DZ(Sb+d,I+d) basis set as in the third row of Table Three was used for the subsequent single point calculations. It would have been preferable to be able to use a 6-311G type basis set for Sb, however, these are not available in Gaussian94 for fifth-row elements.

Results of the single-point calculations yielding molecular first hyperpolarisability tensor elements are presented in the following tables showing the progression of these values with increase of basis set level.

Table Four: Calculated Hyperpolarisabilities for Iodoform.

BASIS SET §	β_{xxx} a.u.	β_{zxx} a.u.	β_{zzz} a.u.	Dipole Moment	Energy (hartrees)
LANL2DZ	163.6	56.9	33.2	0·79D	
6-31G(d,p) I=D95(d)	116.5	38.7	25.0	0·73D	-71.904
6-31++G(d,p) I=D95(d)	108.4	11.4	117.6	0·63D	-71.906
6-31++G(2d,2p) I=D95(d)	101.3	7.0	116.7	0·64D	-71.911
6-31++G(2d,2p) I=D95+(d)	98.2	2.2	12.1	0·71D	-71.912
6-31++G(2df,2pd) I=D95+(df)	102.0	1.9	12.6	0·75D	-71.925
6-311++G(2df,2pd) I=D95+(df)	102.1	4.3	13.6	0·73D	-71.9315
KARNA C&I dbl-zeta(2d)/Stev ECP	19.1	8.6	13.7	0·67D	

§.   '+' indicates that 's' and 'p' diffuse functions are added to the basis set for non-hydrogen atoms. '++' indicates that an 's' diffuse function was also added to the hydrogen basis set. Characters in parentheses indicate the number and type of polarisation functions added. See text for those functions used for each atom type.

Table Five: Calculated Hyperpolarisabilities for Arsenic Triiodide.

BASIS SET §	β_{xxx} a.u.	β_{zxx} a.u.	β_{zzz} a.u.	Dipole Moment	Energy (hartrees)
As & I = straight LANL2DZ	158.1	17.2	0.4	0·77D	-39.441
As=D95(d) I=D95(d)	89.3	12.6	46.4	0·73D	-39.530
As=D95+(d) I=D95+(d)	58.8	0.2	44.2	0·76D	-39.533
As=6-31+G(2df) I=D95+(df)	16.2	8.7	75.0	0·77D	-39.534
As=D95+(df) I=D95+(df)	58.3	0.5	47.8	0·80D	-39.549
As=6-311+G(2df) I=D95+(df)	8.3	3.7	106.5	0·73D	-39.552
As=6-311+G(3df) I=D95+(df)	7.2	7.5	129.7	0·80D	-39.554

§.   '+' indicates that 's' and 'p' diffuse functions are added to the basis set for that atom. Characters in parentheses indicate the number and type of polarisation functions added. See text for those functions used for each atom type.

Table Six: Calculated Hyperpolarisabilities for Antimony Triiodide.

BASIS SET §	β_{xxx} a.u.	β_{zxx} a.u.	β_{zzz} a.u.	Dipole Moment	Energy (hartrees)
Sb & I = straight LANL2DZ	364.9	195.1	96.1	2·55D	-38.775
Sb=D95(d) I=D95(d)	189.5	95.1	134.6	1·99D	-38.852
Sb=D95(d) I=D95+(d)	154.5	66.0	20.3	1·98D	-38.855
Sb=D95(d) I=D95+(df)	150.0	64.0	19.8	1·99D	-38.863
Sb=D95(df^{guess}) I=D95+(df)	159.3	70.7	18.9	2·00D	-38.873

§.   '+' indicates that 's' and 'p' diffuse functions are added to the basis set for that atom. Characters in parentheses indicate the number and type of polarisation functions added. See text for those functions used for each atom type.

Several points are to be noted from these results:

- From the SCF iodoform calculations that used progressively larger basis sets (Table Four), it is seen that adequate provision of diffuse functions to the iodine atoms seems to be rather important. Such an observation is based on an observed stability of tensor element values as basis set level increases. Further augmentation of C and H basis sets with polarisation functions makes relatively little difference.

- Analogous comparison of arsenic triiodide calculations shows that for this molecule there is a major difference in the predicted hyperpolarisability anisotropy depending on the *type* of basis set used for the arsenic atom. The Pople (eg, 6-31+) sets suggest a dominant β_{zzz} component over the 'in-plane' contribution whereas the Dunning set (D95) predicts roughly equal sizes for both elements. The reason for this probably involves the manner in which the multiple primitive gaussian functions are contracted to form the set. This discrepancy is mentioned again later in the chapter. Within the Pople sets, treatment of arsenic valence electrons at the triple zeta level has an impact on the ratio β_{zzz}/β_{xxx} -making the zzz component even more dominant- but again, further augmentation of the As basis set with polarisation functions makes only a slight difference.

- One might also expect this to be the case for calculations performed on antimony triiodide. Values computed for this molecule, however, can only be done in Gaussian94 at the double zeta "D95" level (Pople basis sets not yet being available for elements heavier than Kr). It is not certain that the

observation of the hyperpolarisability elements attaining consistency as basis set size increases, is sufficient evidence to conclude that the relative sizes of these beta elements are reliable. See, for example the previous results for the arsenic compound where the β values at the double zeta level are steady but change dramatically when a triple zeta basis set is employed.

- The off-diagonal 311 component seems to be consistently small.

Results from calculations employing the MP2 method are presented in the following two tables. For AsI_3 MP2 calculations were performed using both the Pople and Dunning basis sets which each gave such different results at the SCF level. The one density functional calculation made for CHI_3 is also included.

Table Seven: *   MP2 and DFT Calculated Hyperpolarisabilities for Iodoform.

BASIS SET §	β_{xxx} a.u.	β_{zxx} a.u.	β_{zzz} a.u.	Dipole Moment
DFT	72.3	12.2	18.9	0·86D
6-31++G(2d,2p) I=D95+(d)	61.9	10.3	16.1	0·80D
6-31++G(2df,2pd) I=D95+(df)	63.0	9.2	14.9	0·83D
6-311++G(2df,2pd) I=D95+(df)	65.1	11.2	15.9	0·80D

§.   Characters have the same meaning as for Table Four.
*   The B3LYP method of Gaussian 94 was used in the test of the DFT technique.

Table Eight: MP2 Calculated Hyperpolarisabilities for Arsenic/Antimony Triiodide.

BASIS SET §	β_{xxx} a.u.	β_{zxx} a.u.	β_{zzz} a.u.	Dipole Moment
As=D95+(df) I=D95+(df)	46.9	15.5	31.2	0·93D
As=6-311+G(2df) I=D95+(df)	30.7	18.4	111.7	0·87D
As=6-311+G(3df) I=D95+(df)	47.5	25.5	136.9	0·92D
Sb=D95(df) I=D95+(df)	72.2	27.4	18.9	2·04D

§.   Characters have the same meaning as for Table Five.

The following important points are noted from these results:

- For each compound, treatment with the MP2 method (or consideration of electron correlation more generally) resulted in increases in size for small β components as compared to the SCF results. This was particularly the case for β_{zzz} and β_{zxx}. This is not unexpected in light of the earlier discussion of electron correlation effects. Conversely, there is a substantial decrease in the size of the large predicted in-plane hyperpolarisability, β_{xxx} by a factor of about two, though the reason for this effect is not clear.

- The static, SCF *and* correlated hyperpolarisabilities calculated here for iodoform do not closely resemble those of Karna's noncorrelated results [10a,11]. In particular, β elements are considerably larger[13] here and the β_{xxx} element more dominant. These results seem to be an improvement in that their absolute magnitudes are greater and, as will be seen from Chapter Five, experimental, gas-phase hyperpolarisabilities are probably larger than those predicted here.

- An important observation stems from comparison of these 'higher-level' hyperpolarisability calculations for the three triiodides. One notices a dramatically different response predicted for AsI_3 when the MP2/6-311+G(3df) method/basis set is employed as compared to MP2/D95. The possibility has to be considered that the former basis set improperly parameterises valence electron distribution for computation of β tensor elements. Such a conclusion is also supported by:

  - the anomalous behaviour of β elements during the series of calculations during which the basis set 'quality' was progressively increased.

  - Semi empirical (MOPAC-PM3) calculation of β for AsI_3 showed the in-plane NLO response as much stronger than that parallel to the z axis.

  - the *change* in β tensor element size (using 6-311+G(3df)) when electron correlation is accounted for is very different for AsI_3 than that of the other triiodide molecules. For example, for CHI_3, from SCF/6-311++G(2df,2pd) to MP2/6-311++G(2df,2pd), β_{xxx} is diminished by a factor of about two. For AsI_3, from SCF/6-311+G(3df) to MP2/6-311+G(3df), all β elements are substantially increased.

  - a similar comparison was noted between SCF-determined hyperpolarisabilities using Dunning and those using Pople basis sets.

---

[13]   There may also be a difference in the numerical coefficients used in Eq(2) between the two works which would make the difference even larger.

- the enormous contrast between predicted microscopic NLO response anisotropy in AsI_3 and SbI_3 which is unexpected given the general similarity between these molecules/materials.

Though both at the double zeta level, there are significant differences between the Pople 6-31 and Dunning D95 basis sets. These lie in the gaussian functions used (they have different exponents and coefficients) and in the way a group of primitive gaussians is contracted to yield the final double zeta function. Because of this, virtual orbital energies as calculated with the two different sets may be of slightly different energy (and this is seen in these outputs). Adding to the likelihood of such differences is the extensive use of polarisation and diffuse functions. With increased chance of outer virtual orbitals being close in energy, differences in order (in energy) of these is also more likely.

Effective core potentials are unlikely to be the cause of the problem as the same set was used for all calculations.

For these reasons, the Pople numbers (those obtained using 6-311-type basis sets) are considered anomalous and in the next chapter, AsI_3 β tensor elements returned using the Dunning D95 basis set will be relied upon when performing the $\chi^{(2)}$ estimations.

From these computations, it can be seen that for each of the compounds, the molecular dipole moment is determined with far greater precision. For the well-parameterised AsI_3 and CHI_3 molecules, the experimental agreement is particularly good - although the experimental values relate to measurements performed in condensed phase.

The one density functional hyperpolarisability calculation that was performed yielded beta tensor elements in close agreement with the MP2 values. Perhaps using a triple zeta basis set would have improved the geometry and dipole moment agreement however, the computational cost would probably be too large and would not be justified given that MP2 computations ran very efficiently. The proximity of density functional and MP2 estimations probably indicates that these two ways of accounting for electron correlation are approximately equivalent.

2.   THE S$_8$ MOLECULE

The results from calculations for each of the S$_8$ ring geometries are presented in Table Nine.

Table Nine

S$_8$ ring geometry	β Tensor elements; MOPAC		β Tensor elements; ab initio		
RI$_3$*3S$_8$	yyy	zzz	yyy	zzz	Point Group
CHI$_3$*3S$_8$	-84.5	10.3	-46	-22.5	C$_{2v}$
AsI$_3$*3S$_8$	-11	2.0	1.9	0.8	C$_{2v}$
SbI$_3$*3S$_8$	-7.3	2.2	1	0.3	C$_{2v}$

These hyperpolarisability elements are calculated at zero frequency and are given in atomic units.

For calculations on all these molecules, large basis sets have been used and it is unlikely that under-parametrisation of the electron distribution causes the disparity in tensor components. An unfortunate consequence of extensive use of extra diffuse and polarisation functions to   augment basis sets is the possibility that a significant 'basis set superposition error' (BSSE) is introduced [8a]. Uncertainty in calculated energies is created due to the probability of spatial overlap of electron density from nearby atoms. Orbital confinement effects [25] may also contribute to error in these predictions. This occurs when the full spatial extent of outer diffuse and polarisation functions cannot be realised due to close proximity of filled orbitals of neighbor atoms and it may be significant - though generally only when considering anions in crystal lattices.

Discussion

It is appropriate to try to place these results in context. There is no experiment which exactly corresponds to the set of conditions that are simulated in the theoretical calculations and the most relevant physical determination of β is a gas-phase EFISHG measurement. The hyperpolarisabilities of several small molecules have been determined in this way in the work of Ward *et al* [21] and these can serve as test of the computational methods.

...

Measured vector parts of β for a few such molecules are shown in Table Ten with SCF hyperpolarisabilities computed in this work (using similar levels as employed for the RI_3 molecules).

Table Ten:

β_V (a.u.) §	CHF_3	CH_3OH	NH_3
static SCF. This work.	$\approx$-16	$\approx$-31	-6.1
static SCF. Bartlett	-19.0		-6.5
from Gas-phase EFISHG	-25.0	-30	-20.9

§ $\beta_V = {}^3/_5(\beta_{xxz} + \beta_{yyz} + \beta_{zzz})$

For the CHF_3 and NH_3 molecules for which β_V was checked, the agreement between these calculations and those of Bartlett [9] is seen to be good. The agreement with experimental values is erratic but quite satisfactory given that for these test calculations neither electron correlation[14] nor non-zero frequency response were taken into account. This brief test supports the magnitudes of calculated β for the RI_3 molecules performed in this work.

The closeness seen between theoretical and gas-phase experimental numbers suggests other reasons for the large discrepancies between Karna's RI_3 calculations in condensed-phase measurements. In particular, these are;

♦ the enhancement of NLO response due to local field effects in such media. This issue is dealt with extensively in Chapters Four and Five.

♦ generally larger NLO responses at optical frequencies as compared to with static fields.

The presumption of a zero-frequency condition in this work is considered a weakness. An idea of the size of the effect that this neglect might have on the hyperpolarisabilities can be gained from comparison between the results of calculations of Bartlett *et al* [9] on small molecules using the time dependent Hartree-Fock method and calculated static values. This shows static-β to be smaller by 5%-15% for most species but by 30% for NH_3. Calculations of β for iodoform by Karna [10a] showed a 10% increase in β_V in going from a static to λ=694nm frequency condition[15].

---

[14] Bartlett showed that for ammonia, agreement with experiment was good when the MP2 method was used.

[15] Related results from the same author [14] showed that the calculated *time-*

These differences are generally reassuringly small and will be used in the discussion in Chapter Five. One cannot, however, extrapolate this result fully to the other RI_3 molecules as due to the proximity of electronic resonance in these substances, so somewhat larger differences are anticipated. Another point of view about static-calculated hyperpolarisabilities is that they have merit because they exclude the complicating factor of response modification due to electronic resonances. Accounting completely for all molecular resonances is rarely possible and so static values can provide a sound baseline for comparison of non-resonant electronic hyperpolarisabilities.

An objective of this work is to use the relative differences between the calculated tensor elements (the anisotropy) as well as their absolute values in later analyses. There is the implication when using the anisotropy of static β values that the error coming from using the zero-frequency condition is the same for all tensor elements. This is unlikely to be the case. Karna's measure of dispersion of β_v which has been mentioned in this chapter, is of little value with respect to the β_{xxx}/β_{zzz} ratio of particular interest in this study since the β_{xxx} element is not included in β_v. These early non-zero-frequency hyperpolarisability calculations for iodoform [10a] estimated β_{xxx} leading to the indication that at optical frequency, the β_{xxx}/β_{zzz} anisotropy is greatly increased. The effect that such an anisotropy change would have on predicted susceptibilities is addressed in Chapter Five. It should be remembered, however, that these were preliminary calculations of a fairly low level (double-zeta, no correlation) and thus carry significant uncertainty.

An estimate of the frequency dependence of β for isolated S_8 was able to be made by using semi-empirical calculations of this quantity. These were performed with the MNDO method using the MOPAC program. A trend whereby the 33 element increased slightly (by $\approx 10\%$) between the static and 0.5 eV conditions was noticed but the overall differences are small.

This part of the study would have benefited had frequency dependent β calculation been possible, nevertheless, useful estimations of the RI_3 and S_8 free-molecule hyperpolarisability and the RI_3 β anisotropy have been made. The hyperpolarisability tensors which have been calculated here can be taken for use in estimating macroscopic nonlinear optical coefficients for the RI_3 octa-sulfur adduct crystals. This is done in the next Chapter.

---

dependent polarisability, α, is ~20% smaller than the experimental quantity.

REFERENCES

1. D.S. Dudis, A.T. Yeates and D. Kost, Prediction of third-order NLO properties of organic molecules. *Adv.Mat.*, **6**, 248 (1994)

2. J.L. Brédas, C. Adant, P. Tackx, A. Persoons and B.M. Pierce, Third-order nonlinear optical response in organic materials: Theoretical and experimental aspects. *Chem.Rev.*, **94**, 243 (1994)

3. A.A. Hasanein, Ab initio computations of polarizabilities and hyperpolarizabilities of atoms and molecules. *Adv.Chem.Phys.*, **85**, 415 (1993)

4. D.R. Kanis, M.A. Ratner and T.J. Marks, Design and construction of molecular assemblies with large second-order optical nonlinearities. Quantum chemical aspects. *Chem.Rev.*, **94**, 195 (1994)

5. D.P. Shelton and J.E. Rice, Measurement and calculations of the hyperpolarisability of atoms and small molecules in the gas phase. *Chem.Rev.*, **94**, 3 (1994)

6. P.N. Prasad and D.J. Williams, *"Introduction to Nonlinear Optical Effects in Molecules and Polymers"* Wiley-Interscience, New York, 1991

7a. Y. Luo, H. Ågren, P. Jørgensen and K.V. Mikkelsen, Response Theory and calculations of molecular hyperpolarisabilities. *Adv.Quant.Chem.*, **26**, 165 (1995);
7b. J. Guan, P. Duffy, J.T. Carter, D.P. Chong, K.C. Casida, M.E. Casida and M. Wrinn, Comparison of local-density and Hartree-Fock calculations of molecular polarisabilities and hyperpolarisabilities. *J.Chem.Phys.*, **98**, 4753 (1993)

8a. I.N. Levine *"Quantum Chemistry"* Fourth Edition, (Prentice Hall, New York, 1991);
8b. J.B. Foresman and E. Frisch *"Exploring Chemistry with Electronic Structure Methods"* (Gaussian Inc., Pittsburgh, 1996)

9. R.J. Bartlett and H. Sekino, Can quantum chemistry provide reliable molecular hyperpolarisabilities?. Chapter Two in; *Nonlinear optical materials: theory and modeling.* eds S.P. Karna and A.T. Yeates, (American Chemical Society Series 628, 1996)

10a. S.P. Karna and M. Dupuis, Frequency-dependent hyperpolarisabilities of haloforms from ab initio SCF calculations. *Chem.Phys.Lett.*, **171**, 201 (1990);
10b. S.P. Karna and M. Dupuis, Frequency-dependent NLO properties of molecules: formulation and implementation in the HONDO program. *J.Comp.Chem.*, **12**, 487 (1991)

11. S.P. Karna, M. Dupuis, E. Perrin and P.N. Prasad, Theoretical and experimental studies of optical nonlinearities of haloforms CHX_3, X=F, Cl, Br, I. *J.Chem.Phys.*, **92**, 7418 (1990)

12. S.P. Karna, E. Perrin, P.N. Prasad and M. Dupuis, Dynamic polarisability of haloforms: Experimental and ab initio theoretical studies. *J.Phys.Chem.*, **95**, 4329 (1991)

13. T. van Mourik and F.B. van Duijneveldt, Ab initio calculations on the C-H⋯O hydrogen bonded systems CH_4-H_2O, CH_3NH_2-H_2O and $CH_3NH_3^+$-H_2O. *J.Mol.Struct.*, **341**, 63 (1995)

14a. Y. Sakai and E. Miyoshi, Theoretical study of geometries and dipole moments of AsX_3 and SbX_3 (X=F, Cl, Br, I) molecules. *J.Chem.Phys.*, **89**, 4452 (1988);

14b. J. Breidung and W.Thiel, A systematic ab initio study of the groupV trihalides MX_3 and pentahalides MX_5 (M=P-Bi, X=F-I). *J.Comput.Chem.*, **13**, 165 (1992)

15. A. Samoc, M. Samoc, P. Prasad and A. Krajewska-Cizio, Second harmonic generation in the crystalline complex antimony triiodide-sulfur. *J.Opt.Soc.Am.B*, **9**, 1819 (1992)

16a. G. Maroulis, *J.Chem.Phys.*, **96**, 6048 (1992);
16b. G. Maroulis, *J.Chem.Phys.*, **94**, 1182 (1991)

17. J.L. Brédas, F. Meyers, B.M. Pierce and J. Zyss, On the second order polarisability of conjugated π-electron molecules with octupolar symmetry: the case of triaminotrinitrobenzene. *J.Am.Chem.Soc.*, **114**, 4928 (1992)

18a. R.C. Binning and L.A. Curtiss, Compact contracted basis sets for third-row atoms: Ga-Kr. *J.Comput.Chem.*, **11**, 1206 (1990);
18b. S. Huzinaga (Ed), *"Gaussian Basis Sets for Molecular Calculations"* Elsevier, Amsterdam, 1984;

19. M.N. Glukhovtsev, A. Pross, M.P. McGrath and L. Radom, Extension of Gaussian-2 (G2) theory to bromine- and iodine-containing molecules: Use of effective core potentials. *J.Chem.Phys.*, **103**, 1878 (1995)

20a. W.R Wadt and P.J. Hay, *Ab initio* effective core potentials for molecular calculations. Potentials for main group elements Na to Bi. *J.Chem.Phys.*, **82**, 284 (1985);
20b. W.J. Stevens, M. Krauss, H. Basch and P.G. Jasien, Relativistic compact effective potentials and efficient, shared-exponent basis sets for the third-, fourth- and fifth-row atoms. *Can.J.Chem.*, **70**, 612 (1992)

21a. J.F. Ward and C.K. Miller, Measurements of nonlinear optical polarisabilities for twelve small molecules. *Phys.Rev.A*, **19**, 826 (1979);
21b. J.F. Ward and I.J. Bigio, Molecular second and third order polarisabilities from measurements of second harmonic generation in gases. *Phys.Rev.A*, **11**, 60 (1975)

22a. P.W. Allen and L.E. Sutton, Tables of interatomic distances and molecular configurations obtained by electron diffraction in the gas-phase. *Acta Cryst.*, **3**, 46 (1950);
22b. T. Bjorvatten, Crystal structure of the 1:3 addition compound iodoform-sulfur ($CHI_3 \cdot 3S_8$). *Acta Chem.Scand.*, **16**, 749 (1962);
22c. J. Trotter, The crystal structure of arsenic triiodide, AsI_3. *Z.Krist.*, **121**, 81 (1965);
22d. R. Enjalbert and J. Galy, Refinement of the structure of arsenic triiodide. *Acta Cryst.*, **36B**, 914 (1980);
22e. Y. Morino, T. Ukaji and T. Ito, Molecular structure determination by gas electron diffraction at high temperatures II. Arsenic triiodide and gallium triiodide. *Bull.Chem.Soc.Jap.*, **39**, 71 (1966)
22f. J. Trotter and T. Zobel, The crystal structure of SbI_3 and BiI_3. *Z.Krist.*, **123**, 67 (1966);
22g. A. Almenningen and T. Bjorvatten, An electron diffraction investigation of the molecular structure of antimony triiodide. *Acta.Chem.Scand.*, **17**, 2573 (1963);
22h. T. Bjorvatten, O. Hassel and A. Lindheim, Crystal structure of the addition compound $SbI_3 \cdot 3S_8$. *Acta Chem.Scand.*, **17**, 689 (1963)

23a.   R.P. Smith, T. Ree, J.L. Magee and H. Eyring, The inductive effect and chemical reactivity I: General theory of the inductive effect and application to electric dipole moments of haloalkanes. *J.Am.Chem.Soc.*, **73**, 2263 (1951);

23b.   R.P. Young, A. Holt and S. Walker, Interdipole distances in hydrogen bonded complexes in solution. *Tetrahedron*, **20**, 2351 (1964)

23c.   M.G. Malone and A.L. Ferguson, *J.Chem.Phys.*, **2**, 99 (1934);

23d.   E.G. Claeys, *J.Organomet.Chem.*, **5**, 446 (1966)

24.   Zernike and J.E. Midwinter, *Applied Nonlinear Optics.* John Wiley, New York (1973)

25.   Fowler and Madden, In crystal polarisabilities of alkali and halide ions. *Phys.Rev.B*, **29**, 1035 (1984)

CHAPTER FOUR

With calculated hyperpolarisabilities of isolated RI_3 and S_8 molecules available, it is possible to construct NLO susceptibilities for the adduct crystals based on these free-molecule β tensors. By building the $\chi^{(2)}$ values using different methods based on different models of the NLO-active lattice, evidence is obtained as to which of the four reasons discussed in Chapter One is most important in explaining the anisotropy in the susceptibility tensors of each of the RI_3*3S_8 complexes.

The determination of 'constructed' NLO susceptibility tensors for each of the RI_3-octasulfur adducts is the subject of this chapter. The different methods employed are:

1. The most straightforward treatment of the RI_3 hyperpolarisabilities uses the so-called "Oriented Gas" model[1] for the molecular crystal. Standard Lorentz factors are applied to this to account for the larger 'local' electric field experienced by the NLO molecule in the crystal environment. Factors are derived for both crystal directions in terms of the refractive indices. The NLO active unit is not actually specified. This approach is termed the *Anisotropic Lorentz Approximation* or *ALA Method*.

2. An alternative treatment deals with the local field problem more rigorously. A single NLO-active entity is detailed and the electric field at this position is explicitly calculated given that it sits in a polarised lattice of known structure. Local-field-factor *tensors* are obtained which describe the microscopic response of the molecule (through its polarisability) as well as the effect of the surrounding polarised crystal structure on the local field experienced by the NLO-active molecule. These factors can be significantly different to those determined by the ALA Method. These approaches are referred to as *Lorentz-Factor-Tensor Methods*.

3. The first of the LFT methods defines the complex as a $RI_3(S_8)_3$ *Supermolecule* and $\chi^{(2)}$ is built by assigning RI_3 hyperpolarisabilities to this entity. Refinement of this model comes through determination of a complete Lorentz-Factor tensor which considers both molecules in the adduct structure. The first of these is called the *LFT-Full* Method. Using this approach, one can also incorporate the NLO response of the S_8 molecule and this is described as the *LFT-Composite Method*.

The theoretical development in this Chapter relies strongly on concepts discussed in Chapter One, specifically the methods introduced by Munn [6].

---

[1] which neglects any interaction between the molecules and any modification by the molecular medium of an applied electric field. Thus, β anisotropy is preserved using this model.

The ALA Method:

1 .   THEORY OF THE ANISOTROPIC LORENTZ APPROXIMATION

Consider a molecular crystal comprised of unit cells containing a single molecule which may be oriented such that its molecular axes do not coincide with crystal axes. Each macroscopic NLO tensor element is then the product of:

- the molecular hyperpolarisability element, β
- the three appropriate cosines transforming each index (i, j, k) from molecular to crystal axes,
- the number density, N, of the molecules in the crystal and
- factors, f, relating the applied field strength outside the sample to that experienced at the molecule. There is one for each electric field in the process and the factor may depend on the direction of application/generation of the field.

Thus:

$$\chi_{IJK}^{(2)} = N \, f_I f_J f_K \, \{\cos \theta_{Ii} \cos \theta_{Jj} \cos \theta_{Kk}\} \beta_{ijk} \qquad (1)$$

Expanding this to the more general case where the number of molecules in the unit cell, Z, is greater than one. This requires summing $\{\cos \theta_{ij} \cos \theta_{jk} \cos \theta_{ki}\} \beta_{ijk}$ over each molecular site in the unit cell [1]. Eq (1) is sometimes used for Z>1 assuming the Einstein convention applies.

The local field factors, f, to be used in this model are usually determined through application of the approximation formulated by Lorentz in 1880 [2a]. This considers the electric field at a molecule as modified by its surroundings. The molecule or cell is presumed to exist within a spherical cavity embedded in a dielectric continuum. The structure of the medium is not explicitely considered in this treatment.

For molecular crystals, the applicability of this model requires the assumption to be made that the crystal is well described as a matrix of non-interacting molecules. This is generally reasonable for molecular materials in which intermolecular attractive forces are weak, such as organic liquids [3], but it is clearly less appropriate for solids where non-uniform fields and charge-transfer interactions exist.

115

Given such a model, the electric field [2b] inside the sphere is made up from:

$$E_f = E_1 + E_2 + E_3 + E_4 \qquad (2a)$$

where E_1 is the externally applied (optical) field and E_2 is the depolarisation reaction field of the medium in response to this. Together, E_1 and E_2 comprise the macroscopic field, E_M. E_3 is the field inside a spherical cavity due to an assembly of charges on the surface of the sphere. This contribution arises because the dielectric medium is also polarised by E_1;

> Consider a sphere of radius, *a*, polarised in a uniform electric field such that equal and opposite charges are distributed on each side of the sphere. The surface charge density at a point on the sphere is given by:
> $$-P\cos\theta$$
> where θ is the angle from the polarisation direction and P is the total amount of charge polarisation.
>
> The radial electric field, E_r, at the centre of the sphere due to an area element dA at this point is:
> $$E_r = P\cos\theta \, dA \; / \; 4\pi\varepsilon_o a^2$$
> and the total field in the polarisation direction due to the entire surface charge is:
> $$E_3 = \int_0^\pi E_r \cos\theta \; / \; 4\pi\varepsilon_o a^2 \; d\theta$$
> Substituting for E_r in the previous expression and integrating yields:
> $$E_3 = P / 3\varepsilon_o$$

The field from multipolar charge distributions within the cavity is denoted by E_4. This is usually assumed to be zero -as it is exactly in the case of dipoles arranged in a cubic array. In such a case, substituting for the terms in Eq (2a) gives (in esu):

$$E_f = E_M + {}^1/_{3\varepsilon_o} \, P \qquad (2b)$$

The bulk polarisation, P, is related to the macroscopic electric field through the linear susceptibility:

$$P = \varepsilon_o \chi^{(1)} \, E_M = \varepsilon_o(\varepsilon - 1) \, E_M \qquad (2c)$$

which when substituted in Eq (2b) and using $n^2 = \varepsilon$, can be rearranged to give:

$$E_f = E_M \left(\frac{n^2 + 2}{3} \right) \qquad (2d)$$

In which the term in parentheses is the well known Lorentz local-field factor. The ALA method is widely used in many spectroscopic and nonlinear optical analyses because of this simple form. However, local fields determined in this way will always preserve (and slightly increase) the anisotropy in the refractive indices from which they are taken and this is not necessarily realistic.

2.   APPLICATION TO $RI_3 \cdot 3S_8$

The structure of these complexes presents the fortuitous case whereby RI_3 molecular and crystal axes coincide meaning direction cosines are unity for all tensor elements [4]. Local-field factors for $RI_3 \cdot 3S_8$ crystals calculated using the anisotropic Lorentz approximation from refractive indices[2] in the manner just described are shown in Table One.

Table One:

Adduct	$f_{\omega,1}$	$f_{\omega,3}$	$f_{2\omega,1}$	$f_{2\omega,3}$	N
$SbI_3 \cdot 3S_8$	2.293	1.817	2.479	1.909	$1.270 \times 10^{27} m^{-3}$
§$AsI_3 \cdot 3S_8$	2.293	1.771	2.500	1.847	$1.283 \times 10^{27} m^{-3}$
$CHI_3 \cdot 3S_8$	2.259	1.714	2.408	1.754	$1.319 \times 10^{27} m^{-3}$

The number densities of RI_3 molecules, N, are also shown in the last column.
§   From the refractive index determinations for this complex, the dispersion is probably slightly smaller than indicated in Chapter Two and so f_{ω} values are probably slightly underestimated and $f_{2\omega}$ overstimated by a small amount. The effect of this on constructed NLO susceptbilities is discussed in Chapter Five.

Hyperpolarisabilities for each of the triiodides are taken as indicated in Table Nine of last Chapter. Using Eq (1) with the appropriate local field factors, one obtains the $\chi^{(2)}$ elements listed in Table Two.

Table Two:

Adduct	$\chi^{(2)}_{111}$ $(x10^{-12}mV^{-1})$	$\chi^{(2)}_{311}$ $(x10^{-12}mV^{-1})$	$\chi^{(2)}_{333}$ $(x10^{-12}mV^{-1})$
$CHI_3 \cdot 3S_8$	3.82	0.48	0.39
$AsI_3 \cdot 3S_8$	2.86	0.70	0.84
$SbI_3 \cdot 3S_8$	4.33	1.3	0.55

These tensor elements (and their anisotropies) will be used in the comparison with experimental and other derived susceptibility tensors. It is interesting, however, to note at this point that the NLO susceptibilitiy of the $AsI_3 \cdot 3S_8$ adduct appears significantly different to that of the other complexes.

---

2 see TableTwo of Chapter Two.

The LFT Method

1.   INTRODUCTION and THEORY

The Lorentz Approximation accounting for local field enhancement is often rather too crude[3]. Weak assumptions made in the ALA method of relating microscopic-macroscopic properties are:

- that due to presumed cubic symmetry within the (ellipsoidal) cavity, the dipole field completely cancels.

- that outside the cavity, the medium is treated as a continuous, polarisable medium of uniform dielectric constant.

Also, from inspection of Eq (2c) in the development of the ALA local field factors in the previous section, one can see that a $f \leftrightarrow \chi^{(1)}$ relationship exists. Yet f must relate $\chi^{(1)}$ and the polarisability, α, as well as relating the applied and local fields. So the anisotropy of f is determined by microscopic factors (manifested as the molecular polarisability) *as well as* macroscopic properties arising from how the molecules are arranged in the condensed phase. This means that the anisotropy of the local field factor does <u>not</u> follow that of the linear susceptibility (and thus refractive index) unless the polarisability of the molecule is isotropic -which is rarely the case. By taking the ALA approach, one obtains the anisotropy of $\chi^{(1)}$ for the anisotropy in f. This can be quite unrepresentative since $\chi^{(1)}$ relies on the product of the molecular polarisability and the local electric fields acting on them. The anisotropies of these can be quite different and even opposite [5a-c] (consider the long axis of an elongated molecule -the polarisability tends to be greatest along this dimension yet intermolecular fields are smaller due to the greater separation) resulting in an uninformative 'average' $\chi^{(1)}$ anisotropy.

It is possible to rectify these shortcomings and determine an f factor incorporating consideration of crystal *and* molecular properties[4]. Firstly though, one needs to start with an entirely different description of the local field.

---

[3] and has been shown to make inaccurate predictions; for example in *p*-terphenyl [5a], *m*-nitroaniline [5b] and in 4-(*N*,*N*-dimethylamino)-2-acetamido-nitrobenzene ('DAN') [5c].

[4]   Important factors involved when relating molecular properties with those of their molecular crystals include the presence of permanent internal fields and non-local polarisability response. Thus, the local-field issue is rather more complex than expected and this especially influences prediction of NLO properties.

A general description of these issues and development of theoretical frameworks incorporating such factors has been the concern of Munn. Refs [6] are important such works relevant to this study. These guided the theoretical explanations which follow.

Consider the 'NLO-phore' molecule in a crystal lattice being polarised by a macroscopic electric field. The total local field experienced at a molecule is the sum of the macroscopic field and the dipole fields from all other point dipoles, i, in the lattice. This may be written [2a]:

$$\mathbf{E}_f = \mathbf{E}_M + \sum_i \frac{(3\boldsymbol{p}_i \cdot \boldsymbol{r}_i)\boldsymbol{r}_i}{r^5} - \frac{\boldsymbol{p}_i}{r^3} \qquad (3)$$

where E_f and E_M have the same meanings as in Eqs (2a-d). The second term is the lattice-sum of dipole fields arising from the regular electrostatic relation for the electric field, presuming *point* dipoles at each point. $\boldsymbol{p}$ is the dipole moment vector, r is the inter-dipole distance, $\boldsymbol{r}_i$ is the vector between molecule and lattice point. The factor $(3\boldsymbol{p}_i \cdot \boldsymbol{r}_i)$ is a scalar containing the angular dependence of the field on the point dipole location.

More generally, the material is considered as Z (where Z>1) inter-penetrating lattices of the distinct molecules of the unit cell - with each bearing an induced dipole moment in the direction of the applied polarising field. A summation over lattice points, i, in a (spherical) 'shell' is performed to arrive at the total crystal field. This is done in a particular manner as briefly described in the next section. One may separate molecules into a number of 'submolecules' to better represent molecular shape and orientation [6f,9a,b]. The fields at each submolecule from each lattice-of-submolecules are individually determined and averaged to give the overall field sum at the molecule.

Eq (3) can be written in the form of Eq (2b):

$$\mathbf{E}_f = \dot{\mathbf{E}}_M + \sum_{k'} L_{k,k'} \cdot p_{k'} / \varepsilon_o v \qquad (4a)$$

where $L_{k,k'}$ is the result of the summation described above and is called the Lorentz tensor. The tensor is dimensionless and is normalised to unit cell volume and so is defined as having a trace of unity. It gives the field arising from each lattice (of point dipoles) at each molecule in the unit cell, for each direction of field application. The local field at a molecule, k, is comprised of fields from dipoles on lattices of the different molecules k' of the unit cell and from point dipoles on the lattice of k molecules - but excluding molecule k itself (thus k may equal k').

The bulk polarisation, P, of Eq (2b) has been replaced in Eq (4a) by a sum of sub-lattice polarisations[5] which for a molecular crystal can be given by [8b]:

$$p_{k'}/\varepsilon_o v$$

where $p_{k'}$ is the dipole moment of molecule k' as it exists in the lattice and v is the unit cell volume.

As in the development of the ALA field factors, the macroscopic (unit-cell) polarisation, P, is substituted into Eq (4a):

$$\sum_{k'} p_{k'}/\varepsilon_o v = P = \varepsilon_o\, \chi^{(1)}\cdot E_M$$

where again, $\chi^{(1)}$ is the linear bulk susceptibility. This leads to:

$$E_f = E_M + \varepsilon_o\, \chi^{(1)}\cdot E_M \sum_{k'} L_{k,k'} \qquad (4b)$$

The local-field-factor-*tensor*, d_k is defined: $\qquad E_f = d_k\, E_M$

and so from Eq (4b):

$$d_k = 1 + Z^{-1}\chi^{(1)} \sum_{k'} L_{k,k'} \qquad (5a)$$

where d_k is the local-field-factor tensor at molecule k and the summation is over all other molecules k' in the unit cell. Z is the number of molecules in the unit cell. Implicitly assumed in this preliminary expression is that each sublattice, k, makes an equal contribution to the susceptibility.

This expression is workable however it is still reliant on the linear susceptibility, the anisotropy of which is the 'bland' average of the frequently opposing[6] anisotropies of the molecular polarisability and the Lorentz-factor tensor.

One recognises that in obtaining $L_{k,k'}$, the *macroscopic* effects of differing local electric fields at the molecule as a result of the molecular packing are accounted for. To incorporate consideration of the molecular polarisability, α, into the local field tensor, d, it is necessary to explicitly express it via the relation:

$$p_k = \alpha_k \cdot E_{f,k}$$

where p_k is the sublattice polarisation and α_k is the 'effective' polarisability of molecule, k, in the crystal. This may be substituted into Eq (4a) to give:

---

[5] Normally, a molecular crystal is parameterised such that sub-lattices correspond exactly with a molecule -though this does not have to be the case.

[6] in practice, the more anisotropic a molecule is in shape, the more anisotropic a_k and $L_{k,k'}$ are likely to be, in opposite directions [5].

$$\mathbf{E}_{f,k} = \mathbf{E}_{M} + \sum_{k'} L_{k,k'} \cdot \mathbf{a}_{k'} \cdot \mathbf{E}_{f,k'} \qquad (5b)$$

where $\mathbf{a}_k = \alpha_k / \varepsilon_0 v$ and is a dimensionless reduced polarisability and v is the

volume of the unit cell. The LHS of Eq (5b) may be expanded as $\sum_{k'} \mathbf{E}_{f,k'} \times \delta_{kk'}$

($\delta_{kk'} = 1$ when $k' = k$ and zero otherwise). The two k' summation terms may then

be combined and the equation rearranged to give:

$$\sum_{k'} (1 - L_{k,k'} \cdot \mathbf{a}_{k'}) \cdot \mathbf{E}_{f,k'} = \mathbf{E}_{M} \qquad (5c)$$

where the unit matrix has been included.

The local-field tensor is then given by:

$$\mathbf{d}_k = \sum_{k'} (1 - L_{k,k'} \cdot \mathbf{a}_{k'})^{-1} \qquad (5d)$$

From which one can see that the anisotropies of macroscopic and microscopic

aspects of the structure are now included in $\mathbf{d}_k$. Difficulties associated in

obtaining appropriate $\mathbf{a}_k$ are dealt with in the next section.

One can also obtain Eq (5d) by substituting the independent expression [9b]:

$$\chi^{(1)} = \sum_{k} \mathbf{a}_k \cdot \mathbf{d}_k$$

into Eq (4b) to give after rearranging:

$$\mathbf{d}_k = 1 + \sum_{k} L_{k,k'} \mathbf{a}_{k'} \, \mathbf{d}_{kk'} \qquad (5e)$$

where the quantity $\mathbf{d}_{kk'}$ is a 3x3 submatrix defined as the specific field factor

relating effects on applied fields at molecule, k, due to lattice k'. $\mathbf{d}_{kk'} = \mathbf{d}_{k'k}$

and given that $\mathbf{d}_k = \sum_{k} \mathbf{d}_{kk'}$, Eq (5e) can be rearranged to yield (5d).

These local field tensors are used in the calculation of $\chi^{(2)}$ tensor elements from

hyperpolarisabilities using an expression analogous to Eq (1) [6b,f]:

$$\chi^{(2)}_{HIJ} = N \, \mathbf{d}_k^{\mathrm{T}}(2\omega) \, \mathbf{d}_k(\omega) \, \mathbf{d}_k(\omega) \, \{\cos\theta_{Hh} \cos\theta_{Ii} \cos\theta_{Jj}\} \beta_{hij}$$
$$(6)$$

2.   *APPLICATION TO RI$_3$*3S$_8$*

Step One

The first of the series of steps in the susceptibility calculation is the determination of the Lorentz-factor tensor, $L_{k,k'}$. A direct lattice dipole summation would be quite straightforward but is hampered by very slow convergence[7]. A technique called the Ewald Method is used in which summation is concurrently performed over the reciprocal and real lattices. This facilitates convergence as the oscillatory part of the summation (from the lattice periodicity) is much more efficient in phase-space. It also has the advantage of leaving a shape-independent Lorentz-Factor tensor. This is, however, rather more complicated mathematically and is dealt with in Refs [7]. An average[8] over submolecules is performed to give $L_{k,k'}$. This subtracts out the contributions to the field at the molecule from submolecules within that molecule in the same unit cell - since a molecule does not polarise itself. This routine is employed in the UMIST program that was used for this work.

As a starting model, the RI$_3$*3S$_8$ complex is specified in the sub-molecular treatment in the following way. A 'super' molecule is defined comprising seven submolecules - at the R and three iodine atomic positions, as well as at 'average' sulfur positions at the center of each of the three S$_8$ rings. The hexagonal unit cell was used (as opposed to the rhombohedral cell) for which Z=3. Cell dimension parameters and atomic coordinates were obtained from appropriate X-ray structure data[9]. These are input in the required manner in a command script with submolecule positions expressed as fractional coordinates.

As indicated above, field contributions from successive lattice shells are calculated -the number of these shells used is the minimum for which a satisfactory convergence criterion is achieved. This was specified to be better than 1 in 1x10^{-5}. For each complex, such a convergence was achieved after summation over seven shells.

---

[7]   since while the field due to a point dipole decreases as r^{-3}, the number of dipoles in a spherical volume increases as r^3.
[8]   The average is performed by summing (k,j;k',j') over all submolecules j and j' and dividing by the square of the number of submolecules that are specified.
[9]   Those for the arsenic triiodide complex were determined in this work -see Appendix One. The iodoform-octasulfur complex structure was determined by Bjorvatten [4a] and the SbI$_3$*3S$_8$ complex by Bjorvatten *etal* [4b].

The result is a 3Zx3Z (super)matrix, *i.e.*, a 3x3 matrix for each molecule-lattice pair and this is the Lorentz-factor Tensor, $L_{k,k'}$. These are shown for each complex in the following tables:

Table Three i.   Lorentz Tensor, $L_{\alpha\beta;k,k'}$ for CHI_3*3S_8

kk'	$\alpha\beta$					
	aa	ab	ac	bb	bc	cc
1,1	-0.8699	0	0	-0.8699	0	2.7398
1,2	0.4958	0	0	0.4958	0	0.00845
1,3	0.4958	0	0	0.4958	0	0.00845

Table Three ii.   Lorentz Tensor, $L_{\alpha\beta;k,k'}$ for AsI_3*3S_8

kk'	$\alpha\beta$					
	aa	ab	ac	bb	bc	cc
1,1	-0.8618	0	0	-0.8618	0	2.7235
1,2	0.4963	0	0	0.4963	0	0.00738
1,3	0.4963	0	0	0.4963	0	0.00738

Table Three iii.   Lorentz Tensor, $L_{\alpha\beta;k,k'}$ for SbI_3*3S_8

kk'	$\alpha\beta$					
	aa	ab	ac	bb	bc	cc
1,1	-0.8267	0	0	-0.8267	0	2.6534
1,2	0.4962	0	0	0.4962	0	0.00765
1,3	0.4962	0	0	0.4962	0	0.00765

Tensors are calculated in the fully orthogonal a, b, c axis system in which b is at 90° to a in the ab plane. The calculations may also be performed in the hexagonal axis system to give identical results.

One can see from these Tables that the off-diagonal elements are zero as predicted by symmetry. The highly anisotropic nature of these tensors is evident remembering that an isotropic structure has a symmetric LFT with diagonal elements equal to $1/3$. The large size of $L_{11;k,k'}$ is consistent with these molecules being stacked in close proximity along the c axis (which is of small dimensions for these crystals). Unit cell elongation can be implied in the direction of an element which tends to one as k' increases in $1k'$, however, this is not relevant for this structure.

It is difficult to interpret the significance of the small differences in tensor elements between the various complexes. The general trend in which they diminish slightly going from CH to Sb is attributed to the increasing unit cell volume which causes the normalised fields to become a little smaller.

Step Two

The next requirement for the local-field tensor calculation is the molecular polarisability, α. For most molecular crystals (Z>1), obtaining this presents a double problem as it is the polarisability of the NLO molecule *in the lattice* which is important - this is different to the free-molecule quantity since it is affected by geometry differences and the local field it experiences in the crystal. Thus, it is not expected that ab initio computed polarisability tensors are at all useful in this case. This leaves measured α's as the only source.

The experimental observable to which α directly contributes is the linear susceptibility, $\chi^{(1)}$. There is a problem however, in extracting microscopic polarisabilities from this bulk quantity as many combinations of individual molecule polarisabilities can result in a given susceptibility. This non-uniqueness problem can be circumvented by assuming that fixed relations exist between the contributions to unit cell $\chi^{(1)}$ from each molecule (other ways are mentioned later). More simply, it is often reasonable to assume for homomolecular crystals that all molecules in the unit cell make equal contribution to the susceptibility [5a,b,9a,b]. Likewise, one assumes that each submolecule within the molecule contributes equally to the total molecular polarisability.

Taking $\quad \chi^{(1)} = \sum_{k'} a_{k'} \cdot d_{k'} \quad$ and substituting for d_k with Eq (5a) and rearranging, an expression for $a_{k'}$ is obtained:

$$a_{k'} = \left(\frac{Z}{\chi^{(1)}} + \sum_{k'} L_{kk'} \right)^{-1} \tag{7}$$

To be consistent with the use of static hyperpolarisabilities, the use of zero frequency susceptibility data would be preferred. For these complexes, however, this is not available and so $\chi^{(1)}$ at optical frequency had to be used[10] and was determined from refractive indices through the relation:

---

[10] This approach was also used by other authors, for example, Hurst and Munn [5b] for their mNA study.

$$\chi^{(1)} = n^2 - 1$$

and input in a command script. Lorentz tensors were taken directly from the output of the program which computes them. These were used directly in the subsequent step for calculation of d_k.

Step Three

Local field tensor elements may now be calculated via Eq (5e) and are shown in Tables Four after averaging over submolecules. Note that they are determined for a single frequency (ω).

Table Four i.   Local-Field factor tensor for, d, CHI_3*3S_8

k	aa	ab	ac	bb	bc	cc
1	1.152	0	0	1.152	0	2.970
2	1.150	0	0	1.154	0	2.970
3	1.151	0	0	1.153	0	2.970

Table Four ii.   Local-Field factor tensor, d, for AsI_3*3S_8

k	aa	ab	ac	bb	bc	cc
1	1.169	0	0	1.169	0	3.111
2	1.169	0	0	1.169	0	3.111
3	1.169	0	0	1.169	0	3.111

Table Four iii.   Local-Field factor tensor, d, for SbI_3*3S_8

k	aa	ab	ac	bb	bc	cc
1	1.214	0	0	1.214	0	3.181
2	1.214	0	0	1.214	0	3.181
3	1.214	0	0	1.214	0	3.181

Tensors are diagonal in this case where molecular and crystal axes coincide. Comparison between these d tensors and the f factors of the ALA Method (shown in Table One) is appropriate. The anisotropies of the two factors are very different. Those calculated with the LFT method are considerably more polarised and in the opposite sense to the f factors. This is not unusual in context with results from other molecular crystals [5a,c] which were discussed earlier. The 33 component of d calculated here indicates that the local field is about three times as great as an applied field in this direction. This is rather large but not unrealistic.

Step Four

Calculation of the second order NLO susceptibility is via Eq (6). Technically, one of the d tensors should be for the harmonic wavelength. For several reasons, however, three local field factors for the *fundamental* wavelength were used[11] and the following elements are obtained:

Table   Five:

Adduct	$\chi^{(2)}_{111}$ $(x10^{-12}mV^{-1})$	$\chi^{(2)}_{311}$ $(x10^{-12}mV^{-1})$	$\chi^{(2)}_{333}$ $(x10^{-12}mV^{-1})$
CHI_3*3S_8	0.77	0.26	2.3
AsI_3*3S_8	0.70	0.46	5.1
SbI_3*3S_8	0.8	0.78	3.4

These tensors are biased toward the 33 element and the following methods aim to rectify this. The supermolecule specification was originally employed because it conforms to the methodology of the suite of programs used for calculating $L_{k,k'}$, $a_{k'}$, d_k and $\chi^{(2)}$ which are designed to be applied to homo-molecular crystals. Munn used a supermolecule approach in the study of effective polarisability of CT complex crystals and noted similar aberration along CT interaction axis.

---

[11]   This removes ambiguity in tensor elements which are equal under Kleinman conditions (and which do not exactly apply at 532nm for these materials) by forcing this condition to apply. The direct error introduced is known to underestimate the susceptibility by a small amount. The neglect of consideration of resonances and so breakdown of the Kleinman assumption can be incorporated in the discussion of resonance effects (in Chapter Five).

The LFT-Full Method:

1.   INTRODUCTION and THEORY

As mentioned in Chapter One, an improvement in the accuracy of $\chi^{(2)}$ predictions is effected by calculation of the Lorentz-Factor tensor using full specification of all molecules in the unit cell.

Consider, then, the Z=3 hexagonal unit cell of the $RI_3 \ast 3S_8$ complex as containing two types of molecules; three RI_3 molecules, each comprising four submolecules at the R and three iodine atomic positions and nine S_8 molecules with submolecules at each of the eight sulfur atom positions. A Lorentz-factor tensor can be calculated for this structure specification as outlined in the previous section.

The procedure for calculation of the Local-Field-factor tensor that was developed in the last section may be followed -in principle- for the full unit cell specification. Due to a software limitation, however, it is currently not possible to determine an effective polarisability: $\sum_k a_k$ for a unit cell containing more than one type of molecule (possibly with different numbers of submolecules in each). Such a quantity would otherwise have been obtained from Eq (7). Therefore it is not possible to calculate the Local-Field tensor via Eq (5e). Accordingly one returns to Eq (5a) to determine d_k. This may be rewritten as follows:

$$d = 1 + \left(L_{II} + 3L_{IS}\right) \frac{\chi^{(1)}_{adduct}}{Z} \tag{8}$$

This zero-frequency Local-Field-factor tensor was used with the hyperpolarisabilities in Eq (1) as was done in the supermolecule case to determine the NLO susceptibility.

2.   APPLICATION TO $RI_3 \ast 3S_8$

The Lorentz-tensor could be calculated as usual using the hetero-molecular crystal specification. The averaged Lorentz-tensor elements[12] were sorted into L_{II} and L_{IS} subtensors which were then used in the calculation of d. L_{II} and

---

[12] averaged over j and j' to give $L_{kk'}$ for each molecule.

L_{IS} were also used in the next approach and it is more appropriate to show them there. They are in Tables Eight (i-iii).

Local-Field-factor tensors determined with this method (Eq (8)) for each of the complexes are shown in Tables Six(i-iii). Again, the d are for the fundamental wavelength, 1064nm.

Table Six i.   Local-Field factor tensor for CHI_3*3S_8

	aa	ab	ac	bb	bc	cc
d	2.2043	0	0	2.2043	0	2.490

Table Six ii.   Local-Field factor tensor for AsI_3*3S_8

	aa	ab	ac	bb	bc	cc
d	2.2745	0	0	2.2745	0	2.5640

Table Six iii.   Local-Field factor tensor for SbI_3*3S_8

	aa	ab	ac	bb	bc	cc
d	2.3106	0	0	2.3106	0	2.6126

The 11 and 33 elements of the NLO susceptibility were obtained through use of Eq (6) and are shown in Table Seven.

Table Seven:

Adduct	$\chi^{(2)}_{111}$ (x10^{-12}mV^{-1})	$\chi^{(2)}_{333}$ (x10^{-12}mV^{-1})
CHI_3*3S_8	3.33	1.17
AsI_3*3S_8	2.56	2.44
SbI_3*3S_8	4.1	1.55

Even from a brief glance at these coefficients, it is clear that the skewed nature of previous constructed $\chi^{(2)}$ tensors is not replicated here. This seems to indicate that this property is rather sensitive to unit cell specification.

The LFT-Composite Method:

1.   INTRODUCTION and THEORY

The previous methods either made gross assumptions about the environment in which the NLO-phore exists, or this entity was treated in an approximate 'super-molecule' fashion. In the previous *LFT-Full* basis, explicit molecular polarisability contribution to the local field factor was excluded. Such approaches prevented the consideration of differing polarisabilities and hyperpolarisabilities from the different RI_3 and S_8 parts of the complex. To this point, response from the complexing partner -S_8- has been neglected.

The former shortcoming leads to error in the estimation of the local field factor (tensor) and so in the predicted $\chi^{(2)}$ elements. A failure to account for all component hyperpolarisabilities neglects the possibility that each contributes to the macroscopic NLO response. A methodology based on the LFT treatment which does deal with different components of a hetero-molecular crystal has been devised and applied to the RI_3*3S_8 complexes.

Consider again the RI_3*3S_8 adduct crystal as comprised of a RI_3 lattice and three S_8 lattices, interpenetrating to form the overall structure. A modified Eq (6) for the nonlinear susceptibility is defined which incorporates contribution to $\chi^{(2)}$ from both of these hyperpolarisable components:

$$\chi^{(2)}(-\omega_3;\omega_1,\omega_2) = \sum_k d_k^T(\omega_3) \cdot b_k(-\omega_3;\omega_1,\omega_2) : d_k(\omega_1)\, d_k(\omega_2)$$

(9)

where $b_k = \beta_k/\varepsilon_0 v$ and v is the volume of the unit cell. Other symbols have their usual meanings. The summation is over the RI_3 and the three S_8 lattices.

Consider the general expression Eq (5e) with the intention of determining the different d_k at RI_3 and S_8 molecules as required in Eq (9):

$$d_k = 1 + \sum_{k'} L_{kk'} \cdot a_{k'} \cdot d_{kk'}$$

In this case, in order to incorporate a molecular basis in the LF factor tensor, d_k, one cannot presume that each molecular site in the unit cell has the same polarisability and contributes equally to $\chi^{(1)}$. Clearly, this is not appropriate for this system where two distinct molecular components are contained in the unit cell.

So to derive an expression for an overall d_k composed from the constituent lattices, the individual $a_k \cdot d_k$ contibutions are examined. The equation:

$$\chi^{(1)} = \sum_k a_k \cdot d_k$$

is thus modified according to the stoichiometry of the complex:

$$\chi^{(1)} = a_I \cdot d_I + \sum_{k=1}^{3} a_{Sk} \cdot d_{Sk} \qquad (10)$$

where the I and S subscripts refer to the RI_3 and S_8 lattices, respectively.

The problem then arises of how to obtain polarisabilities of component molecules as they exist in the crystal. Again, the method is used whereby the relationship between the polarisabilities of the component molecules is sought[13] (although they are not deemed to be equal in this case). The ratio of $a_k \cdot d_k$ terms (which might be described as 'sub-susceptibilities' of the entire lattice) is designated ρ and Eq (10) becomes:

$$\chi^{(1)} = \left(1 + \sum_{k=1}^{3} \rho_{Sk} \right) a_I \cdot d_I \qquad (11)$$

where

$$\rho_{Sk} = \frac{a_{Sk} \cdot d_{Sk}}{a_I \cdot d_I} \qquad (12)$$

---

[13]   It is possible to derive a single nonlinear equation incorporating a_k for two different molecules in a unit cell via expressions for the local-field at each of the molecules. This was done for naphthalene and other similar molecules and solutions were determined using the Lorentz-tensor and by presuming equivalence between the molecules [8a].
A nonlinear matrix equation relating $\chi^{(1)}$ and a was determined for an anthracene complex and solutions determined by taking a suitable starting polarisablity for one of the molecules [8c].
One can also work out a range of acceptable effective polarisabilities algebraically using arbitrary parameters in the matrix defining ρ (see later) [9a,c,10].

There is still no experimental data which indicates what this ratio might be. A simple plausible assumption is therefore made:

$$\rho_{Sk} = \chi_S \Big/ \chi_I \qquad (13)$$

in which χ_S is the linear susceptibility of the homomolecular S_8 crystal and χ_I is the susceptibility of the homomolecular RI_3 crystal. Such a claim is justified by arguing that these susceptibilities arise from the molecules of interest in *a* crystal environment, which, although different to the adduct crystal environment, is still a much better approximation than trying to use gas-phase polarisability data (for example). Also, $\chi^{(1)}$ information is available for the homomolecular crystals of the parent compounds [footnote14].

Substituting Eq (13) into Eq (12) and Eq (11) allows expressions for the 'sub-susceptibilities' to be obtained:

$$a_I \, d_I = \left(\chi_I \big/ Z \, \bar{\chi}\right) \chi^{(1)}_{adduct}$$

$$\qquad (14)$$

$$a_{Sk} \, d_{Sk} = \left(\chi_S \big/ Z \, \bar{\chi}\right) \chi^{(1)}_{adduct}$$

where $\bar{\chi}$ is the weighted average of linear susceptibilities:

$$\bar{\chi} = \left(\chi_I + 3\chi_S\right) \big/ 4$$

These can be substituted in (5e) to yield:

$$d_I = 1 + \left(L_{II}\chi_I + 3L_{IS}\chi_S\right) \frac{\chi^{(1)}_{adduct}}{Z \, \bar{\chi}}$$

$$\qquad (15)$$

$$d_S = 1 + \left(L_{SI}\chi_I + 3L_{SS}\chi_S\right) \frac{\chi^{(1)}_{adduct}}{Z \, \bar{\chi}}$$

. where L_{IS} etc are the Lorentz-factor sub-tensors between the particular lattices. These are averages over all such kk' combinations. For example, $L_{IS} = L_{SI}$ is the average of the fields calculated between an RI_3 molecule and each of the nine S_8 molecules in the cell. For symmetry reasons, it is necessary to use a scalar average over crystallographic axes of the linear susceptibility of the homomolecular RI_3 and S_8 crystals. χ_I and χ_S were[14]:

S_8 χ_S	3.05
CHI_3 χ_I	3.00
AsI_3 χ_I	5.13
SbI_3 χ_I	6.01

These local-field-factor tensors are then used in Eq (9) with the appropriate hyperpolarisabilities to give the overall $\chi^{(2)}$ of the crystal.

2.   APPLICATION TO $RI_3 * 3S_8$

In this treatment, the cell was specified as containing twelve molecules - exactly as in the previous *LFT Full* approach. Lorentz-factor tensors were able to be calculated in this specification using the same software as used for the LFT supermolecule treatment. A sample input file with fractional coordinates for $AsI_3 * 3S_8$ is shown in Appendix One. In this case, the averaged Lorentz-tensor elements[15] were sorted into L_{II}, L_{IS}, and L_{SS} sub-tensors which were then used 'manually' in Eq (15) with the averaged $\chi^{(1)}$ to give the composite local-field-factor tensors.

---

[14] χ_S was determined as an average of the principle-axis χ_{ij} values for orthorhombic sulfur (S_8) crystals which were taken from Ref [10]. Analogous χ_I for the RI_3 materials were worked out from the relation, $\chi = n^2 - 1$. The refractive indices used were those listed in Table Five of Chapter One. These n were for slightly different frequencies (between 633nm and 671nm) for each of the RI_3 compounds and this does introduce a small but consistent error. The χ_I for CHI_3 is slightly overestimated with respect to that of AsI_3 and χ_I for SbI_3 is slightly underestimated with respect to that of AsI_3. The effect this has on the predicted $\chi^{(2)}$ anisotropies is discussed briefly in Chapter Five.
[15]   averaged as for *LFT-Full* method -see footnote 12.

Table Eight i.   Averaged Lorentz sub-Tensors for CHI_3*3S_8

kk'	$\alpha\beta$					
	aa	ab	ac	bb	bc	cc
L_{II}	-0.4751	0	0	-0.4751	0	1.9502
L_{IS}	0.4773	0	0	0.4773	0	0.0454
L_{SS}	0.2279	0	0	0.2279	0	0.5443

Table Eight ii.   Averaged Lorentz sub-Tensors for AsI_3*3S_8

kk'	$\alpha\beta$					
	aa	ab	ac	bb	bc	cc
L_{II}	-0.4584	0	0	-0.4584	0	1.9168
L_{IS}	0.4813	0	0	0.4813	0	0.03744
L_{SS}	0.2191	0	0	0.2191	0	0.5618

Table Eight iii.   Averaged Lorentz sub-Tensors for SbI_3*3S_8

kk'	$\alpha\beta$					
	aa	ab	ac	bb	bc	cc
L_{II}	-0.4254	0	0	-0.4254	0	1.8508
L_{IS}	0.4796	0	0	0.4796	0	0.0407
L_{SS}	0.2191	0	0	0.2191	0	0.5618

It is noteworthy that the size of the differences between equivalent Lorentz-tensor elements of the different complexes are small. Also, within this range, there is a diminishing trend in the absolute size of L_{II} elements across the series. As mentioned for the supermolecule Lorentz-Factor tensors, this might simply be due to change in unit cell size. Curiously, however, there is no consistent trend in L_{IS} elements. The larger $L_{IS}(1,1)$ for AsI_3*3S_8 is probably due to the fact that AsI_3 actually has a larger spread in the ab plane, yet the unit cell is a little smaller in this dimension.

Local-field-factor tensors d_I and d_S calculated with the *LFT-Composite* Method through the use of Eqs (15) are shown in Tables Nine. A quantity, $d_{'cell'}$, is also included. This is the appropriate weighted average of d_I and d_S and is provided so that all of the local-field tensors generated by the various methods of this Chapter may be compared.

Table Nine i.   Local-Field factor tensor for CHI_3*3S_8

k	aa	ab	ac	bb	bc	cc
d_I	2.2185	0	0	2.2185	0	2.4734
d_S	2.4572	0	0	2.4572	0	2.2028
$d_{'cell'}$	2.233	0	0	2.233	0	2.270

Table Nine ii.   Local-Field factor tensor for AsI_3*3S_8

k	aa	ab	ac	bb	bc	cc
d_I	1.7434	0	0	1.7434	0	3.1970
d_S	2.6207	0	0	2.6207	0	2.1513
$d_{'cell'}$	2.226	0	0	2.226	0	2.413

Table Nine iii.   Local-Field factor tensor for SbI_3*3S_8

k	aa	ab	ac	bb	bc	cc
d_I	1.6254	0	0	1.6254	0	3.4789
d_S	2.6676	0	0	2.6676	0	2.1614
$d_{'cell'}$	2.228	0	0	2.228	0	2.491

Local field factors at the sulfur molecule indicate a reasonably isotropic environment - although components are a little larger in the xy (a,b) plane. The d_S are relatively constant across the series although it is curious that the d_S cc element for AsI_3*3S_8 is not part of a trend as is the case for other elements. For the factors at the RI_3 molecule, however, one can see that the d_I sub-tensor is very polarised (though not as much as the d in the supermolecule treatment). A trend in polarisation toward the cc(33) component of d_I across the series is also observed and this goes against the weaker opposite trend for d_S. This reflects the significantly different complexed-molecular geometries. There is a large difference between d components of the iodoform and antimony complexes which is also due to the smaller linear susceptibility of the CHI_3*3S_8 crystal.

Finally, the nonlinear susceptibilities are presented in Table Ten. In calculating these, two geometric factors needed to be considered. For the 11 component coming from the sulfur molecules, one must multiply the individual molecular response by:

$$1+2\cos 30 = 2.732$$ (rather than 3.0) due to their relative orientations in the xy plane. The orientation of the sulfur molecule with respect to the trigonal axis is also important. From the crystal structures, the plane of the sulfur ring is almost perpendicular to this axis in each of these compounds and so no correction need be applied to the 33 component.

Table Ten:

Adduct	$\chi^{(2)}_{111}$ $(\times 10^{-12} mV^{-1})$	$\chi^{(2)}_{333}$ $(\times 10^{-12} mV^{-1})$
$CHI_3 * 3S_8$	12.3	2.7
$AsI_3 * 3S_8$	3.7	5.02
$SbI_3 * 3S_8$	3.2	4.0

These NLO susceptibilities are not skewed toward a particular tensor element as was the case for those from the other methodologies. They are also larger and thus more realistic. They are discussed in context with the other results in the next Chapter.

REFERENCES

1a.   J. Zyss and D.S. Chemla in; *Nonlinear Optical Properties of Organic Molecules and Crystals.* eds D.S. Chemla and J. Zyss, (Academic Press, 1987);

1b.   J. Zyss and J.L. Oudar, Relations between microscopic and macroscopic lowest-order optical nonlinearities of molecular crystals with one- or two-dimensional units. *Phys.Rev.A,* **26**, 2028 (1982)

2a.   C.J.F. Böttcher, *Theory of Electric Polarisation* Vol. 1 (Elsevier, 1973);

2b.   C. Kittel, *Introduction to Solid State Physics.* 6th ed (Wiley, 1986)

3.   B.F. Levine and C.G. Bethea, Second- and third-order hyperpolarisabilities of organic molecules. *J.Chem.Phys.,* **63**, 2666 (1975)

4a.   T. Bjorvatten, Crystal structure of the 1:3 addition compound iodoform-sulfur (CHI_3*3S_8). *Acta.Chem.Scand.,* **16**, 749 (1962);

4b.   T. Bjorvatten, O. Hassel and A. Lindheim, Crystal structure of the addition compound SbI_3*3S_8. *Acta.Chem.Scand.,* **17**, 689 (1963)

5a.   J.H. Meyling, P.J. Bounds and R.W. Munn, Breakdown of the anisotropic Lorentz approximation in *p*-terphenyl. *Chem.Phys.Lett.,* **51**, 234 (1977);

5b.   M. Hurst and R.W. Munn, Theory of molecular opto-electronics IV -prediction of $\chi^{(2)}$ for *meta*-nitroaniline. *J.Mol.Electron.,* **2**, 139 (1986);

5c.   R.W. Munn, Theory of molecular opto-electronics IX: Calculation of $\chi^{(2)}$ from theoretical hyperpolarisabilities for DAN. *Int.J.Quant.Chem,.* **43**, 159 (1992)

6a.   R.W. Munn, Theory of molecular opto-electronics: from the molecule to the crystal. *J.Mol.Electron.,* **4**, 31 (1988);

6b.   M. Hurst and R.W. Munn, Theory of molecular opto-electronics I -macroscopic and microscopic response. *J.Mol.Electron.,* **2**, 35 (1986);

6c.   M. Hurst and R.W. Munn, Theory of molecular opto-electronics II -environmental effects on molecular response. *J.Mol.Electron.,* **2**, 43 (1986);

6d.   M. Hurst and R.W. Munn, Theory of molecular opto-electronics III -effect of molecular elongation. *J.Mol.Electron.,* **2**, 101 (1986);

6e.   R.W. Munn, Delocalisation and dimensionality effects on local electric fields in molecular materials. *Synth.Metals,* **64**, 117 (1994);

6f.   R.W. Munn, Electric dipole interactions in molecular crystals. *Mol.Phys.,* **64**, 1 (1988)

7a.   D.A. Dunmur, The local electric field in anisotropic molecular crystals. *Mol.Phys.,* **23**, 109 (1972);

7b.   P.G. Cummins, D.A. Dunmur R.W. Munn and R.J. Newham, Applications of the Ewald method I -calculation of multipole lattice sums. *Acta Cryst.,* **A32**, 847 (1976)

8a.   P.G. Cummins, D.A. Dunmur and R.W. Munn, The effective molecular polarisability and local electric field in molecular crystals. *Chem.Phys.Lett.,* **22**, 519 (1973);

8b.   F.P. Chen, D.M. Hanson and D. Fox, The effective polarisability and local electric field in molecular crystals. *Chem.Phys.Lett.,* **30**, 337 (1975);

8c.   R.W. Munn, R.J. Phillips and C.J. Eckhardt, Dielectric theory of weak charge-transfer crystals I -effective polarisabilities. *Chem.Phys.,* **135**, 1 (1989)

9a. P.J. Bounds and R.W. Munn, Effective molecular polarisabilities in some aromatic hydrocarbon crystals. *Chem.Phys.*, **24**, 343 (1977);

9b. A.H. Price, J.O. Williams and R.W. Munn, Dielectric tensors, effective polarisabilities and local electric field in pyrene crystals. *Chem.Phys.*, **14**, 413 (1976);

9c. F.P. Chen, D.M. Hanson and D. Fox, Molecular crystal spectral: The effective molecular polarisability and local electric field. Durene and naphthalene. *J.Chem.Phys.*, **63**, 3878 (1975)

10. P.J. Bounds and R.W. Munn, *Chem.Phys.*, **39**, 165 (1979)

CHAPTER FIVE

Through the use of experimental and theoretical methods described in the previous chapters, coefficients describing the macroscopic NLO responses for RI_3*3S_8 crystals are now available. It is now possible to examine how *microscopic* NLO properties of the RI_3 molecules give rise to the *bulk* NLO response of the adduct crystals. It is possible to identify effects responsible for differences in $\chi^{(2)}$ structure between members of this series of complexes.

An overall similarity of microscopic NLO response was noted in Chapter Three upon cursory inspection of computed hyperpolarisabilities of the RI_3 molecules. This suggested that investigation of other factors explaining $\chi^{(2)}$ anisotropy differences was warranted. The possible suggestions for this phenomenon that were mentioned in Chapter One are now discussed in this Chapter.

This Chapter is structured as follows:

1. <u>Results are assembled</u> from each section of this study:
    - Computed hyperpolarisabilities for the isolated RI_3 molecules are listed.
    - NLO susceptibility estimations from the Anisotropic Lorentz Approximation and Lorentz Factor Tensor - Supermolecule, Full and Composite Methods are tabulated.

2. <u>The Methodology</u> which was outlined in Chapter One to resolve the question of differing $\chi^{(2)}$ anisotropies in these complexes is followed:
    - Comparisons are made of the anisotropies of 'constructed' and measured NLO susceptibilities and of the computed RI_3 hyperpolarisabilities.
    - The contribution to the crystal NLO response from the sulfur molecule is considered.
    - Absorption spectra of the complexes and the issue of anisotropic resonance enhancement is discussed.
    - The local-field-factor tensors calculated in Chapter Four are inspected.

3. <u>Further questions</u> arising from these results are discussed. For example, the importance of the consideration of the environment in which the NLO active molecules exist is an issue raised by the results of this study.

4. <u>Errors and uncertainties</u> are discussed.

Assembly of Results

In Table One, calculated hyperpolarisability tensor components for each of the triiodide molecules are presented together with the NLO susceptibilities measured for the octa-sulfur adducts and the $\chi^{(2)}$ predicted for these complexes using the techniques described in Chapter Four.

1.   PRELIMINARY OBSERVATION

As discussed in Chapter Three, the hyperpolarisability tensor for AsI_3 calculated at the MP2 level using (large) Pople basis sets was most unusual. In units of 10^{-40} m^{4}V^{-1}, it was $\beta_{333} \approx 5.0$ and $\beta_{111} \approx 1.7$
A β_{333} as large as this actually yields a $\chi^{(2)}$ in very good agreement with experiment, but it is felt that the very large difference in β anisotropy is anomalous and thus the elements returned by the MP2/D95 calculation (as used for SbI_3) are used here.

2.   SIZE OF PREDICTED SUSCEPTIBILITIES

Comment is warranted on the absolute size of the predicted susceptibilities as compared to the measured $\chi^{(2)}$ tensor elements. One notices from Table One that the experimental components are significantly larger than their computed counterparts. Since the local-field effects should be fully accounted for, the following are possible reasons for this observation:

- Underestimation of calculated β will carry through to give underestimates of predicted $\chi^{(2)}$. Neglect of non-zero frequency consideration in the computation of hyperpolarisabilities probably results in an underestimation of the size of β - as discussed in Chapter Three. There may also be a 'residual underestimation' of β by the ab initio routine.

- The local field factor tensor, d, used in the calculation of $\chi^{(2)}$ with the LFT methods are those for the fundamental wavelength although in fact, one of the factors should be for the frequency of the harmonic beam and this will be larger at 2ω frequency.

- It might be that $\chi^{(2)}$ elements are generally enhanced because of the nearby electronic resonance. Differing resonance enhancement for different $\chi^{(2)}$ elements is expected to occur as is discussed later but a general enhancement may also exist.

Table One: i-iii

CHI_3 Ab Initio Hyperpolarisabilities $\beta_{333} \approx 0.6$ $\beta_{111} \approx 2.4$ $\times 10^{-40}\ m^4 V^{-1}$	ALA	$\chi^{(2)}$	
		333	0.39pm/V
		111	3.82pm/V
	LFT supermolecule	$\chi^{(2)}$	
		333	2.7pm/V
		111	0.8pm/V
	LFT Full	$\chi^{(2)}$	
		333	1.17pm/V
		111	3.33pm/V
	LFT Composite	$\chi^{(2)}$	
		333	2.7pm/V
		111	12.3pm/V
	EXPERIMENT*	$\chi^{(2)}$	
		333	4.6pm/V
		111	42pm/V

AsI_3 Ab Initio Hyperpolarisabilities $\beta_{333} \approx 1.1$ $\beta_{111} \approx 1.7$ $\times 10^{-40}\ m^4 V^{-1}$	ALA	$\chi^{(2)}$	
		333	0.84pm/V
		111	2.86pm/V
	LFT supermolecule	$\chi^{(2)}$	
		333	5.1pm/V
		111	0.7pm/V
	LFT Full	$\chi^{(2)}$	
		333	2.44pm/V
		111	2.56pm/V
	LFT Composite	$\chi^{(2)}$	
		333	5.0pm/V
		111	3.7pm/V
	EXPERIMENT	$\chi^{(2)}$	
		333	23pm/V
		111	52pm/V

SbI_3 Ab Initio Hyperpolarisabilities $\beta_{333} \approx 0.7$ $\beta_{111} \approx 2.6$ $\times 10^{-40}\ m^4 V^{-1}$	ALA	$\chi^{(2)}$	
		333	0.55pm/V
		111	4.3pm/V
	LFT supermolecule	$\chi^{(2)}$	
		333	3.9pm/V
		111	0.9pm/V
	LFT Full	$\chi^{(2)}$	
		333	1.55pm/V
		111	4.1pm/V
	LFT Composite	$\chi^{(2)}$	
		333	4.0pm/V
		111	3.2pm/V
	EXPERIMENT	$\chi^{(2)}$	
		333	22.6pm/V
		111	16.2pm/V

---

* As described in Chapter Two, there was some uncertainty about the coherence length for the experimental geometry measuring the 333 component of $\chi^{(2)}$ for $CHI_3 * 3S_8$. This is around 6pm/V if the larger value of l_c is used.

- There is a possibility that the 'effective' hyperpolarisability of the unit cell is increased by the presence of the CT interaction between the sulfur and iodine atoms. This might be expected to increase the NLO response in each of the tensor elements - perhaps by more in the I_3 plane.

- The occurrence of field-induced effects may lead to enhancement of bulk NLO response. Such effects were described in Chapter One; polarisation of the NLO-phore molecule by reaction and permanent local (dipole) fields could lead to increase in β.

- The RI_3 molecular geometry as it exists in the adduct crystal is slightly different to the free-molecule geometries used for ab initio β calculation. The hyperpolarisabilities of these may be different.

The absolute sizes of the predicted coefficients show they are not excessively underestimated. For $CHI_3 \cdot 3S_8$ the predicted $\chi^{(2)}$ are too small by a factor of ≈ 4 and for $SbI_3 \cdot 3S_8$ by a factor of ≈ 5. It is relevant to note that in many studies where comparison is made between computed β and those determined by EFISHG [1], similar discrepancies have been noted.

It is interesting to put these constructed susceptibilities in context with other predictions of homomolecular crystal $\chi^{(2)}$ from free molecule hyperpolarisabilities. These were all for organic molecular crystals (in which molecular and crystal axes did not coincide). In each case, a significant difference was noted between the anisotropy of the LFT local field tensor as compared to the ALA field factor. There were also off-diagonal elements in the LFT and local field factor tensor.

Hurst and Munn performed such calculations in 1986 for _m_-nitroaniline [2a]. Hyperpolarisabilities computed using the CNDO semi-empirical method were used and the molecule was treated as three sub-molecules. They noted that their (nominally) zero frequency 'constructed' NLO susceptibility was in fairly good agreement with experimentally determined values. The 311 element was, however, underestimated by about a factor of three.

The same group later calculated $\chi^{(2)}$ tensors for MBANP and NMBA[1] again using CNDO hyperpolarisabilities [2b]. These were also smaller than experimental results although there was some uncertainty in the conversion of calculated $\chi^{(2)}$s

---

[1] 2-(α-methyl benzylamino)-5-nitropyridine and 4-nitro-4'-methyl(benzylidene aniline) respectively.

in the **a, b, c*** axis system to the measured $d_{I,J,K}$ coefficients.   A general agreement was attained for NMBA whereas for MBANP it was very poor.   The quality of the CNDO hyperpolarisabilities was questioned.

The 4-(*N,N*-dimethylamino)-2-acetamido-nitrobenzene (DAN) molecular crystal was studied by Munn in 1992 [2c] also using CNDO hyperpolarisabilities.   In this case, the agreement with experimental $\chi^{(2)}$s was not nearly as good -the theoretical value was 2-6 times too small and not account for the anisotropy. The possibility was noted, however, that for this system, intermolecular hydrogen bonding is important between certain functional groups and that this is not accounted for in the CNDO βs.   This issue is relevant to the present case *i.e.*, molecular charge distributions and hence their NLO response may be significantly different in the crystal environment as compared to the free molecule. Such differences are almost impossible to accurately reproduce - even with modern ab initio computational techniques.   Perhaps the greater mismatch reported here is due in part to an analogous neglect of the S--I charge transfer interaction.

For the reasons outlined earlier, the discrepancy in absolute size of $\chi^{(2)}$ elements is regarded with only mild concern.   This margin is the same as that seen for the $\chi^{(2)}$ predictions for the DAN molecular crystal discussed earlier this chapter. Rather, the relatively close agreement in anisotropy seen for the two non-absorbing complexes is gratifying.

Following the Methodology

1.   *Comparison of COMPUTED HYPERPOLARISABILITIES*

The computed β tensors for each of the RI_3 molecules are compared in accordance with the methodology outlined in Chapter One.   It is seen that the NLO response for the isolated molecules is largest in the I_3 plane for each triiodide.   The SbI_3 and CHI_3 molecules have very similar predicted hyperpolarisabilities which is perhaps a little curious given their differing

geometries and the difference in chemical nature of the R-group. Arsenic triiodide has a significantly different anisotropy of its computed hyperpolarisability to that of the other RI_3 molecules.

This suggests that any differences between the NLO properties of CHI_3*3S_8 and SbI_3*3S_8 adducts must be due to;

- differing local field corrections applying in these crystals.
- differing resonance enhancements for the $\chi^{(2)}$ elements of the two complexes.
- that an NLO response from the sulfur molecule contributes to the two lattices but by differing extents.
- it might be that different field-induced effects operate in these crystals. Geometry and β changes could be sensitive to permanent local fields which may be quite different.
- differing non-local effects may occur in these crystals, including CT interaction strength which may influence β.

Conversely, the different hyperpolarisability tensor determined for AsI_3 means that inherent RI_3 β difference *may* solely explain the differences in $\chi^{(2)}$ for the AsI_3*3S_8 adduct. This is unlikely given that other effects must be acting to cause the $\chi^{(2)}$ differences between the other adducts. The β tensor differences of AsI_3 will of course play a role in the $\chi^{(2)}$ differences exhibited by this complex.

2.   *Comparison of MEASURED $\chi^{(2)}$ WITH COMPUTED HYPERPOLARISABILITIES*

In Chapter One, this comparison was proposed as being useful in indicating if a set of local field factors operated consistently across this adduct series. Such a demonstration would mean that Hypothesis Two (in which $\chi^{(2)}$ tensor differences in the series are mostly due to β and local field factor tensor differences) does not apply.

The $^{11}/_{33}$ anisotropies of both computed RI_3 hyperpolarisabilities and of measured RI_3*3S_8 $\chi^{(2)}$ are shown for each RI_3/RI_3*3S_8 pair in Table Two.

Table Two

	Computed β_{11}/β_{33}	Experimental $\chi_{11}^{(2)}/\chi_{33}^{(2)}$
CHI_3*3S_8	4.0	9.1
AsI_3*3S_8	1.5	2.3
SbI_3*3S_8	3.7	0.72

From these results, it is evident that the differences between hyperpolarisability and NLO susceptibility anisotropies vary greatly between the RI_3 / RI_3*3S_8. Therefore it is not possible to rule out Hypothesis Two as a cause. It does not *necessarily* mean that Hypothesis Two is important, as a consistent anisotropy difference may be masked by resonance effects or $\chi^{(2)}$ contributions from S_8. This evidence implies that local field factor differences and/or resonance enhancement differences and/or S_8 contribution differences explain experimental $\chi^{(2)}$ anisotropy differences in this series (and so is no more conclusive than the previous comparison of β tensors).

An apparent trend in the anisotropies of experimental RI_3*3S_8 susceptibilities is not replicated in the anisotropy of calculated hyperpolarisabilities of the isolated RI_3 molecules. In this regard, the earlier result of Samoc *et al* [3] has been confirmed, namely, the computed anisotropy of the gas-phase SbI_3 molecule's NLO response is very different to that which was measured in the octasulfur adduct. This is in contrast with the agreement seen between such anisotropies for CHI_3 and CHI_3*3S_8 - a result also confirmed by the experimental and theoretical results of this work.

3. Comparison of PREDICTED $\chi^{(2)}$ WITH MEASURED $\chi^{(2)}$

Constructed susceptibilities determined using each of the methods outlined in the last chapter are now examined and compared with the experimentally derived coefficients. These comparisons may show that only β and local-field-factor differences dictate $\chi^{(2)}$ tensor differences if good agreement is seen with one of the methods.

i. The $\chi_{11}^{(2)}/\chi_{33}^{(2)}$ ratios using $\chi^{(2)}$ elements predicted using the ALA model are presented in Table Three. Comparing these firstly with the β_{11}/β_{33} ratio, one can see that in each case, the anisotropy of $\chi^{(2)}$ is about twice that of the

hyperpolarisability. This occurs because three ALA f factors appear with β in the expression for computing $\chi^{(2)}$ (Eq (1) in Chapter Four) and all have similar anisotropies - large elements in the xy plane and smaller elements perpendicular to this. Therefore, this treatment exacerbates the anisotropy of $\chi^{(2)}$. The combination of $f_\omega f_\omega f_{2\omega}$ multiplied by β leads to an increase in the anisotropy of a factor of about two in this case - the exact amount depends on crystal birefringence (dictating f anisotropy) and the anisotropy of the computed β.

Table Three

	Computed β_{11}/β_{33}	ALA $\chi^{(2)}_{11}/\chi^{(2)}_{33}$	Experimental $\chi^{(2)}_{11}/\chi^{(2)}_{33}$
CHI_3*3S_8	4.0	9.8	9.1
AsI_3*3S_8	1.5	3.4	2.3
SbI_3*3S_8	3.7	7.8	0.72

This model deems the NLO response of the adduct crystal to be much stronger in the plane of the iodine atoms than perpendicular to it. While this was theoretically predicted to be the case for the free molecules, such a result is not necessarily plausible for the $\chi^{(2)}$ of the adduct crystals in general. This is evident from the measured susceptibilities. Another noteworthy point is the comparison between ALA-derived $\chi^{(2)}_{11}/\chi^{(2)}_{33}$ ratios and measured $\chi^{(2)}_{11}/\chi^{(2)}_{33}$ ratios. There is a reasonable agreement in these anisotropies for CHI_3*3S_8, a scant and uncertain agreement for AsI_3*3S_8 and none at all for SbI_3*3S_8 (the ALA prediction is even of the wrong sense). Some pattern might have been expected if there was a systematic error introduced by this method.

As indicated in the last chapter, the ALA model is known to misrepresent the local field acting at the NLO active centre (which is unspecified using this method) and the agreement in the anisotropy that is seen for CHI_3*3S_8 is therefore considered to be coincidental. The comparison of these $\chi^{(2)}$ tensors with measured NLO susceptibilities is seen to be unable to provide information on the question of differing measured $\chi^{(2)}$ tensor anisotropies.

ii.   Susceptibilities predicted using the Lorentz-Tensor method for an adduct structure approximated as comprising three super-molecules per hexagonal

unit cell were potentially more promising[2]. From first glance one notes that the anisotropy of these $\chi^{(2)}$ tensors is opposite to that determined by the ALA method. This result is a rather dramatic change from the previous case and it is also unrealistic. It is also curious in being completely different to the anisotropy of the calculated hyperpolarisabilities[3]. It is, however, able to be explained if these susceptibilities are instead regarded as showing very suppressed $\chi^{(2)}_{11}$ elements and/or slightly enhanced $\chi^{(2)}_{33}$ elements.

Such a skewed $\chi^{(2)}$ anisotropy can in fact be predicted when modelling the structure as supermolecules. The problem can be seen to stem from two errors introduced in the determination of the Lorentz factor tensor:

♦   The determination of $L_{kk'}$ considers fields at each submolecular point from each submolecular lattice. It then subtracts fields at submolecules from submolecules within the same molecule to prevent self-polarisation effects being simulated. Thus in a supermolecule specification the electric fields calculated at submolecules 'S_{av}' due to R and I submolecules (and vice versa) are actually excluded. Yet for accurate consideration of the NLO response of the RI_3 molecule it is important to account for lattice points most closely surrounding this 'NLO-phore' molecule. This is true above and beyond any consideration of a CT interaction between these molecules. The sulfur-iodine (CT) axis in these structures is closest to the crystallographic xy plane (especially for CHI_3). Thus, it is fields in the xy plane that are largest[4] between these submolecules and these are ignored from the submolecular-averaged Lorentz-factor tensor determination. Because, the tensor is normalised, such components are 'diluted' and too small in the resultant averaged Lorentz tensor and conversely, the z or 33 elements are a little overestimated.

♦   As well as this shortcoming, treating the S_8 ring as a single submolecule further causes 11-component diminishment. The increased distance of the center sulfur submolecule from the RI_3 molecule as compared to the actual I--S

---

[2]   comprised of seven equally-polarisable atoms (sub-molecules) at the R, I and S_8 ring center positions. This is a homo-molecular description of the structure.

[3]   This is not at all impossible. That a NLO susceptibility has a different anisotropy to the corresponding hyperpolarisability is not surprising in light of the similar relation between α and $\chi^{(1)}$ anisotropies in molecular crystals (it may even be opposite).

[4]   From basic electrostatics, the field in a plane or along a line containing dipoles arranged with their dipole vector in that plane is large and positive and is negative and decays quickly perpendicular to it. For a linear or planar array of dipoles with their dipole vectors aligned perpendicular to the plane, the field in the plane is smaller than in the former situation and still decays rapidly perpendicular to the plane [4].
        The situation in the supermolecule is such that the R-I-S axis is nearly linear and oriented much closer to the 1,2 crystal plane than to the 3 axis. Thus, field application in the x and y direction resembles the former situation more closely than the latter, resulting in large (1,1) and (2,2) components between submolecules on this R-I-S line. Fields applied in the z direction more closely resemble the latter situation meaning smaller (3,3) components. This is borne out from the *LFT-Composite* work described in the previous chapter in which such an anisotropy is observed for the L_{IS} sub-tensor.

distance in the adduct means that field contributions between point dipoles lying on S atoms and on I atoms (within different molecules) will be smaller. As just discussed, it is the 11 component which will most affected. It is suggested that this effect is of secondary importance to the previous point.

Because of this aberration, these 'LFT Supermolecule' tensors are not of use for comparative purposes with measured $\chi^{(2)}$ but it is interesting to note the effect of using a supermolecule cell specification for these heteromolecular crystals. It may generally be the case that $\chi^{(2)}$ for such charge-transfer complexes is poorly predicted when modelled in this way. A similar effect was noticed when employing a supermolecule specification in the work predicting effective polarisabilities in CT complexes of anthracene [5].

iii. It is evident that $\chi^{(2)}$ tensors attained where unit-cell atomic positions are fully parameterised do not appear unduly biased to either 33 or 11 element. They are still an incomplete parametrisation due to the neglect of molecular polarisability in the determination of d but they incorporate explicit local field calculation for the actual adduct structure and so are a large improvement over the ALA results.

For the iodoform complex, the computed anisotropy is of the correct sign but is not as large as the measured $\chi^{(2)}$ anisotropy. For $AsI_3 \cdot 3S_8$ also, this method predicts a quite different (smaller) anisotropy than is seen experimentally. For the antimony complex, this model leads to prediction of a dominant $\chi^{(2)}_{11}$ element whereas a larger $\chi^{(2)}_{33}$ is observed.

Despite the problems with the first two construction methods and the limitations of this one, it can reasonably be said that the agreement mentioned earlier with measured NLO susceptibility anisotropies is not apparent. This would mean that it is not *solely* inherent β tensor differences in combination with local field differences that explain the phenomenon of differing $\chi^{(2)}$ anisotropies in these complexes. The corollary to this is that one or more of the other factors mentioned must be playing a part.

Interestingly, one can see from this comparison that the anisotropies of *LFT-Full* $\chi^{(2)}$ tensors roughly imitate the β tensors (at least $\chi^{(2)}_{FULL}$ anisotropies are more like those of β than $\chi^{(2)}_{MEAS}$). This provides further independent evidence that local-field-factor differences across the series are not so different as to be able to explain the large $\chi^{(2)}$ tensor differences.

4.   *SUMMARY OF COEFFICIENT COMPARISONS*

Overall, the comparisons that have been discussed have returned rather inconclusive answers:

- The comparison of computed RI_3 hyperpolarisabilities both within the adduct series and with experimental $\chi^{(2)}$ tensors led to the conclusion that more than just β differences between the triiodide molecules are needed to explain the $\chi^{(2)}$ tensor differences.

- The final comparison was more conclusive, suggesting that local-field-factor differences across the series do not play a major role in explaining this.

Thus, the other techniques suggested in the Methodology are now examined for clues as to the importance of the alternative explanations.

5.   *SULFUR CONTRIBUTION*

The *LFT-Composite* method is an extension of the *LFT-Full* method in which the microscopic NLO response of S_8 is incorporated into the NLO-susceptibility prediction. The idea behind the use of such an approach was that if the $\chi^{(2)}$ elements thus yielded were in good agreement with experimental adduct susceptibilities, then this would strongly suggest that the hyperpolarisability of the sulfur molecule is important in determining the appearance of the adduct $\chi^{(2)}$ tensor. This importance would, of course, be in combination with proper consideration of the β of the RI_3 molecule and the appropriate local-field-factors for the particular adduct structure.

One sees upon inspection of these *LFT-Composite* $\chi^{(2)}$ tensors that the agreement with measured NLO susceptibilities is much better than for previous constructed tensors. This is attributed to two factors. The first is the effect of the addition of the NLO response of the sulfur molecules. The other is that local-field-factors are much more realistic through full representation of the complex in distinct molecular components (as with the *LFT-Full* method) and that in this case, polarisability contributions to d from both molecules are included.

149

The *LFT-Composite* $\chi^{(2)}$ anisotropy computed for the iodoform complex is about half that of the experimentally derived tensor. The $^{11}/_{33}$ ratios are ~4.5 and 9 respectively, although this latter ratio is reduced to 7 if the alternative $\chi^{(2)}_{33}$ element is used. This agreement is quite good. For the arsenic complex the agreement is poor, $^{11}/_{33}$ is ~0.75 for the constructed $\chi^{(2)}$ tensor and 2 for the measured $\chi^{(2)}$. In this case, however, it is believed that there is a significant resonance enhancement of the $\chi^{(2)}_{11}$ element - this will be addressed later. For $SbI_3 {*} 3S_8$, the predicted $\chi^{(2)}$ anisotropy is 0.8 versus the measured 0.7. This is a very good agreement although these values can be expected to be a little further apart after consideration is made of weak absorption at 532nm, leading to weak enhancement of the $\chi^{(2)}_{11}$ element. This was also the only method which correctly predicted the sense of the anisotropy for this adduct.

In using this method, the assumption was made that the ρ of the adduct crystal -the ratio of polarisabilities of the different molecules in the unit cell- was approximately equal to the ratio between the susceptibilities of S_8 and RI_3 crystalline compounds. How this affects the anisotropy of the constructed $\chi^{(2)}$ is not clear. This is especially so for χ_S because the orientations of S_8 molecules do not map exactly between the adduct and homo-molecular crystal structures[5]. It might be expected, however, that by taking the susceptibilities of orthorhombic sulfur for the scalar average, χ_S, the anisotropy of the S_8 lattice in these crystals is somewhat underestimated. In any case, the effective estimated anisotropy used in the $\chi^{(2)}$ calculation is zero, due to the susceptibilities being averaged over all crystallographic axes. This will lead to a slight underestimation of the $\chi^{(2)}$ anisotropy. This can be seen by looking at the d_k tensors for the individual RI_3 and S_8 lattices comprising the adduct crystal.

Another interesting aspect may be noted from the *LFT-Compo* $\chi^{(2)}$ results. It appears that the metal triiodide adducts seem to have a similar *non-resonant* NLO response. It is interesting to realise that this arises because the differing hyperpolarisabilities and sulfur contributions (and to a small extent, the local-field-factors) coincidentally combine to create this similarity. If faced with just the bulk responses, it would be impossible to work backwards to predict the actual RI_3 and S_8 contributions for each adduct - which are clearly quite different.

---

5   In the orthorhombic S_8 crystal, the 16 molecules in the unit cell are arranged with one axis of the mean-ring-plane parallel to the c-axis [6]. The axis perpendicular to this plane is aligned along (but not parallel to) the a axis. Molecules are aligned with opposite orientations of their mean-ring-plane axes (ie, they do not all lie 'flat' in a crystal plane as is the case in the adduct crystals). The anisotropy in $\chi^{(1)}$ would be expected to be larger if the latter arrangement applied.

The significant NLO response of the sulfur molecules in the CHI_3*3S_8 lattice appears to be due to appreciable geometry distortions induced in this molecule in this complex and this is discussed later.

Sulfur Conclusion

Apart from the AsI_3*3S_8 complex, NLO susceptibility anisotropies calculated with this LFT method are in good agreement with those derived experimentally. With respect to the overall question, this result provides very strong evidence that the Fourth Hypothesis of the Chapter One methodology is most important, namely, sulfur (donor molecule) contributions *do* matter.

6.   *CONSIDERATION OF ABSORPTION*

The presence of molecular electronic resonances will cause absorption of either fundamental or second harmonic radiation. This can have a profound effect on the observed nonlinear optical effect. Certain NLO processes may be advantaged[6], however, such effects are generally unwanted in more fundamental studies due to the uncertainty they introduce [7]. The losses due to absorption of harmonic radiation were mentioned in Chapter Two.

These complexes are yellow or orange-yellow and thus absorb slightly at the harmonic wavelength of this study - 532nm. This is shown in Appendix Two in diffuse reflectance spectra which were measured on powders of the complexes. It is evident from these that the arsenic compound is much more absorptive at 2ω than the antimony and iodoform complexes. AsI_3*3S_8 was further examined by measuring polarised absorption spectra for single crystals of this complex. A strong dichroism at 2ω is observed with A at 532nm is about 3.5 times as great in the xy plane - though this figure is uncorrected for scattering and reflection differences. It is reasonable to presume that the CHI_3*3S_8 and SbI_3*3S_8 complex crystals exhibit similar polarised absorption behaviour.

It is possible therefore, that the higher $\chi^{(2)}$s seen for AsI_3*3S_8 are attributable to an effective hyperpolarisability enhancement stemming from the proximity of the

---

6   For example, third order effects such as third harmonic generation and intensity-dependent refractive index changes can also be significantly enhanced in the region of electronic resonances - they are also needed in anomalous-dispersion phase-matching [8].

(fundamental two-photon) resonance in this material. Two photon absorption as a material property is actually given by the imaginary part of the *third-order* susceptibility; $\chi^{(3)}(-\omega;\omega,\omega,-\omega)$. The resonance itself may affect other NLO processes such as frequency mixing - as is noticed here.

Most importantly for the question of $\chi^{(2)}$ anisotropies, the strongly polarised nature of this absorption can account for the even larger NLO response in the xy plane (see Table One) which was greater-than-predicted by the LFT-Compo method just discussed.

In principle, it is possible to roughly estimate the extent of this resonance enhancement by using the relations mentioned in Chapter One, Eqs (7) & (9) for two- and three-level system approximations (2LS & 3LS) respectively. The 2LS is appropriate for the vector part of β whereas the 3LS is needed to examine resonance effects on β tensor elements of octupolar character.

In practise, however, it is not possible to determine λ_{max} and thus ω_{nm} or f from the reflection spectra of the complexes. Solution spectra of RI_3 are unsatisfactory due to very different absorption characteristics in the different environments. Furthermore, rapid decomposition results in interference from I_2 absorption. No estimates are available for the transition dipole moments needed for the 3LS expression. For these reasons, such an estimation was not possible, however, if one considers the *LFT-Composite* $\chi^{(2)}_{11}$ element as $\approx$4-5 times smaller than the nonresonant $\chi^{(2)}$ (as it seems to be for the other adducts), this would mean a resonance enhancement of about three times which is plausible. Such an effect greatly overwhelms the underestimation ($\approx$9%) of this element that was caused by the neglect of absorption of second harmonic radiation.

Due to this resonance, $AsI_3 \cdot 3S_8$ was less useful for examining the relationship between electronic (non-absorptive) and structural properties and the NLO susceptibility in these adducts. It is possible that the different absorption characteristics for this complex are connected to a slightly different CT interaction, however, there is no supporting evidence for this from the interatomic distances given by the X-ray structures.

7. *EXAMINATION OF TENSORS*

It was suggested in Chapter One that further insight into the cause for the anisotropies of $\chi^{(2)}$ tensors could be obtained by looking at the anisotropies of the local-field-factor tensors. In this section, those d determined using the *LFT-Full* and *LFT-Composite* methods are examined.

The evidence to this point suggests that differing local-field-factor tensors for each of these complexes *is not* a major explanation for their observed differing NLO susceptibilities. This is corroborated by the calculated *LFT-Full* d tensors which show small (<5%) and relatively uniform change across the RI_3*3S_8 series (see Tables Six i-iii of Chapter Four). Turning to the $d'_{cell'}$ calculated using the *LFT-Composite* method, again one notices only small changes in the tensor elements across the series: for the 33 component, it varies by $\approx 9\%$ and remarkably, for the 11 component the local field factor is virtually the same for each adduct.

Other points arise from this analysis. The individual contributions from d_I and d_S are evident from the determination of $d'_{cell'}$ using the *LFT-Composite* method. It is remarkable to see that the rather isotropic 'unit cell' local field factor tensor comes about from the averaging of *one* d_I tensor which is strongly weighted in 33 elements, with *three* d_S tensors weighted toward 11 elements. Inspection of individual d_k tensors shows some differences between the various lattices, for example, the 33 component of d_I for CHI_3*3S_8 is very much smaller than those for SbI_3*3S_8 or AsI_3*3S_8 and conversely, the 11 components are much larger. This is to be expected since the latter two adducts have a more similar structure whereas CHI_3*3S_8 has a 'flatter' form (see scale pictures in Figure Six of Chapter One).

The lattice of S_8 molecules is of different dimensions in each adduct. This is expected, given the RI_3 geometry differences. This leads to only a fairly small spread in d_S across the series. Presumably, that the size and anisotropy of d_S (opposite to d_I) almost cancels the anisotropy of d_I is coincidental.

8 .   IN SUMMARY

<u>Firstly, with respect to the central $\chi^{(2)}$ anisotropy question:</u>

It appears that the differences in the $\chi^{(2)}$ tensor across this series of isomorphous complexes <u>are not</u> explicable by <u>only</u> considering the hyperpolarisability of the RI_3 molecule - even with the local fields experienced by this molecule in the S_8 lattice properly accounted for.

Results from this study independently show that this is the case:

- Comparisons of computed hyperpolarisabilities, measured $\chi^{(2)}$ and various 'constructed' NLO susceptibilities indicated that local-field-factor tensor differences across the series were not a major cause of $\chi^{(2)}$ anisotropy differences in RI_3*3S_8 crystals.

- Inspection of local-field-factor tensors shows only small variation in d across the RI_3*3S_8 series and this leads to the same conclusion.

This implies that the Third and Fourth hypotheses of the Chapter One Methodology are of significant importance in rationalising bulk NLO properties from molecular hyperpolarisabilities in these complexes. It was also shown that significant contributions to $\chi^{(2)}$ come from the complexing partner (S_8) molecule in these adducts. This is especially so for CHI_3*3S_8. Clearly, the proximity of the electronic resonance of the material (stemming from the triiodide molecules) is also a major factor determining the bulk susceptibility of these adduct crystals. This is especially illustrated by the response of AsI_3*3S_8.

<u>Secondly, with respect to other complexes:</u>

The results from these experimental and theoretical $\chi^{(2)}$ determinations show that the process of construction of NLO susceptibility from computed hyperpolarisabilities can give a reasonable prediction of the size and anisotropy of bulk NLO response in hetero-molecular 'complex' crystals such as these. General conclusions that might be drawn from this work include:

- a full tensorial consideration of the local field issue is necessary. The Lorentz Factor tensor for the crystal lattice tensor should be calculated using a sensible specification of the molecules in the unit cell.

- when local field factor tensors are determined using an LFT approach, they are very often different to ALA counterparts and that this may lead to a dramatically different anisotropy of $\chi^{(2)}$.

154

- use of a supermolecule specification for the complex is inadvisable - primarily due to the absence of consideration of nearest neighbor field contributions to the Lorentz tensor.

- contributions to $\chi^{(2)}$ from the partner molecule should be taken into account. In this case, the S_8 ring in its distorted form significantly increased the overall response. This has not been shown previously.

This work has shown the importance of dealing properly with hetero-molecular crystals where both molecules contribute to $\chi^{(2)}$. It is quite likely that these conclusions also apply to other closely related series of 'adducts', for example, the differences noted in the bulk NLO response of $CHI_3 \ast 3Qn$ with respect to the $CHI_3 \ast 3S_8$ response [9], might be (partly) due to differing contributions from the donor quinoline molecule as well as differing local fields experienced by the CHI_3 molecule in this lattice.

Other Conclusions:

Although it is interesting and worthwhile to know of the NLO response of $AsI_3 \ast 3S_8$, this complex has not been of great use in confirming the utility of the *LFT-Composite* treatment of hetero-molecular complexes. This is due to the probable operation of a two-photon resonance enhancement mechanism which overwhelms the underlying non-resonant $\chi^{(2)}$ anisotropy and against which it may have been possible to see some agreement with $\chi^{(2)}$ predicted from AsI_3 hyperpolarisability. This is a limitation of this method -one must look for additivity in NLO response from different adduct components *at frequencies removed from resonances in either component*. It would be beneficial to measure these $\chi^{(2)}$ elements using several fundamental sources further into the IR so that this complicating factor would not be present.

Finally, this is the first time a hetero-molecular CT complex type material has been examined at in this way. Other conclusions following from these results:

- the geometry of molecules as they exist in the lattice can have an important bearing on bulk NLO behaviour.

- hetero-molecular treatment of a lattice to include different hyperpolarisability contributions is possible without a Lorentz-Factor Tensor treatment of the local fields.

Other Issues

1. THE CHARGE-TRANSFER INTERACTION

The charge-transfer interaction which is responsible for the complex formation must have an effect on the way the overall NLO response of the crystal develops from the free-molecule RI_3 hyperpolarisability. This might be on both the anisotropy of the $\chi^{(2)}$ tensor as well as affecting the overall size of the response.

It has been shown that the effective polarisability, α_k, of a molecule in a general lattice of molecules is different to the free-molecule polarisability, α_k^0 [11-13,16]. This is largely because of effects induced in the molecule from fields at the molecule coming from (i) permanent molecular charge distributions on the lattice and (ii) dipoles induced on lattice points by an applied electric field. As well as these *local* effects, however, are *non-local* effects whereby field application at a position remote from the molecule leads to some response and change of property of the molecule (such as polarisability). This can be expressed [10,11]:

$$A_{lk} = \alpha_{lk} + \sum_{l'k'} \tau_{lk,l'k'}$$

where A_{lk} is the total polarisability of molecule k in unit cell l, and is different to the effective molecular polarisability α_{lk} because of extra distortions imposed on the molecule from short-range interactions (such as those CT interactions in these adducts) which are the means through which non-local response occurs. $\tau_{lk,l'k'}$ is the polarisability induced in the molecule from non-local effects on other molecules k' in the same and in other cells l'.

Non-local effects may be manifested within a molecular volume or between molecular volumes and the presence of a charge-transfer interaction may provide a mechanism for the latter type of non-local effect. This has been discussed in terms of 'field-induced charge-transfer' in [4]. Given the existence of a CT 'bond' in the crystal, it can be seen that the polarisabilities of both donor and acceptor molecules will be different due to their partially ionic nature. As well as this, field-induced charge-transfer will result in further polarisability change. Also, if attempting to use homomolecular crystal data, different crystal structures may well obfuscate any differences seen as occurred for [4].

The non-local contribution to the polarisability, $\tau_{lk,l'k'}$, should be quantified as this would allow some idea of the importance of such effects on the effective hyperpolarisability. In practice, this is not possible due to lack of knowledge of the amount of induced CT.

The CT interaction is expected to have an appreciable effect on the electron distribution at the iodine atom. A Raman experiment was performed to see if this effect is similar for each triiodide [this is presented in Appendix Three]. The results indicate that the bond attains significantly greater covalent character upon complexation with S_8 (by a factor of ≈ 2) but that this induced change is almost the same for each adduct. The change in bond polarisability derivative also indicates that the charge-transfer to the iodine acceptor is significant. It is plausible to suggest that this may affect NLO response.

Can the extent that this 'iodine-sulfur bond' affects the overall NLO response be deduced by examining the difference between the constructed and measured $\chi^{(2)}$ quantities? In particular, one would look for differences between $\chi^{(2)}$ elements derived from the *LFT-Composite* treatment and the experimental susceptibilities. In principle this is possible, however, in practice this is not at all feasible since:
- The assumptions made in parametrising the system to perform the *LFT-Composite* $\chi^{(2)}$ construction are too severe. The first of these is the approximation that the linear susceptibility of both the RI_3 and S_8 components when determining local field factor tensors for each of these lattices. The other is the use of linear susceptibilities at *optical* frequency for $\chi^{(2)}$ calculation using static computed β.
- An extremely high degree of reliability in the computed hyperpolarisabilities of the free molecules would be required.
- the complicating absorption needs to be avoided (or accurately accounted for).

Thus it is not possible to say exactly how the charge-transfer interaction contributes to the NLO response of these complexes. With the use of more advanced ab initio computations, CT interaction contributions to β in 'super-molecular' systems such as these might be predicted.

2.   CONTRIBUTION FROM DISTORTED S_8 RINGS

One notices a large difference in the contribution to the predicted adduct susceptibilities from the octa-sulfur lattice for the iodoform complex as compared to the other two. This stems directly from the much larger hyperpolarisability manifested by the more distorted S_8 ring which exists in CHI_3*3S_8. Figure One illustrates the differing distortion. This also illustrates that NLO response can be very sensitive to molecular geometry.

Octa-sulfur exists as a puckered 8-membered ring which, when undistorted as in the gas-phase, belongs to the D_{4d} point group. By symmetry, this noncentrosymmetric molecule will exhibit a β at non-zero frequencies and this response is governed by a single tensor element, β_{123}. At zero frequency this element too becomes zero.

While an undistorted S_8 molecule in the adduct lattice will exhibit an NLO response, it would only be in the 'off-diagonal' condition required to measure β_{123}. It is only when the symmetry of the molecule is lowered through distortions imposed by the combination of charge-transfer interaction, permanent local fields and the crystal lattice potentials, that other tensor elements appear such that a contribution to $\chi_{11}^{(2)}$ and/or $\chi_{33}^{(2)}$ is made.

It was noticed in Chapter Three that the static β calculated for the various S_8 ring structures vary markedly across the series and that β is sensitive to octa-sulfur geometry - seemingly increasing with the amount of 'distortion' (and vanishing when exact D_{4d} symmetry is attained). It is difficult to procure evidence as to why the ring shapes are so different in these materials but there is probably a connection with the strength of the iodine-sulfur interaction. In CHI_3*3S_8 one sees the shortest iodine-sulfur interatomic distance of 3.5Å. This stronger interaction may be responsible for extra distortion of the S_8 ring -especially the S atoms closest to the bonding sulfur. This is indicated in Figure One.
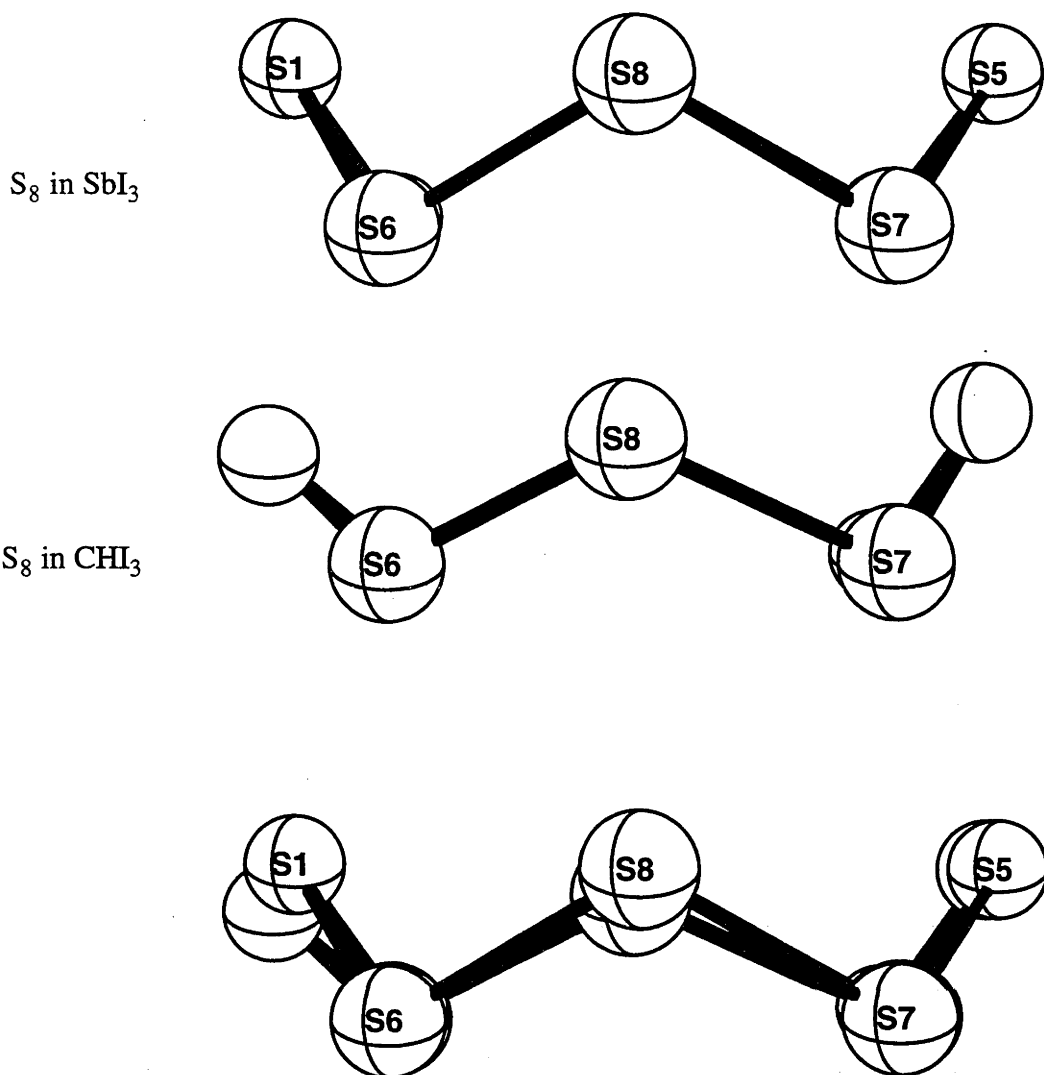
S_8 in SbI_3

S_8 in CHI_3

Figure One: Models of S_8 molecules as they exist in two CHI_3*$3S_8$ lattices. The view is along the axis containing the S3/S8 atoms so that distortion in S1 is most visible. An view with S7 atoms overlaid is shown to highlight the geometry difference.

Ring-geometry distortions are a sum of those produced by the regular crystal potential, any distortion arising from the permanent DC field and that due to the iodine-sulfur CT interaction. RI_3 in-adduct geometries are only slightly different to those optimised ab initio molecular geometries. See Table Nine in Chapter Three.

This result showing significant S_8 contribution to the NLO susceptibility seems to be in conflict with earlier work showing the $\chi^{(2)}$ response to come mainly from RI_3 [Refs 23,24 of Chap 1]. The experiments reported in those studies were not, however, intended to be conclusive on this question.

2.   NLO EFFECTS INDUCED BY PERMANENT FIELDS

The question was raised by Samoc *et al* [3] whether an 'EFISHG-type' mechanism operates in some adduct crystals to augment the vector part (or just the $\chi^{(2)}_{33}$ component) of the NLO susceptibility. This was briefly described in Chapter One as a valid possibility. A permanent internal electric field exists due to the RI_3 molecular dipole moment and the suggestion was that this field induces a β in the S_8 molecules. In fact, this is not well described as an EFISH process since such a term suggests a field-induced bulk nonlinearity arising from removal of the orientationally averaged centrosymmetry in a fluid medium. The mechanism proposed here is an example of an *all-electronic* effect of β enhancement induced in a molecule by a permanent internal electric field.

Strong evidence supporting that such a mechanism operates would be to show that there is a definite correlation between the size of the RI_3 molecular dipole moment, μ, and the $\chi^{(2)}_{11}/\chi^{(2)}_{33}$ anisotropy ratio[7]. One would expect a positive correlation -though not necessarily a straight line dependence. One could also use correlation between μ and the "effective hyperpolarisability" if this could be reliably calculated. Further supporting evidence would be provided if it could be demonstrated that electric field application to the 'in-adduct' S_8 geometries results in an enhancement of that molecule's hyperpolarisability.

The suggested correlation requires use of nonresonantly enhanced $\chi^{(2)}$ coefficients. Such an exercise also requires μ - ideally for the molecule as it exists in the adduct crystal. In practice, such a correlation would be difficult with only three members of this series. In any case, it has been seen that $SbI_3 \cdot 3S_8$ has a significantly larger '33' NLO response than $CHI_3 \cdot 3S_8$ and the dipole moment of SbI_3 is about twice that of CHI_3 in the gas phase. This originally prompted the 'permanent-field-enhancement' theory. $AsI_3 \cdot 3S_8$, however, has a

---

[7] Using such a correlation as evidence for a physical mechanism is quite different to the intuitively appealing course of simply trying to relate μ with free-molecule hyperpolarisability as was discussed by Levine and Bethea [14]. It was concluded there that this has no basis for σ-electron molecules and that such a relation for conjugated π-electron systems is inaccurate.
Incidentally, there is no *a priori* justification to relate a polarisability or hyperpolarisability (distortabilities of bound electric charges by an applied field) to the static moments of distribution of these charges although an empirical relation between μ and α seems to exist for RI_3 molecules (using the expression of LeFèvre [15] connecting bond stretching frequency with bond polarisability, these α correlate well with μ).

nonresonant $\chi_{11}^{(2)}/\chi_{33}^{(2)}$ ratio close to that of $SbI_3 * 3S_8$, yet AsI_3 has an isolated dipole moment much closer to that of CHI_3 which does not fit the trend of the other two.

It is informative to look at the internal fields and in-adduct dipole moments for $CHI_3 * 3S_8$ and $SbI_3 * 3S_8$ which have the smallest and largest RI_3 dipole moments respectively.

Theoretical investigation of dipole moments and permanent electric fields of polar molecules within crystals has been discussed in the work of Munn [16] and such predictions have been made for the case of HCN crystals [17]. The procedure developed there for computing both quantities in homo-molecular crystals involves calculating:

- molecular dipole moment as a function of local electric field (using MO computational chemistry techniques) and
- local-field at the molecule as a function of dipole moment.

The point at which the two functions cross gives the estimate for both μ and $\mathbf{E}_f$.

Given the Lorentz-factor tensor for the structure, the latter can be worked out from the earlier formalism in Chapter Four, where local field was given by Eq (4a):

$$\mathbf{E}_f = \mathbf{E}_M + \sum_{k'} L_{k,k'} \cdot p_{k'} / \varepsilon_o v$$

For hetero-molecular crystals, the situation is complicated since a dipole moment on one type of molecule will induce a μ on the others. This then contributes to the local-field, thereby modifying the dipole moments etcetera. To properly estimate a local field, contributions from all these dipoles must be included self consistently. In this case, however, it is useful to consider the local electric field at molecular sites simply arising from a RI_3 dipole moment and neglecting the contribution to this field from the polarised sulfur molecules. By doing this, relative differences in the local-fields in the two lattices will be apparent. These will be meaningful despite the assumption since -to a first approximation- the contribution from the sulfur lattices of the two adducts will be similar.

In the specific case of zero applied-field, $\mathbf{E}_M = 0$. For the hexagonal $RI_3 * 3S_8$ unit cell, Z=3, and taking the complete submolecular specification (as for the *LFT-Composite* Method), the above equation simplifies to:

$$\mathbf{E}_f = 3(L_{\mathrm{II}} + 3L_{\mathrm{IS}})\mu / \nu \, \varepsilon_o \qquad (1a)$$

for $\mathbf{E}_f$ at the iodoform molecule and

$$\mathbf{E}_f = 3(L_{\mathrm{SI}} + 3L_{\mathrm{SS}})\mu / \nu \, \varepsilon_o \qquad (1b)$$

for $\mathbf{E}_f$ at the octa-sulfur molecule. The Lorentz sub-tensors (averaged fields at a molecule from dipoles on sub-lattices) are as described and calculated in Chapter Four (Table Eight). These expressions rely on the assumption of there being a dipole moment on the RI_3 molecules only.

Only $\mathbf{E}_{f,33}$ (the local field in the crystal/molecule z direction) need be determined since, by symmetry, components in other directions are zero when a z-oriented dipole is on RI_3. Thus, the 33 components of the $L_{kk'}$ subtensors are used in Eqs (1) to give $\mathbf{E}_f$ for various dipole moment magnitudes (see Table Four).

Table Four

Site of Local Field (au)	μ_z 0.5D	μ_z 2.5D
CHI$_3$ 33	1.01×10^{-3}	5.04×10^{-3}
SbI$_3$ 33	9.18×10^{-4}	4.59×10^{-3}

To determine the dipole moment as a function of $\mathbf{E}_f$, field-dependent μ were computed for both the CHI_3 and SbI_3 molecules within Gaussian94 - exactly as for the MP2 β calculations which are described in Chapter Three. The computed free-molecule dipole moment for iodoform is $\approx 0.8D$ along the C--H bond axis. When an electric field of 0.001au is applied along this axis, μ increases to $\approx 1.0D$ and when a field of 0.01au is used, a value of $\approx 2.6D$ is obtained. These are sufficiently reliable to be used for estimating the in-adduct μ value for $CHI_3 \cdot 3S_8$.

For the antimony triiodide molecule, a slight problem arises in that the dipole moment of free SbI_3 was not particularly well reproduced in ab initio calculations[8]. This introduces some uncertainty as to where the intercept of the two linear functions will occur. A 'zone' for the intercept is therefore defined by plotting the μ versus $\mathbf{E}_f$ function using all-computed dipole moments and then 'shifting' this to the observed $\mathbf{E}_f = 0$ dipole moment (1.58D) maintaining the same gradient. Both lines are depicted in Figure Two.

---

[8] The literature value is 1.58D. The closest ab initio prediction was $\approx 2.0D$ (Chapter Three, Tables Six and Eight).

Once an in-crystal dipole moment has been estimated from the intercept of the E_f and μ functions, it can be used in Eq (1b) to estimate the local-field strength existing at the sulfur molecules of the two complexes
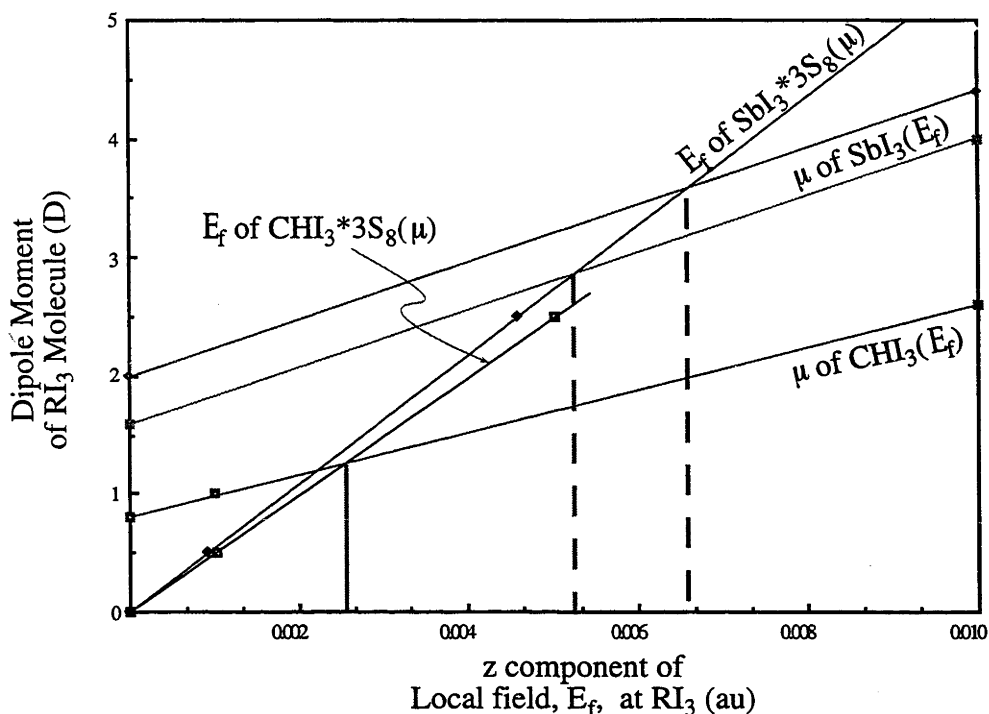

Figure Two: The Graph contains:
      Dependence of molecular Dipole Moment (in Debye -vertical axis) on the z component of the local electric field E_f (in atomic units) at the RI_3 molecule.
      Dependence of the z component of the local electric field E_f at the RI_3 molecule on the molecular Dipole Moment.
The dashed lines indicate the different possible intercepts for SbI_3*3S_8. Note the similarity in the plots of local-electric-field as a function of μ for both adducts.

From the intercept of the iodoform $E_f(\mu)$ function with the $\mu(E_f)$ function in Figure Two, one arrives at a value of **1.26D** as the in-crystal dipole moment and an estimate of the permanent local-field in the z direction of $\approx 2.55 \times 10^{-3}$ a.u. Using this dipole moment in Eq (1b), a value of $\approx 2.04 \times 10^{-3}$ a.u. is predicted for the z-direction permanent local field at the octa-sulfur molecule.

A range of values were obtained for the in-crystal dipole moment and the local electric field at the SbI_3 molecule in SbI_3*3S_8. A figure toward the lower end is more likely if one accepts the straight line using the experimental SbI_3 dipole moment of $\approx 1.6D$. In such a case, the in-crystal moment is predicted to be **2.85D** and the permanent local-field, $\approx 5.25 \times 10^{-3}$ a.u. Such a dipole moment would give rise to a field at the octa-sulfur molecule of $\approx 4.58 \times 10^{-3}$ a.u.

Despite the uncertainty for SbI_3*3S_8, it is clear that the local electric field in the z direction at the S_8 molecule is larger by at least a factor of two in the SbI_3 adduct than in CHI_3*3S_8. The question remains whether the difference in these fields may explain $\chi^{(2)}$ differences. It is conceivable that these fields induce a β_{ZZ} in the S_8 molecule as their magnitudes are large[9] -three orders of magnitude greater than the static external fields usually applied in an electro-optic experiment (although an order of magnitude smaller than those predicted to occur in the crystal of the highly polar HCN molecule [17]). The induction of such an effect may also be nonlinear in E_f.

The results of this brief analysis lead to the rather open conclusion that such a mechanism of selective β tensor enhancement of one molecular component by a permanent internal electric field is quite possible. The >two-fold difference in E_f at the S_8 molecule between the lattices may therefore contribute to the relatively larger $\chi^{(2)}_{33}$ of SbI_3*3S_8. This does not, however, confirm or rule out the existence of such an effect.

Also from this demonstration, a close similarity in the two E_f vs μ functions for the two lattices is noticed. The difference in the size of the z component of local field is therefore mostly determined by the difference in the behaviour of μ with E_f. In this regard, the antimony molecule has a similar slope to the $\mu(E_f)$ function for iodoform but as it starts from a larger value, it can give rise to much larger fields. This also explains why antimony triiodide experiences a proportionally greater increase in μ. From the slope of the $E_f(\mu)$ plots, it is curious to note that in the antimony complex, there is a slightly *lesser* E_f at RI_3 due to a dipole moment of fixed size than occurs for the CHI_3*3S_8 lattice. This must be due to adduct crystal structure difference as it arises from the Lorentz sub-tensor differences between the two adducts.

As indicated earlier, if it could be shown that a 33 component of the hyperpolarisability tensor of S_8 is induced/enhanced by the application of a z-direction field, this would strongly suggest that these permanent internal field strength differences do play an important role in determining the anisotropy of the complex $\chi^{(2)}$. It happens, however, that calculation of hyperpolarisability in an applied external electric field is not possible within the Gaussian suite of programs so this aspect remains incomplete.

---

[9] approximately 1×10^9 Vm^{-1} in SI units.

Errors and Uncertainties

1.   IN EXPERIMENTAL $\chi^{(2)}$

Uncertainties in the experimentally determined NLO coefficients have been mentioned in Chapter Two in this thesis. Of particular significance are:

(i)   the refractive index determinations for the $AsI_3 {\ast} 3S_8$ crystal. These were determined from the Sellmeier fit of fairly old experimental data of West [18] but were shown to add negligible uncertainty to experimental $\chi^{(2)}$ anisotropies.

(ii)   the determination of reliable $I_{2\omega}$ values for the $RI_3 {\ast} 3S_8$ crystals in the Maker Fringe experiment was hampered by crystal surface degradation in many samples. A slight underestimation of $I_{2\omega}$ may persist leading to underestimation of measured $\chi^{(2)}$ values but this will not not affect the $\chi^{(2)}$ anisotropy.

(iii)   absorption of second harmonic radiation generated in these crystals caused an underestimation of the $\chi^{(2)}_{11}$ NLO coefficient by a factor of about 9% and of $\chi^{(2)}_{33}$ by about 2.5%. Because these two diagonal elements are affected differently, the measured $\chi^{(2)}_{11}/\chi^{(2)}_{33}$ anisotropy is expected to be underestimated by approximately 3.6%.

2.   IN CONSTRUCTED $\chi^{(2)}$

In the determination of the various constructed $\chi^{(2)}$, several assumptions were made and these unavoidably introduce some error. Some of these were mentioned in Chapter Four:

(i)   In the construction of NLO susceptibilities, effective cell polarisabilities were calculated in order to incorporate molecular response into the local field factor tensors. This used refractive index data and so the error in the determination of n for $AsI_3 {\ast} 3S_8$ in particular, reappears in this part of the study. A test calculation was performed to examine the effect of error in this quantity on the constructed $\chi^{(2)}$.

165

A maximum underestimation of 2% in n_ω of AsI_3*3S_8 is presumed (based on the error analysis presented in Chapter Two). Using indices which are larger by this amount results in $\chi^{(2)}$ predictions which are larger[10] by $\approx 7\text{-}11\%$. So the value of this coefficient is rather sensitive to change in n, however, this uncertainty is an *upper limit* and the actual underestimation of constructed $\chi^{(2)}$ values caused by using West's n data for AsI_3*3S_8 is believed to be much smaller than this.

(ii)   In the determination of the *LFT-Composite* NLO susceptibilities, there is error introduced by using the average *homomolecular* crystal susceptibility ratio, χ_S/χ_I for ρ, which should actually be the ratio of 'sub-lattice susceptibilities' of the RI_3 and S_8 molecules in the adduct lattice. As well as this, the χ_S and χ_I used are the scalar averages of $\chi^{(1)}$ over all crystal axes. This latter point is less severe for the more isotropic orthorhombic sulfur but for strongly birefringent RI_3 crystals[11], the averaging assumption is more drastic. One can expect that some underestimation of the anisotropy of $\chi^{(2)}_{COMPOSITE}$ tensors results.

It is difficult to say in which direction the anisotropy of *LFT-Composite* $\chi^{(2)}$ errs and by how much through use of the χ_S/χ_I ratio. This is because the relationship between (RI_3 or S_8) molecular lattices in the homomolecular crystal and those in the adducts is not straightforward. This is especially the case for S_8 where there are 16 molecules in the unit cell with rather different orientations to the S_8 lattice in the RI_3*3S_8 complexes. This was discussed earlier this Chapter where it was concluded that $\chi^{(2)}_{11}/\chi^{(2)}_{33}$ may be underestimated.

(iii)   Error is introduced in each of the constructed $\chi^{(2)}$ determinations by taking all local field tensors, d_k, for 1064nm in the expression Eq (6) of Chapter Four. Instead, one of these d_k should be for 532nm. The underestimation that this assumption causes can be determined by examining the ratio of d_k tensor elements calculated for ω frequency to those at 2ω.

---

[10]   As an example, for AsI_3*3S_8 using the supermolecule specification, $\chi^{(2)}_{11}$ increased from 5.1 to 5.7pm/V and $\chi^{(2)}_{33}$ increased from 0.7 to 0.75pm/V.

[11]   These have a large n ($\chi^{(1)}$) in the direction corresponding to in-the-plane of the RI_3 iodine atoms and a much smaller n perpendicular to this.

This was tested for $AsI_3 \cdot 3S_8$ in the supermolecule specification by examining the $d^3_{1064nm} \Big/ d^2_{1064nm} d_{532nm}$ ratio where the numerator was the factor used in Eq (6) of Chapter Four and the denominator that which should properly be used. One finds, however, that the resultant underestimation in $\chi^{(2)}$ is only by $\approx 2.4\%$ for $\chi^{(2)}_{11}$ and by $\approx 6.3\%$ for $\chi^{(2)}_{33}$ elements. This also means that a small increase in the $\chi^{(2)}_{11} \Big/ \chi^{(2)}_{33}$ ratio is caused by calculating $\chi^{(2)}$ in this way.

This method was employed because it implies Kleinman symmetry is valid which results in a simpler $\chi^{(2)}$ tensor[12]. These materials are not dispersionless, however, meaning that the 'actual' $\chi^{(2)}$ tensor has certain 'new' elements - in this case, the following previously equal elements become 311=312≠131=113. In any case, the focus has not been on these elements and so the use of d^3 for 1064nm in Eq (6) is not considered an overly serious shortcoming.

The error in the *LFT-Composite* $\chi^{(2)}$ estimations is more complicated to deduce due to the added consideration that needs to be made of dispersion in homo-molecular susceptibilities which appear in determining the Lorentz factor tensor. Presumably, neglect of a d_k factor for 532nm and imposition of the Kleinman condition has a similar effect on these elements as on the supermolecule values just described.

All these errors have resulted in predicted underestimations of $\chi^{(2)}$ values and so these effects will compound - the total error is probably of the order of 15-20%. The two predicted effects on the $\chi^{(2)}_{11} \Big/ \chi^{(2)}_{33}$ anisotropy ratio are opposite suggesting that some cancellation of error in determination of this quantity occurs.

---

[12]   This approach is the same as used in which d tensors at both fundamental and harmonic frequencies were used and then the discrepancy between Kleinman-related elements in the resultant $\chi^{(2)}$ tensor were examined. For example, Munn and Smith [2b] noted differences in such elements of about 10%.

REFERENCES

1. D. Pugh and J.O. Morley, Molecular hyperpolarisabilities of organic materials. in; *Nonlinear Optical Properties of Organic Molecules and Crystals* eds D.S. Chemla and J. Zyss, (Academic Press, 1987).

2a. M. Hurst and R.W. Munn, Theory of molecular opto-electronics IV -prediction of $\chi^{(2)}$ for *meta*-nitroaniline. *J.Mol.Electron.*, **2**, 139 (1986);

2b. R.W. Munn and S.P.B. Smith, Theory of molecular opto-electronics X -calculations for MBANP and NMBA. *Adv.Mat.Opt.Electron.*, **1**, 65 (1992);

2c. R.W. Munn, Theory of molecular opto-electronics IX: Calculation of $\chi^{(2)}$ from theoretical hyperpolarisabilities for DAN. *Int.J.Quant.Chem,.* **43**, 159 (1992)

3. A. Samoc, M. Samoc, P. Prasad and A. Krajewska-Cizio, Second harmonic generation in the crystalline complex antimony triiodide-sulfur. *J.Opt.Soc.Am.B*, **9**, 1819 (1992)

4. S.E. Mothersdale and R.W. Munn, Calculation of planewise dipole sums for anthracene crystal. *J.Chem.Phys.*, **97**, 4536 (1992)

5. R.W. Munn, R.J. Phillips and C.J. Eckhardt, Dielectric theory of weak charge-transfer crystals I -effective polarisabilities. *Chem.Phys.*, **135**, 1 (1989)

6. R.W.G. Wyckoff, *Crystal Structures*, Vol 1 (Interscience 1965)

7a. S.K. Kurtz in H. Rabin and C.L. Tang (Eds), *Quantum Electronics*, (Academic Press; New York, 1975);

7b. S.K. Kurtz in F.T. Arecchi and E.O. Schulz-Dubois (Eds), *Laser Handbook*, Vol1, (North Holland; Amsterdam, 1972);

7c. D. Chemla and P. Kupecek, Analyse des experiences de génération de second harmonique. *Rev.Phys.App.*, **6**, 31 (1971)

8. P.A. Cahill, K.D. Singer and L.A. King, Anomalous-dispersion phase-matched second-harmonic generation. *Optics Letters*, **14**, 1137 (1989)

9. A. Samoc, M. Samoc, D. Kohler, M. Stähelin, J. Fünfschilling and I. Zschokke-Gränacher, Linear and second-order optical properties of the trigonal adducts of triiodomethane with sulfur and quinoline. *Nonlinear Optics*, **2**, 13 (1992)

10. R.W. Munn, and T. Luty, Effective and non-local polarisability response in molecular assemblies. *Chem.Phys.*, **81**, 41 (1983)

11. R.W. Munn, Electric dipole interactions in molecular crystals. *Mol.Phys.*, **64**, 1 (1988)

12a. R.W. Munn and S.M. Bourne, The polarisability of iodoform in the crystal. *Chem.Phys.Lett.*, **75**, 403 (1980);

12b. T. Luty, On the effective molecular polarisability in molecular crystals. *Chem.Phys.Lett.*, **44**, 335 (1976);

13. R.W. Munn, Unified theory of the dielectric properties and lattice vibrational intensities of the HCN crystal. *Chem.Phys.*, **59**, 269 (1981)

14. B.F. Levine and C.G. Bethea, Second and third order hyperpolarisabilities of organic molecules. *J.Chem.Phys.*, **63**, 2666 (1975)

15. R.G.W. LeFèvre, Stretching frequencies and longitudinal polarisabilities of bonds. *Proc.Chem.Soc.*, 363 (1959)

16. M. Hurst and R.W. Munn, Theory of molecular opto-electronics II -environmental effects on molecular response. *J.Mol.Electron.*, **2**, 43 (1986)

17. D.G. Bounds, A. Hinchliffe, R.W. Munn and R.J. Newham, The dipole moment of HCN in the crystal. *Chem.Phys.Lett.*, **29**, 600 (1974)

18. C. D. West, Sulfur-iodide crystals $RJ_3 3S_8$ structure unit and optical properties. *Z.Krist.*, **94**, 459 (1937)

APPENDIX ONE

Crystal Structure Determination for AsI_3*3S_8.

X-ray crystal structures have been previously determined for the complexes CH_3*3S_8 and SbI_3*3S_8 [1,2]. In this study, the isomorphous adduct AsI_3*3S_8 was also characterised in this manner:

The sample was a deep yellow fragment broken from a prism-shaped crystal which was grown as described in Chapter Two. The measurements were performed on a Rigaku AFC6S diffractometer using Mo-Kα radiation for which the absorption coefficient was 56.7cm^{-1}. Hexagonal cell dimensions were ascertained from 25 reflections in the range: 2θ between 50·56° - 54·84°.

> Thus, the space group was determined to be R3m with
> a = 24.7392 Å, c = 4.4123 Å, Vol = 2338 Å^3

Overall, 648 unique reflections were collected (from 1401 total). R_{int} = 0.034. The least-squares refinement was performed in the teXsan program and converged with unweighted and weighted agreement factors of R=0.019 and R_w=0.022. The standard deviation was 1.26. The predicted p is 2.61gcm^{-3} (Lit; 2.608 gcm^{-3} [3]). Unit cell diagrams generated in the refinement step were shown in Chapter One; in these, thermal ellipsoids indicate 50% probability levels.

Data from this structure determination which has been used in this study are:

- molecular geometry parameters were used in comparing computed molecular geometries in Chapter Three.

As-I (Å)	2.574
I-As-I (degrees)	99.7
As-I-S (degrees)	169.68
I-S (Å)	3.571

The geometry of the sulfur molecule was taken directly from fractional coordinates.

- fractional coordinates for all atoms were used to specify (sub)molecule positions in the unit cell when calculating the Lorentz-factor Tensor, $L_{kk'}$, in Chapter Four. These are shown on the next page for the $AsI_3·3S_8$ hexagonal unit cell as they were input in the command script for this purpose. They were generated from the primary atomic coordinates yielded from this sructure determination.

170

```
#!/bin/sh
time lorsub << next
AsI3*3S8 Lorentz factor
         tensor
24.7392 24.7392 4.4123 90.0
        90.0 120.0

12 4 8 8 8 4 8 8 8 4 8 8

0.0 1.0 1.27422
-0.05302 1.05302 1.0
-0.05302 0.89397 1.0
0.10603 1.05302 1.0
  -0.13241 1.13241 0.75375
  -0.08318 1.21581 0.97658
  -0.09135 1.28164 0.73265
  -0.15958 1.29373 0.93157
  -0.24100 1.24100 0.69787
  -0.21581 1.08318 0.97658
  -0.29373 1.15958 0.93157
  -0.28164 1.09135 0.73265

  -0.13241 0.73518 0.75375
  -0.21581 0.70102 0.97658
  -0.28164 0.62700 0.73265
  -0.29373 0.54669 0.93157
  -0.24100 0.51800 0.69787
  -0.08318 0.70102 0.97658
  -0.15958 0.54669 0.93157
  -0.09135 0.62700 0.73265

  0.26482 1.13241 0.75375
  0.29898 1.08318 0.97658
  0.37300 1.09135 0.73265
  0.45331 1.15958 0.93157
  0.48200 1.24100 0.69787
  0.29898 1.21581 0.97658
  0.45331 1.29373 0.93157
  0.37300 1.28164 0.73265
```

```
0.33333 0.66667 0.94089
0.28032 0.71968 0.66667
0.28032 0.56063 0.66667
0.43937 0.71968 0.66667

 0.20092 0.79908 0.42042
 0.25016 0.88247 0.64324
 0.24198 0.94831 0.39932
 0.17375 0.96040 0.59824
 0.09233 0.90767 0.36454
 0.11753 0.74985 0.64324
 0.03960 0.82625 0.59824
 0.05169 0.75802 0.39932

 0.20092 0.40184 0.42042
 0.11753 0.36768 0.64324
 0.05169 0.29367 0.39932
 0.03960 0.21335 0.59824
 0.09233 0.18466 0.36454
 0.25016 0.36768 0.64324
 0.17375 0.21335 0.59824
 0.24198 0.29367 0.39932

0.59816 0.79908 0.42042
0.63232 0.74985 0.64324
0.70633 0.75802 0.39932
0.78665 0.82625 0.59824
0.81533 0.90767 0.36454
0.63232 0.88247 0.64324
0.78665 0.96040 0.59824
0.70633 0.94831 0.39932
```

```
0.66667 0.33333 0.60755
0.61365 0.38635 0.33333
0.61365 0.22730 0.33333
0.77270 0.38635 0.33333

0.53426 0.46575 0.08708
0.58349 0.54914 0.30991
0.57531 0.61498 0.06599
0.50708 0.62706 0.26491
0.42567 0.57433 0.03120
0.45086 0.41651 0.30991
0.37294 0.49292 0.26491
0.38502 0.42469 0.06599

0.53426 0.06851 0.08708
0.45086 0.03435 0.30991
0.38502 -0.03966 0.06599
0.37294 -0.11998 0.26491
0.42567 -0.14867 0.03120
0.58349 0.03435 0.30991
0.50708 -0.11998 0.26491
0.57531 -0.03966 0.06599

0.93149 0.46575 0.08708
0.96565 0.41651 0.30991
1.03966 0.42469 0.06599
1.11998 0.49292 0.26491
1.14867 0.57433 0.03120
0.96565 0.54914 0.30991
1.11998 0.62706 0.26491
1.03966 0.61498 0.06599
9 0.000001
1 9 9
1 1
next
```

Indented coordinates are for sulfur atoms grouped as S_8 rings. The four-line-groupings of fractional coordinates are the As and three I atoms, respectively. The three numbers for each atom are its x, y, and z hexagonal-cell coordinates.

{The first five and last four lines are other codes and parameters for the calculation of $L_{kk'}$. The line: 12 4 8 8 8... specifies the number of submolecules, followed by how they are grouped as molecules.}

References

1.   T. Bjorvatten, Crystal structure of the 1:3 addition compound iodoform-sulfur (CHI_3*3S_8). *Acta Chem.Scand.*, **16**, 749 (1962)

2.   T. Bjorvatten, O. Hassel and A. Lindheim, Crystal structure of the addition compound $SbI_3 \cdot 3S_8$. *Acta Chem.Scand.*, **17**, 689 (1963)

3.   C. D. West, Sulfur-iodide crystals $RJ_3 \cdot 3S_8$: structure unit and optical properties. *Z.Krist.*, **94**, 459 (1937)

APPENDIX TWO

Visible Absorbtion Spectra.

The compounds studied here are either yellow / orange-yellow and so have absorbtion edges close to the green second-harmonic wavelength, 532nm. Resonance enhancement of second-order NLO response is possible through two-photon absorption of fundamental radiation at 1064nm, thus, it was important to quantify the absorption in this spectral region.

Electronic absorbtion spectra of each of the crystalline $RI_3{}^*3S_8$ adducts were measured using the diffuse reflectance method. Finely crushed and sieved samples were 'diluted' with spectroscopic grade KBr powder which limited degradation by atmospheric moisture. Spectra were recorded within minutes of the samples being prepared.

The measurements were recorded with a Varian Cary-45 spectrophotometer using the diffuse reflectance capability.
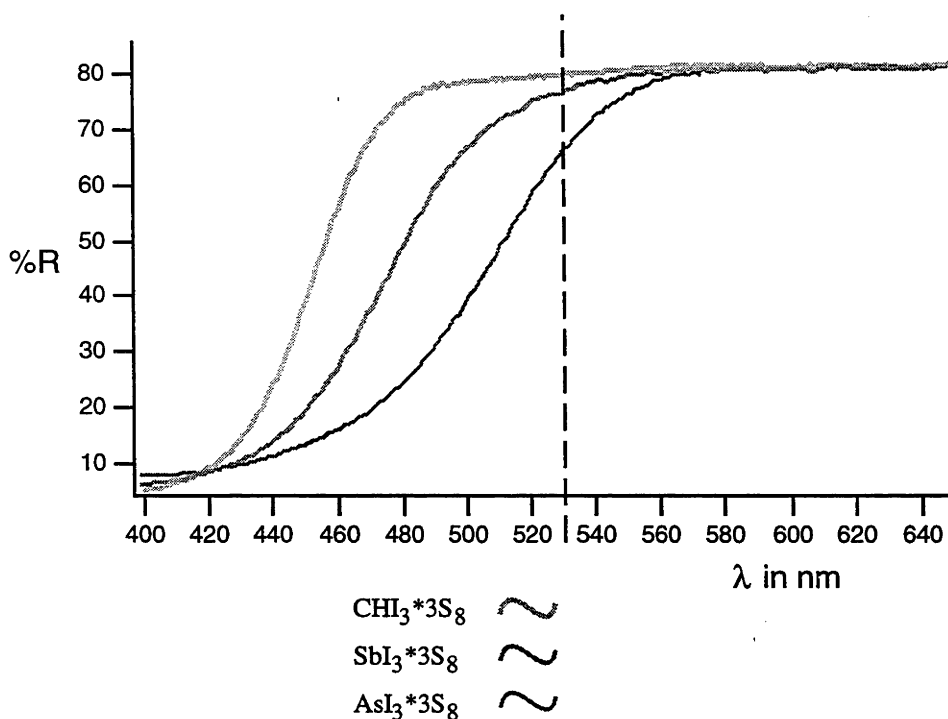
Figure One: Diffuse reflectance spectra of the RI_3*3S_8 adducts. Spectra are normalised to 80% maximum reflectance.

For the arsenic adduct, it is apparent that appreciable absorption occurs at 532nm. SbI_3*3S_8 absorbs a little at this wavelength but only about a quarter that of AsI_3*3S_8. CHI_3*3S_8 is virtually transparent in this region.

The most absorptive material, AsI_3*3S_8, was further examined by measuring the absorption of single crystals in different polarisations. This was done using a custom built, single-beam instrument designed for the purpose of measuring absorption spectra of small crystals. Absorption (at room temperature) of 532nm light polarised parallel and perpendicular to the crystal c-axis was examined in two AsI_3*3S_8 crystals of good quality. After baseline correction, the coefficients for polarisation in the ab plane were $4.7cm^{-1}$ and $5.1cm^{-1}$ for the different crystals. For polarisation parallel to the c-axis, the absorption coefficient was $1.4cm^{-1}$ for both crystals. This represents an average difference in α for the two crystal axes of about 3.5. These figures are uncorrected for differing reflection losses of the two polarisation geometries. It might therefore be expected that the birefringence is overestimated, yet is clearly large.

APPENDIX THREE

Raman Experiments

A quantitative comparison of the complex-forming I····S interaction in the RI_3*$3S_8$ adducts is desirable in order to see if this is sufficiently different for R = CH, As or Sb to be able to account for the observed $\chi^{(2)}$ differences in these materials. A suitable and measurable physical property must be used which is sensitive to the perturbation caused by the close proximity of the octa-sulfur molecule to the iodine atom.

Other bond parameters that will be affected by the changes induced upon complexation are; the *bond polarisability* and the *bond polarisability derivative*. This latter quantity, $\partial\alpha/\partial r$, is the change in bond polarisability accompanying moderate changes in distance between two nucleii -such as occurs during an R--I bond vibration. It is strongly correlated to the degree of bond covalency [1-3] and is measurable by conventional Raman spectroscopy. This is the property that was employed in this study to compare changes induced on the RI_3 molecule.

Methodology and Theory

In these experiments, the differences between the $\partial\alpha/\partial r$ of R--I bonds existing in the homomolecular RI_3 crystal and in the RI_3*$3S_8$ adduct are measured. Such differences indicate how the nature of the R--I bond is modified upon forming the octa-sulfur adduct. Since the structures of AsI_3 and SbI_3 are rather similar, differences in the extent of $\partial\alpha/\partial r$ change manifested for each triiodide upon entering the matrix are considered to mostly reflect differences in the iodine-sulfur CT interaction.

THEORY

A non-zero $\partial\alpha/\partial r$ for a particular stretching mode allows a Raman signal to be expressed and scattering *intensity* is proportional to the extent of this polarisability change occurring during an active mode.

Plazcek was one of the first to describe Raman intensity as an important physical quantity, thus, the intensity of radiation scattered in a Raman process can be given by [1]:
$$I = N_n \frac{64\pi^2}{3c^2} (v_0 - \Delta v)^4 P_{nm}^2$$
where Δv is the mode frequency and v_0 is the exciting frequency. N_n is the number of molecules in initial state n. The P_{nm}^2 factor is the probability of the occurrence of the transition between states n and m. It is proportional to $\frac{I_0}{\Delta v} \alpha'^2$ where α'^2 represents the combined longitudinal polarisability and polarisability anisotropy derivative with respect to change in bond length.

After incorporating a Boltzman factor to account for the number of species existing in the initial state n [1,4]:

$$I_p = (v_0 - \Delta v)^4 \frac{I_0 \times N \times K}{\Delta v \left(1 - \exp(-h\Delta v/kT)\right)} 45 \left(\frac{\partial\overline{\alpha}}{\partial Q_p}\right)^2 \left(\frac{6}{6 - 7\rho}\right) \qquad (1)$$

where I_p is the intensity of the pth normal vibration mode, Q_p, (when measured at 90° to incident intensity, I_0). In this expression, only the longitudinal (diagonal) polarisability change $\frac{\partial\overline{\alpha}}{\partial Q_p}$ is explicitly included. The change in the polarisability anisotropy is accounted for by the factor containing the depolarisation ratio, ρ.

$\frac{\partial\overline{\alpha}}{\partial Q_p}$ may be simply related to $\partial\alpha/\partial r$ using the assumptions of Wolkenstein [1,4] that α is only affected by stretching of that particular bond. The influence of bending modes and stretching of other bonds is neglected.

Relative bond-polarisability derivative measurements can be performed thereby circumventing difficulties associated with absolute intensity measurement [1]. The appropriate expression for comparison of symmetric A_1 stretch modes (for which depolarisation ratios can be neglected) is:

$$\frac{I_2}{I_1} = \frac{M_2}{M_1} \left(\frac{v_0 - \Delta v_2}{v_0 - \Delta v_1}\right)^4 \frac{\Delta v_1}{\Delta v_2} \frac{1 - \exp(-h\Delta v_1 / kT)}{1 - \exp(-h\Delta v_2 / kT)} \left(\frac{\overline{\alpha'_2}}{\overline{\alpha'_1}}\right)^2 \qquad (2)$$

here, $\dfrac{M_2}{M_1}$ indicates the mole fraction of the components being compared and

$\left(\dfrac{\overline{\alpha'_2}}{\overline{\alpha'_1}}\right)$ is the ratio of individual bond-polarisability derivatives, $\dfrac{\partial\overline{\alpha}}{\partial r}$.

Eq (2) is used in this experiment to estimate $\left(\dfrac{\overline{\alpha'_2}}{\overline{\alpha'_1}}\right)$ for $RI_3*3S_8\text{-}RI_3$.

Experimental Aspects

Spectra were collected using a custom set-up which reliably yields excellent Raman spectra due to utilisation of a 0.75m double monochromator and sensitive cooled-PM detection. A 647nm krypton laser line was used as the exciting source. The spectra were measured at low temperature ($\approx$15 K).

Samples were measured as RI_3 - RI_3*3S_8 pairs. Finely powdered samples of both compounds were prepared (such that passed through a 65μm sieve). Weighed amounts of each were mixed and sintered into a pellet. The addition of KBr powder as a diluent was sometimes necessary to obtain a pellet of adequate thickness. Measurements were made on AsI_3*3S_8 and SbI_3*3S_8.

Pellets of $AsI_3\text{-}AsI_3*3S_8$ and of $SbI_3\text{-}SbI_3*3S_8$ were prepared as well as ones containing just AsI_3 and SbI_3. Spectra were recorded in the frequency range of the RI_3 "A_1" stretch mode as previously determined by the work of Hayward [5] and Fernando [6]. Numerous points on the pellet were probed with the non-focussed laser and averages of peak-heights were used.

Results

Overlaid Raman spectra of AsI_3-AsI_3*3S_8 and of SbI_3-SbI_3*3S_8 measured in the manner described are presented in Figures One and Two.
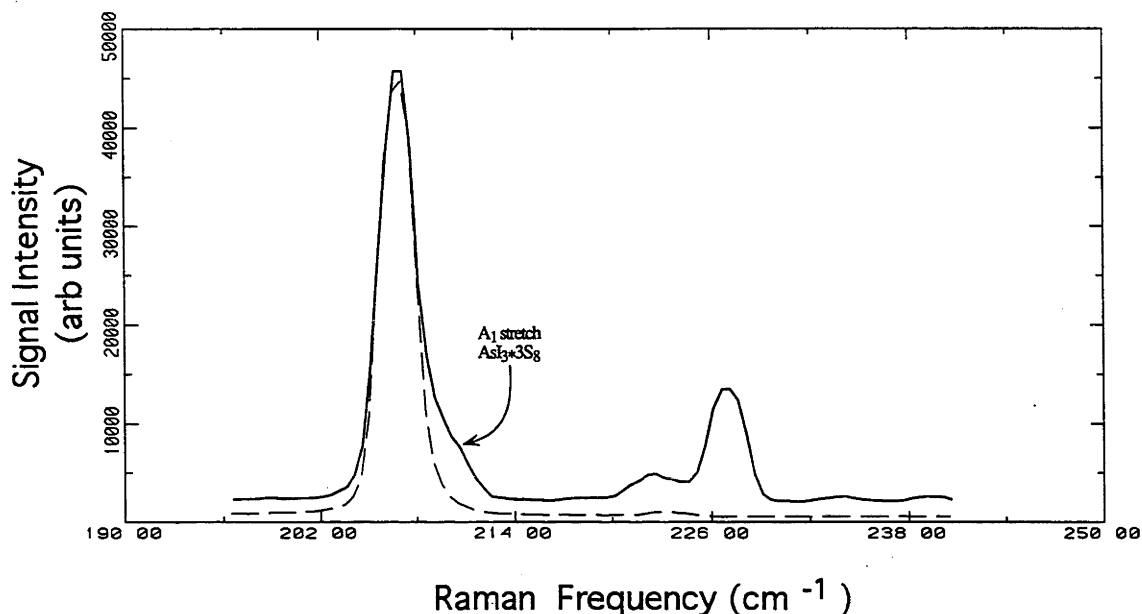
Figure One: Raman spectra at ~10K of a pressed pellet of AsI_3 and AsI_3*3S_8 powders (full line) and that of AsI_3 alone (dashed).
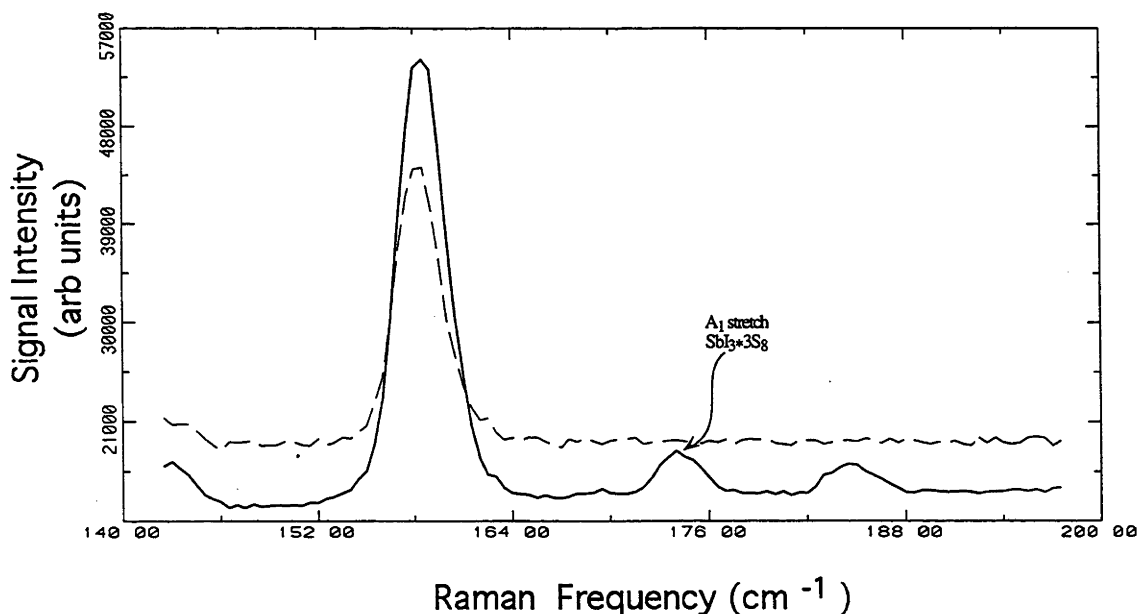
Figure Two: Raman spectra at ~10K of a pressed pellet of SbI_3 and SbI_3*3S_8 powders (full line) and that of SbI_3 alone (dashed).

The peaks due to the R--I A_1 stretch in RI_3*3S_8 can be seen to be significantly less intense than in RI_3, even considering the mole-fraction ratio of ≈ 0.4.

The parameters taken from these spectra for use in Eq (2) are presented in Table One. A subscript of 1 indicates a quantity for the RI_3 component and 2 refers to an RI_3*3S_8 property. The excitation wavelength, v_0, was 15453.56 cm^{-1}. At low temperature, the ratio of Boltzmann factors equals 1 and is not needed in the determination of $\left(\dfrac{\overline{\alpha}_2'}{\overline{\alpha}_1'}\right)$.

Table One:

	M_2/M_1	Δv_1 cm^{-1}	Δv_2 cm^{-1}	I_2/I_1
AsI_3*3S_8 - AsI_3	0.385	206.8	210.6	12.5/126
SbI_3*3S_8 - SbI_3	0.47	158.45	174.2	11.5/117

Using the values of Table One in Eq (2) yields:

$\left(\dfrac{\overline{\alpha}_2'}{\overline{\alpha}_1'}\right)$ for AsI_3*3S_8 / AsI_3 of **0.51** ± 0.02

and

$\left(\dfrac{\overline{\alpha}_2'}{\overline{\alpha}_1'}\right)$ for SbI_3*3S_8 / SbI_3 of **0.49** ± 0.02

These results show that $\partial\alpha/\partial r$ for the R-I bond during the A_1 stretch is reduced upon complexation. The extent of this reduction is virtually the same for both complexes.

Summary

One can understand that the magnitude of the bond-polarisability derivative is determined by the bond 'covalency' by first considering the extreme case of an ionic bond in which α is simply a sum of the ion polarisabilities and hence, $\partial\alpha/\partial r$ must be zero. Conversely, α for a fully covalent bond will be very sensitive to nuclear separation and so $\partial\alpha/\partial r$ will be large. Long and Plane [3] have developed an expression which proportionally relates a 'bond covalency parameter' with $\partial\alpha/\partial r$.

A reduction in $\partial\alpha/\partial r$ may therefore be taken to mean that the covalency of the vibrating bond decreases. This is what is seen for the R--I bonds when

incorporated in the S_8 adduct. This is consistent with MO and electrostatic arguments presented in Chapter One indicating that the C-T interaction adds charge density to the iodine acceptor thus increasing ionic character of the R-I bond.

It is not possible to infer anything about the extent of the covalency reduction from these results since the applicability of the relation of Long and Plane is not certain for solid samples. Also, the error introduced by the Wolkenstein assumptions in this case is not known, nor is it easy to predict. The result showing very similar $\partial\alpha/\partial r$ changes for SbI_3 and AsI_3 upon forming the octa-sulfur adduct is, however, significant.

References

1. R.E. Hester, "Raman Intensities and the Nature of the Chemical Bond." in *Raman Spectroscopy* ed H.A. Szymanski (Plenum, 1967)

2. E.R. Lippencott and G. Nagarajan, Absolute Raman intensities of symmetrical stretching modes in some molecules and ions from delta-function model of chemical binding. *Bull.Soc.Chim.Belges.*, **74**, 551 (1965)

3. T.V. Long and R.A. Plane, Calculation of absolute Raman intensities of A_1 modes of molecules and ions from a delta-function potential model. *J.Chem.Phys.*, **43**, 457 (1965)

4. G.W. Chantry in *The Raman Effect. Vol 1.* ed A. Anderson (Dekker, 1971)

5. G.C. Hayward and P.J. Hendra, The Raman and far infra-red spectra of solid charge-transfer complexes -II. Iodoform complexes of 1,4-diselenan, 1,4-dithianand S_8. *Spectrochim.Acta.*, **23A**, 1937 (1967)

6. W.S. Fernando, Single crystal Raman spectra of $SbI_3 \cdot 3S_8$, $CHI_3 \cdot 3S_8$, $AsI_3 \cdot 3S_8$. *J.Inorg.Nucl.Chem.*, **43**, 1141 (1981)

....a perceptual act....as in a wooden jigsaw puzzle —is not a sum of elements to be distinguished from each other and analysed discretely, but a pattern, that is to say a form, a structure: the element's existence does not precede the existence of the whole, it comes neither before or after it, for the parts do not determine the pattern, but the pattern determines the parts: knowledge of the pattern and of its laws, of the set and its structure, could not possibly be derived from discrete knowledge of the elements that compose it.

....in isolation, a puzzle piece means nothing —just an impossible question, an opaque challenge. But as soon as you have succeeded, after minutes of trial and error, or after a prodigious half-second flash of inspiration, in fitting it into one of its neighbours, the piece disappears, ceases to exist as a piece. The intense difficulty preceding this link-up —which the english word «puzzle» indicates so well —not only loses its «raison d'etre», it seems never to have had any reason, so obvious does the solution appear. The two pieces so miraculously conjoined are henceforth one, which in its turn will be a source of error, hesitation, dismay, and expectation.

George Perec   *«Life, A User's Manual»*